

University at Albany, State University of New York
Scholars Archive

[Legacy Theses & Dissertations \(2009 - 2024\)](#)

[The Graduate School](#)

1-1-2023

Novel nickel-loaded activated carbon cathodes for hydrogen production in microbial electrolysis cells

Daniel Alejandro Moreno Jimenez

University at Albany, State University of New York, dmorenojimenez@albany.edu

The University at Albany community has made this article openly available.
Please share how this access benefits you.

Follow this and additional works at: <https://scholarsarchive.library.albany.edu/legacy-etd>

 Part of the [Environmental Engineering Commons](#)

Recommended Citation

Moreno Jimenez, Daniel Alejandro, "Novel nickel-loaded activated carbon cathodes for hydrogen production in microbial electrolysis cells" (2023). *Legacy Theses & Dissertations (2009 - 2024)*. 3200. <https://doi.org/10.54014/BATS-0QCN>

This Dissertation is brought to you for free and open access by the The Graduate School at Scholars Archive. It has been accepted for inclusion in Legacy Theses & Dissertations (2009 - 2024) by an authorized administrator of Scholars Archive.

Please see [Terms of Use](#). For more information, please contact scholarsarchive@albany.edu.

NOVEL NICKEL-LOADED ACTIVATED CARBON CATHODES FOR HYDROGEN
PRODUCTION IN MICROBIAL ELECTROLYSIS CELLS

by

Daniel Alejandro Moreno Jimenez

A Dissertation

Submitted to the University at Albany, State University of New York
In Partial Fulfillment of
the Requirements for the Degree of
Doctor of Philosophy

College of Engineering & Applied Science
Department of Environmental & Sustainable Engineering
Spring 2023

To my family

Abstract

Microbial electrolysis cells (MECs) can electrochemically produce green hydrogen from waste streams. Although MECs are excellent options for implementing an energy recovery process while treating wastewater, the cathode side still hinders practical applications. Platinum (Pt) has been the top reference for hydrogen evolution reaction (HER) in MECs, however, Pt is not practical due to the high capital cost. Inexpensive nickel-loaded activated carbon (Ni/AC) cathodes were recently developed for replacing Pt in MECs and have shown comparable performance to Pt. This dissertation aims to breakthrough the current cathode challenges regarding the catalytic activity, manufacturing, and operational concept toward a cost-competitive scaling-up process of MECs. First, the electroactivity of the Ni/AC cathode was improved by increasing the oxygen (16.9%) and nitrogen (124%) containing species on the AC surface using nitric acid oxidation. The acid-treated AC (t-AC) showed 21% enhanced wettability which reduced the charge transfer resistance (33%) and ohmic resistance (6.7%) of the cathode. Ni/t-AC achieved 84% higher hydrogen production rates ($0.35 \pm 0.02 \text{ L-H}_2/\text{L-d}$) than the control (pristine AC). Second, increases in polyvinylidene fluoride binder loading (60%), during the manufacturing process, demonstrated to increase by 47% the hydrogen production rates in MECs, yet all cathodes showed a decline in electroactivities ($\leq 9.2\%$) after MEC cycles. It is unclear how the binder content will impact the performance on a large scale. Third, to overcome this drawback, we have examined a novel binder-free flowable cathode. Ni/AC powders were suspended in a buffering solution as a cathode with no electrode fabrication processes. The Ni/AC flow cathode with higher Ni content and minimum Ni/AC loading (4 Ni-atom% and 0.125 wt-AC%, noted as Ni_x/AC_Y , X is nickel content, and Y is powder loading. Hereafter: $\text{Ni}_4\text{AC}_{0.125}$) demonstrated the highest catalytic activities ($-0.86 \text{ V vs. Ag/AgCl}$ at -10 A/m^2) and Faradaic response (1.6 F/g) among Ni/AC flow cathodes tested. This

result indicates that pseudo-capacitive behavior toward Faradaic reactions can be promoted by increasing Ni loadings on AC particles. The MEC with Ni₄AC_{0.125} flow cathode produced comparable hydrogen production rates (1.62 ± 0.15 L-H₂/L_{reactor}-d) to the Pt control (1.64 ± 0.09 L-H₂/L-d), and 40% higher than the blank (without Ni/AC, 1.29 ± 0.02 L-H₂/L-d). There was a 10% increase in hydrogen production rates with the lowest carbon black (CB) blending (CB: 0.06 wt.%) in a Ni₂/AC_{0.125} flow cathode but hydrogen production rates were not further improved as CB content increased. The new Ni/AC flow cathodes showed ~5 times higher hydrogen production rates than previous stationary Ni/AC cathodes. To understand the underlying factors in the flow cathode system, Ni₄AC_{0.125} flow cathodes were further examined by coupling different current collectors (Ni foam, nickel mesh, stainless steel mesh, and Ti sheet). Flowable powders promoted more positive HER potentials at the cathode with the different current collectors, with the Ni foam flow cathode displaying the most positive values (-0.82 V vs. Ag/AgCl). In addition, intrinsically electroactive collector materials produced a higher accumulated charge toward HER than Ti (electrochemically inactive). These results suggest a synergistic effect between collector electroactivity and catalysts powders. There was a voltage drop across the flow cathode volume (≥ 0.49 V vs. Ag/AgCl, 2 cm distant from the current collector), indicating that suspended particles are likely active closer to the current collector rather than in the bulk catholyte. Finally, the nickel foam flow cathode produced 48% higher hydrogen production rates (2.33 ± 0.25 L-H₂/L-d) in MECs than the Ti flow cathode (1.57 ± 0.14 L-H₂/L-d) under the same conditions, demonstrating that the intrinsic electroactivity toward HER and the projected area, of the current collector, play a crucial role in the overall performance of flow cathodes.

Acknowledgment

I would like to express my sincere gratitude to Professor Kyoung-Yeol Kim for being very supportive throughout my years in the Ph.D., for his advice and mentoring. Beyond that, I want to thank Prof. Kim for sharing his work philosophy and values which were the best example to become a better researcher.

I also want to express my gratitude to Prof. Rixiang Huang for providing helpful comments on my research, sharing great professional and personal advice, and promoting a more united graduate student group. The first Ph.D., group in the ESE department.

I would like to thank Professor Michael Yeung and Professor Harry Efstathiadis for their advice and helpful comments on analytical techniques and material synthesis, and for always providing very motivating words.

I want to thank my fiancée Diana Brito for her insightful comments as a peer-grad student and for her love and support, thank you for being with me in every step. This milestone is ours.

A mi mamá, Lolys Moreno, por siempre creer en mi.

I would like to acknowledge my colleagues who have helped me in the laboratory in one way or more. Yukesh Kanna R., Lingqun Zeng, Yamini Kumaran, and Tianhong Mu.

Finally, this work was supported by the Mexican National Council for Science and Technology (CONACYT) through the scholarship 2019-000028-01EXTF-00114.

Table of contents

Abstract	iii
Acknowledgment	v
Table of contents	vi
List of figures	ix
List of Tables	xi
Preface.....	xii
CHAPTER 1	1
General introduction	1
1.1. Background	1
1.2. Research objectives	2
1.3. Dissertation outline	3
CHAPTER 2	5
Literature review.....	5
2.1. Wastewater treatment and energy	5
2.2. Energy-extracting wastewater technologies.....	5
2.3. Microbial electrolysis cells.....	10
2.3.1. MECs for sustainable hydrogen production	11
2.3.2. Cathodes for microbial electrolysis cells	12
2.3.3. Ni/AC cathodes background	15
2.3.4. Cathode operational modes.....	16
2.3.5. Flow electrodes background	17
CHAPTER 3	19
Impact of activated carbon wettability and polyvinylidene fluoride binder loading on Ni/AC cathodes.....	19
3.1. Introduction	19
3.2. Materials and methods	22
3.2.1. Nitric acid treatment of AC powder.....	22
3.2.2. AC/Ni cathode fabrication.....	22
3.2.3. Abiotic electrochemical test.....	24
3.2.4. MEC reactor construction and operation.....	25
3.2.5. Analytical methods and calculations.	26
3.3. Results and discussion.....	28

3.3.1.	Surface characterization of AC/Ni cathodes using XPS, XRD, and FT-IR.....	28
3.3.2.	Wettability and Ni adsorption capacity of AC powder.....	30
3.3.3.	Abiotic electrochemical test for catalytic activity towards HER.....	32
3.3.4.	Hydrogen production rates in MECs.	35
3.3.5.	Average current densities, energy yields, and cathodic hydrogen recoveries.	37
3.4.	Conclusions	40
CHAPTER 4.	42
Flowable Ni-loaded AC cathodes for hydrogen production and operational optimization.	42	
4.1.	Introduction	42
4.2.	Materials and methods	44
4.2.1.	Ni loading on AC particles.	44
4.2.2.	Ni/AC flow cathode experiment.....	45
4.2.3.	Abiotic electrochemical test.....	47
4.2.4.	MEC reactor setup and operation.	48
4.2.5.	Analytical methods and calculations.	49
4.3.	Results and discussion.....	49
4.3.1.	Characterization of Ni/AC flow electrodes.....	49
4.3.2.	Abiotic electrochemical performances with different Ni/AC loadings.	51
4.3.3.	Impact of different Ni loadings on Ni/AC flow cathode.	54
4.3.4.	MEC performances with Ni/AC flow cathodes at 4 h cycle.....	56
4.3.5.	MEC performances with Ni/AC flow cathodes at 24 h cycle.....	58
4.3.6.	Impact of carbon black on the Ni/AC flow cathode.	61
4.4.	Perspectives on the Ni/AC flow cathode application in MECs for hydrogen production.	
	64	
CHAPTER 5.	66
Flowable Ni-loaded activated carbon cathode coupled with different current collectors	66	
5.1.	Introduction	66
5.2.	Materials and methods	69
5.2.1.	Ni loaded on AC particles.....	69
5.2.2.	Ni/AC flow cathode preparation.....	70
5.2.3.	Abiotic electrochemical tests.	70
5.2.4.	MEC reactor setup and operation.	72
5.2.5.	Analytical methods and calculation.	73
5.3.	Results and discussion.....	74
5.3.1.	Characterization of Ni/AC catalyst powders.	74

5.3.2. Electrochemical activity of the flow cathode with different current collectors.....	74
5.3.3. MEC performance with different current collectors.....	81
5.4. Conclusion.....	84
CHAPTER 6	85
Recommendations for future studies	85
APPENDIX A.....	87
Supplementary information	87
APPENDIX B	90
Formal permission for the published paper and figures.....	90
B.1. Permission for adapted CHAPTER 3.....	90
B.2. Permission for the adapted figure 2.3 in CHAPTER 2. Literature review.....	91
B.3. Permission for the adapted figure 2.4 in CHAPTER 2. Literature review.....	92
B.4. Permission for the adapted figure 2.6 in CHAPTER 2. Literature review.....	94
References.....	95

List of figures

Fig. 2. 1. conventional activated sludge treatment process.....	6
Fig. 2. 2. Schematic representation of a Microbial fuel cell.	7
Fig. 2. 3. MFC with different configurations. A) upflow, tubular type MFC with inner graphite bed anode and outer cathode, ¹⁹ B) upflow, tubular type MFC with anode below and cathode above, the membrane is inclined, ²⁰ C) flat plate design where a channel is cut in the blocks so that liquid can flow in a serpentine pattern across the electrode, ²¹ D) single-chamber system with an inner concentric air cathode surrounded by a chamber containing graphite rods as anode, ²² and E) staked MFC, in which 6 separate MFCs are joined in one reactor block. ²³ Adapted with permission from Environ. Sci. Technol. Logan et al. (40)17, 5181-5192. 2006. ²⁴	8
Fig. 2.4. Microbial fuel cell air-cathode pilot plant. Image adapted with permission from Elsevier, water research. Ruggero Rossi et al. (215)118208. 2022. ²⁶	9
Fig. 2. 5.Schematic representation of a two-chambers Microbial Electrochemical Cell (MEC) separated with an Anion Exchange Membrane (AEM).....	11
Fig. 2.6.Top: experimentally measured exchange current, log (j_0), for hydrogen evolution over different metal surfaces plotted as a function of the calculated hydrogen chemisorption energy per atom, ΔE_H (top axis). Single data of crystals are indicated by open symbols. Bottom: The result of the simple kinetic model now plotted as a function of the free energy for hydrogen adsorption, $\Delta G_H^*=\Delta E_H+0.24$ eV. Adapted with permission from © 2005 The Electrochemical Society. J. K. Norskov et at. 2005, 152(3)J23-J26. ³⁷	14
Fig. 3. 1. High-resolution XPS spectra in the a) N 1s, and b) O 1s regions of Ni-adsorbed activated carbon (AC/Ni) and Ni-adsorbed acid-treated activated carbon (t-AC/Ni).....	29
Fig. 3. 2. Surface characterization methods, a) XRD patterns for t-AC/Ni and AC/Ni powders with reference peaks matching SiO ₂ crystal impurities and b) FT-IR spectra for t-AC (upper red line) and pristine AC (bottom black line) powders.....	30
Fig. 3. 3. Comparison of contact angles, a) selected dynamic contact angle plot (1 of 5 data sets) for AC and t-AC tablets, and b) mean values for tablets and electrodes. Error bars indicate mean±standard deviation (n ≥ 5) from testing random points across the surface.....	31
Fig. 3. 4. Contact angle for acid-treated AC (t-AC) and pristine AC tablets. Error bars indicate mean±standard deviation (n ≥ 5) from testing different points across the surface.....	31
Fig. 3. 5. Tafel polarization curves for electrochemical activity analyses of different nickel-functionalized AC cathodes.....	34
Fig. 3. 6. Nyquist plots for t-AC/Ni and AC/Ni catalysts by EIS analyses. The inserted figure is the equivalent circuit used for fitting the spectra through the fit and simulation method.	35
Fig. 3. 7. Hydrogen production rates normalized by the reactor volume and cycle time (L-H ₂ /L-day) and average current densities represented as I _{avg,90} . Error bars indicate mean±standard deviation (n ≥ 10).....	36
Fig. 3.8. Current density productions over 10 days for MECs with different AC/Ni cathodes....	39
Fig. 3.9. Cathodic hydrogen recovery (%, r _{cat}) and energy yield (%, ηE) in MECs with different cathodes tested. Error bars indicate mean±standard deviation (n ≥ 10).	40
Fig. 4.1. Photo of the flow electrode MEC setup used in this study. Closed-loop connection from the glass-bottle reservoir to the cathode chamber for flow cathode recirculation.	46

Fig. 4.2. X-ray photoelectron spectroscopy spectra fitting for (A) Ni ₄ /AC synthesized by hydrothermal method and (B) Ni ₂ /AC synthesized by adsorption method.	50
Fig. 4.3. Current-potential curves of Ni/AC flow cathodes at different Ni/AC powder loadings by (A) LSV and (B) CV tests.....	53
Fig. 4.4. Current-potential curves for Ni/AC flow cathodes, stainless-steel (SS) mesh blank, and Pt control by cyclic voltammetry tests.....	53
Fig. 4.5. GEIS test for Ni/AC flow cathodes with different Ni ₂ /AC powders loadings (≥ 0.25 wt.%). The insert figure represents the equivalent circuit model used to fit the spectra.....	53
Fig. 4.6. Abiotic electrochemical characterization of Ni/AC flow cathodes with different Ni content (2 and 4 Ni-at.%), compared to SS mesh blank and Pt control. (A) current-potential curve by LSV and (B) GEIS tests, the inserted figure represents the equivalent circuit model used to fit the spectra.	55
Fig. 4.7. MEC test results with Ni/AC flow cathodes, compared to SS mesh blank and Pt control at 4 h cycles. (A) Hydrogen production rates normalized by the reactor volume and cycle time (L-H ₂ /L-day) and average current densities represented as I _{avg,90} . (B) Cathodic hydrogen recovery (% , r _{cat}) and energy yield (% , ηE). Error bars indicate mean ± standard deviation (n ≥ 3).....	58
Fig. 4.8. MEC test results with Ni/AC flow cathodes, compared to SS mesh blank and Pt control at 24 h cycles. (A) Hydrogen production rates normalized by the reactor volume and cycle time (L-H ₂ /L-day) and average current densities represented as I _{avg,90} . (B) Cathodic hydrogen recovery (% , r _{cat}) and energy yield (% , ηE). Error bars indicate mean ± standard deviation (n ≥ 3).	60
Fig. 4.9. Current generations over the cycles in MECs with Ni/AC flow cathodes, SS mesh blank, and Pt control. (A) current generations at 4 h cycle, (B) current generations at 24 h cycle, and (C) current generations for a single cycle over 24 h.	61
Fig. 4.10. Impact of carbon blank as an additive in flow cathodes at 4 h cycles. (A) Hydrogen production rates normalized by the reactor volume and cycle time (L-H ₂ /L-day) and average current densities represented as I _{avg,90} . (B) Cathodic hydrogen recovery (% , r _{cat}) and energy yield (% , ηE) Error bars indicate mean ± standard deviation (n ≥ 3).	63
Fig. 4.11. Abiotic electrochemical characterization of Ni ₂ /AC _{0.125} flow cathodes amended with carbon black by LSV.	63

Fig. 5.1. Schematic representation of the abiotic cell used for electrochemical characterization. The working electrode (We) is connected to the different current collectors tested (SS mesh, Ni mesh, Ti or Ni foam).	72
Fig. 5.2. MEC reactor and experimental setup.	73
Fig. 5.3. Current-potential curves. A) Current collector in plain PBS for blank test, B) Ni/AC flow cathode coupled with different current collectors.....	75
Fig. 5.4. Potentiostatic EIS for different current collectors in plain PBS (blank test).	76
Fig. 5.5. Flow cathode coupled with different current collectors. A) charge transferred toward HER, B) simplified model of the current collector interphase phenomena 1) HER at the current collector interphase with PBS, 2) HER at Ni/AC clusters attached to the current collector (left, color grey) and, 3) direct electron transfer to the flowable catalyst powders (right, color red). ..	77
Fig. 5.6. Voltage induced at the probe at different working electrode potentials.....	79
Fig. 5.7. Voltage induced at the probe (2 cm far from the current collector) using flow cathode coupled with different current collectors.	79
Fig. 5.8 .Comparison of MEC performances (hydrogen production rate, current density, cathodic hydrogen recovery, and energy yield) using flow cathodes coupled with Ni foam and Ti.	83

Fig. 5.9. Current generation over the 4 h cycles in MECs with flow cathodes coupled with Ni foam and Titanium (Ti) current collectors.....	83
Fig. A 1. High-resolution XPS spectra in the C 1s regions of (A) Ni-adsorbed acid-treated activated carbon (t-AC/Ni) and (B) Ni-adsorbed activated carbon (AC/Ni).	87
Fig. A2. Nickel adsorption on AC and t-AC (A) experimental equilibrium isotherm data of AC/Ni and t-AC/Ni, (B) Langmuir isotherm model and, (C) Freundlich isotherm model.	88
Fig. A 3. Nickel redox potentials determined by cyclic voltammetry test for Ni/AC catalysts in a 3-electrode cell using catalytic ink.	89

List of Tables

Table A 1. Nickel adsorption test parameters resulted from fitting the data set using Freundlich and Langmuir isotherm models.	89
---	----

Preface

I, Daniel Alejandro Moreno Jimenez, declare that this dissertation titled “Novel nickel-loaded activated carbon cathodes for hydrogen production in microbial electrolysis cells” and the work presented in it is my own. I, the dissertation author, was the primary researcher and first author for the following studies or articles. The studies included here are part of the programmatic line of research that comprised the dissertation in a coherent and sequenced investigation.

Chapter 3 is adapted with permission from: Daniel A. Moreno-Jimenez and Kyoung-Yeol Kim. Elsevier, Bioresource technology, 350 (2022) 126881. Enhanced wettability improves catalytic activity of nickel-functionalized activated carbon cathode for hydrogen production in microbial electrolysis cells. [Doi.org/10.1016/j.biortech.2022.126881](https://doi.org/10.1016/j.biortech.2022.126881). ©2022 Elsevier. The authors (CC-BY-NC-ND). Formal permission is provided in Appendix B1.

Chapter 4 is adapted with permission from: Daniel A. Moreno-Jimenez, Yamini Kumaran, Harry Efstathiadis, Moon-Hyun Hwang, Byong-Hun Jeon, and Kyoung-Yeol Kim. *Manuscript submitted (in Peer Review)*. Flowable nickel-loaded activated carbon cathodes for hydrogen production in microbial electrolysis cells.

Chapter 5 is adapted with permission from: Daniel A. Moreno-Jimenez, and Kyoung-Yeol Kim. *Manuscript in preparation*. Impact of different current collectors on a nickel-loaded activated carbon flow cathode for hydrogen production in microbial electrolysis cells.

The articles are included in the dissertation with permission from the publisher and/or authors. Any deviations from the original wording of these articles are only to conform to the format

requirements of this dissertation. Permission to reuse the articles has been included in Appendix B1, and permission for adapted figures displayed in Chapter 2 (literature review), has been provided in Appendix B as follows: permission for Figure 2.3 is in appendix B2, permission for Figure 2.4 is in appendix B3, and permission for figure 2.6 is in appendix B4.

CHAPTER 1.

General introduction.

1.1. Background

10 million metric tons of hydrogen are produced in the United States each year, mainly for petroleum refining processes and ammonia production. The biggest problem is that most of the hydrogen production is currently performed via natural gas reforming (95%) with important carbon emissions. In addition, the hydrogen demand is likely to increase significantly over the upcoming years due to the introduction of hydrogen in other sectors, such as the transportation sector and the energy sector (including ammonia as an energy carrier, hydrogen for thermal industrial processes, power generation, energy storage and grid balancing).¹ Thus, sustainable pathways for hydrogen production are necessary to introduce a transformative hydrogen economy which will address the climate change challenges. However, the biggest issue with sustainable hydrogen production is the cost. The department of energy (DOE) has established a target of \$2/kg by 2025, and \$1/kg of hydrogen by 2030 via sustainable hydrogen production pathways, which includes water electrolysis, biomass conversion, direct solar water splitting, and others.^{2,3} Among the different sustainable pathways, water electrolysis is one of the most attractive options since this technology can be potentially deployed at all scales and can be coupled with renewable power suppliers to achieve near-zero carbon emissions. Water electrolysis is highly efficient, yet the electricity consumption in conventional water splitting accounts for the highest fraction of the production cost.^{2,4} To reduce the cost of hydrogen production, electrolysis processes with low energy demand should be developed. One attractive option is microbial-assisted electrolysis that uses microbial anodes, in an electrochemical cell, to retrieve energy embedded in wastewater

streams and use it toward hydrogen evolution reaction (HER).⁵ Domestic, industrial, and animal wastewater together represent a huge potential in the U.S., for energy recovery ($\sim 1.5 \times 10^{11}$ kWh of potential energy, 17 GW of power).⁶ The advantage of microbial-assisted electrolysis devices such as Microbial Electrolysis Cells (MECs) is the combination of two sustainable hydrogen production pathways, which are i) biomass conversion, and ii) water electrolysis. The use of MECs for hydrogen production implies the utilization of wastewater streams as source of energy and, the possibility of hydrogen production at a lower applied potentials than the conventional water splitting.^{5,7-9} Microbial anodes in MECs can utilize industrial, municipal, or agricultural wastewater streams as a substrate and the external applied potential can be supplied using renewable power sources such as solar photovoltaic, other microbial electrochemical technologies, thermoelectric technology, and others.¹⁰ Those advantages place MEC technology as an excellent option to integrate a hydrogen economy into the next generation of water treatment and resource recovery facilities.

This dissertation aims to breakthrough the current challenges related to the cathode manufacturing methods and performance limitations toward the scaling-up process of MEC using nickel-loaded activated carbon cathodes as a technology platform.

1.2. Research objectives

This study aims to evaluate nickel-loaded activated carbon (Ni/AC) cathodes with different fabrication and operational methods to improve overall hydrogen production rates in MECs. First, the approach to improve cathode performance is based on enhancing the wettability properties of Ni/AC cathodes by incorporating higher fractions of oxygen and nitrogen functionalities on the AC support. Second, modifying the binder loadings and measuring the impact on electroactivity

and hydrogen production rates. Third, introducing and optimizing a novel cathode operational approach based on flowable electrodes. And fourth, understanding the role of current collectors in the flow cathode system by evaluating different materials in terms of electroactivity and charge transferred towards HER.

The specific objectives of this dissertation are:

1. To study the impact of incorporating oxygen and nitrogen containing species on the surface properties of AC support and the effect on the electrochemical activity and H₂ production rates in the solid-type Ni/AC cathode.
2. To assess the impact of increased PVDF binder loading for solid-type AC/Ni cathodes.
3. To understand the fundaments of the novel Ni/AC flow cathode system in MECs by evaluating different operational parameters such as flow cathode concentration (wt/v.%), cycle time, conductive additives (i.e., carbon black), and impact of different current collector materials.

1.3. Dissertation outline

This dissertation is sectioned as follows. Chapter 2 provides a literature review to understand the fundamentals of MECs, advantages, challenges, operation, and performance. Chapter 3 accomplishes objective 1, stating the impact of oxygen and nitrogen functionalities on the AC support and Ni/AC solid-type cathode. Also, chapter 3 integrates objective 2, stating the influence of polyvinylidene fluorine binder loading on the electroactivity and hydrogen production rates using Ni/AC solid-type cathodes. Chapter 4 introduces the novel Ni/AC flow cathode using different powder loadings, and different Ni loadings and relates the first insights regarding operational parameters, such as cycle time and the presence of conductive additives. Chapter 5

assesses the influence of different current collector materials on the charge transfer process towards the flowable powder and charge transfer at the current collector surface to understand the role of current collectors in the novel flow cathode. Chapter 6 offers perspectives for flow cathodes utilization in MECs and necessary future studies and approaches that could lead to operational and performance improvements for hydrogen production using flowable cathodes in MECs.

CHAPTER 2.

Literature review.

2.1. Wastewater treatment and energy

Wastewater treatment plants (WWTPs) are often the largest energy consumers in many municipalities. An estimated of 3 to 4% of the U.S., electricity consumption is used for the operation of wastewater treatment facilities.^{11,12} This fraction correspond to 30.2 TWh per year and more than 21 million metric tons of greenhouse gases emissions.¹³ Energy is consumed throughout the plant, but the most intensive use is given by the aeration systems and mechanical pumping in WWTPs.¹⁴ The energy needed for a typical domestic WWT employing anaerobic activated sludge processes and anaerobic digestion (AD) is 0.6 kWh per m³ of wastewater treated, about half of that is used for providing electrical energy to the aeration tank.¹² Thus, the overall energy demand is huge worldwide, and represent an important source of carbon emissions, since the current water sector is largely depends on fossil fuels. However, wastewater contains embedded energy which might be around 5 times larger than the required for treatment, mostly conformed by latent thermal energy (80%), chemical (20%), and potential energy for hydraulic applications.¹⁵ This embedded energy can be used to offset the energy expenditures during the treatment process and achieve a near-zero carbon emissions from the water sector.

2.2. Energy-extracting wastewater technologies.

The typical wastewater process usually includes several components including screening, grit removal, primary settling tank, aeration tank (or activated sludge), secondary settling tanks, filtration, disinfection, and sludge treatment (Fig. 2. 1).¹⁵ All of those units are usually energy

consuming and carbon-intensive. To extract the embedded energy in wastewater streams, other energy-extracting technologies could be adapted to existing WWTPs, such as anaerobic digestors, membrane reactors, salinity gradients, osmotic energy recovery process, or fuel cells to convert from a carbon-intensive facilities to near-zero carbon.

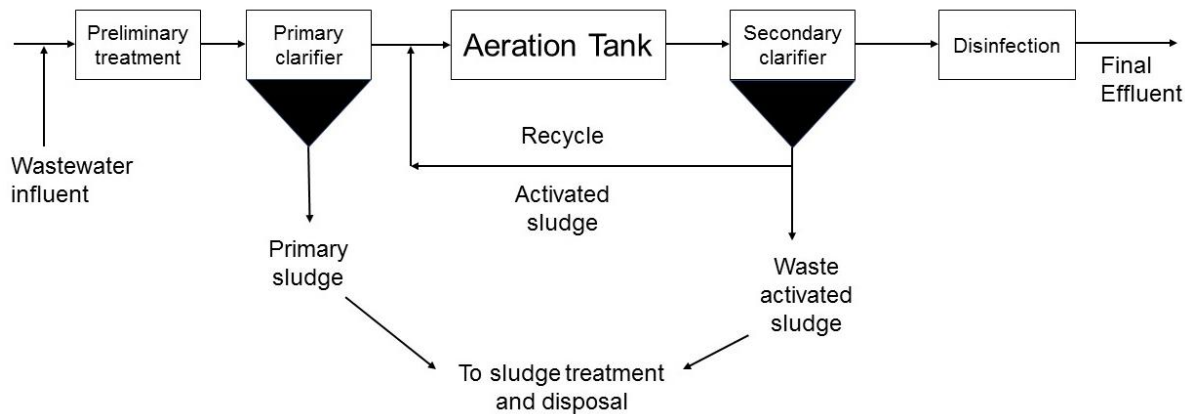


Fig. 2. 1. conventional activated sludge treatment process.

Anaerobic digestion has been commonly used to stabilize sludge with biogas production. WWTPs integrating anaerobic digestion have demonstrated self-sufficient or even energy positive. For example, the WWTP in Bern (Switzerland) uses co-digestion of sludge with green and food waste to produce twice as much energy in the form of biomethane than the energy consumed from the grid for operation.¹⁶ Another example is Grevesmuhlen WWTP in Germany, which produced 113% of its annual energy consumption on-site from biogas through an engine combustion, even part of the electricity generated on-site(>20%) is being traded with the grid operator, generating revenue.¹⁷ Other examples are Gresham WWTP in Oregon, USA., with 17.2 GWh biogas annual production, through co-generators, and heat. East Bay Municipal Utility, District WWTP, Oakland, USA., with 90 GWh of annual biogas production using an internal combustion engine to

generate power 100% of the electricity consumed on-site.¹⁵ The installed power capacity in WWTPs is mainly based on combustion through engine generators, which might still not be beneficial in a deep decarbonized energy sector in the future.

Instead of electricity generation by internal combustion engines, electricity can be produced from the utilization of organic substrate in microbial fuel cells (MFCs). MFCs use microbes to drive the anodic oxidation of organic matter (OM) and generate electrons that are transferred to the cathode for the oxygen reduction reaction (ORR) (Fig. 2. 2). Current density crossing the external circuit can be harvested or directly utilized to power electronic applications while in the anode, the oxidation of OM reduces the chemical oxygen demand (COD) to meet the water treatment standards.

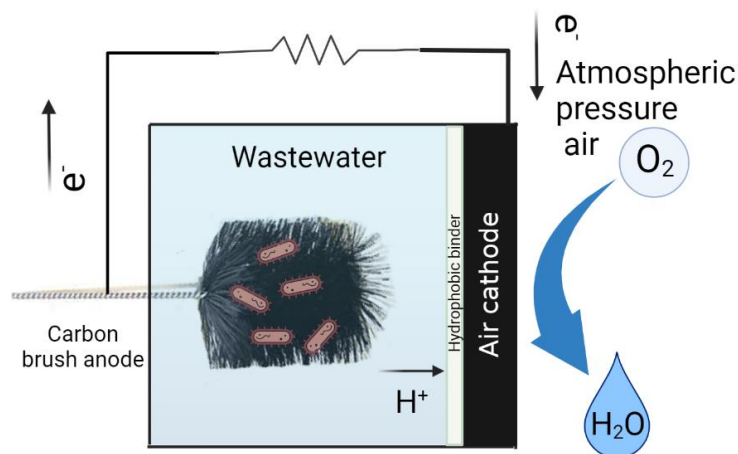


Fig. 2. 2. Schematic representation of a Microbial fuel cell.

MFC technology has reached power densities over 1 kW/m³ (reactor volume) under laboratory conditions.¹⁸ Microbial systems are constructed using a variety of materials, and in an increasing number of configurations (Fig. 2. 3).

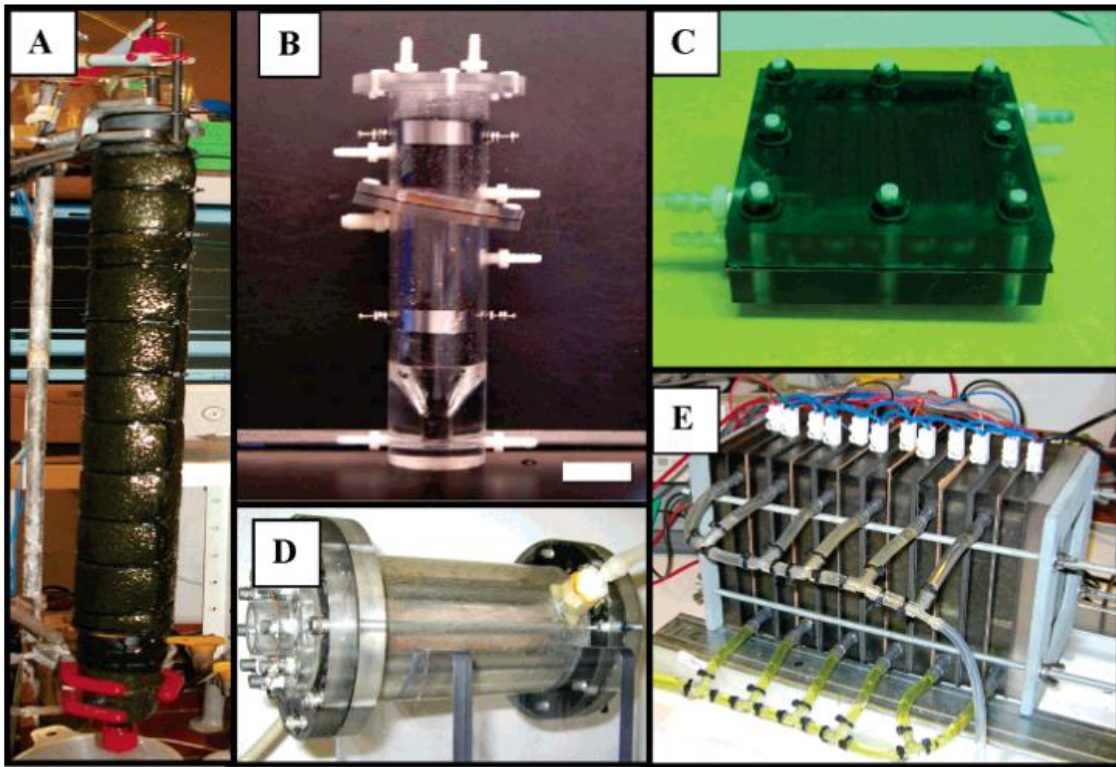


Fig. 2. 3. MFC with different configurations. A) upflow, tubular type MFC with inner graphite bed anode and outer cathode,¹⁹ B) upflow, tubular type MFC with anode below and cathode above, the membrane is inclined,²⁰ C) flat plate design where a channel is cut in the blocks so that liquid can flow in a serpentine pattern across the electrode,²¹ D) single-chamber system with an inner concentric air cathode surrounded by a chamber containing graphite rods as anode,²² and E) staked MFC, in which 6 separate MFCs are joined in one reactor block.²³ Adapted with permission from Environ. Sci. Technol. Logan et al. (40)17, 5181-5192. 2006.²⁴

Electricity is generated in MFCs using a biocompatible anode. The most versatile anodic material is carbon in different forms, such as graphite plates, rods, granules, and high porosity substrates (felt, cloth, paper, fibers, foam, brush, etc.). Those materials have been extensively used and are relative inexpensive and easy to handle.²⁴ There are two recent general configurations for MFCs, 1)

integrating a separator, which divide the anode and cathode into two different chambers, or 2) a single-chamber MFC integrating an air-cathode exposed to the ambient air (Fig. 2. 2). Ion exchange membranes are usually used for separation between the liquid substrates and ambient air. The most common membranes are fabricated by Nafion (Dupont CO., USA). However, the single chamber reactor design does not integrate a membrane separator, instead a polymer binder layer blended with the cathode allow to separate the wastewater from the ambient air, such design is called MFC air-cathode.²⁵ Air-cathode MFC design seems to be most developed version of MFCs for scaling up processes. The largest air-cathode MFC tested today nowadays is an 850 L (1400 L total liquid volume) reactor using real primary domestic wastewater discharged at a field site (Fig. 2.4).²⁶ The study integrated 17 bush anode modules and 16 air-cathodes, capable of producing an average energy of 0.46 ± 0.35 W (0.043W/m^2 normalized by the cross-sectional area of an anode) at a current of 1.54 ± 0.9 A.

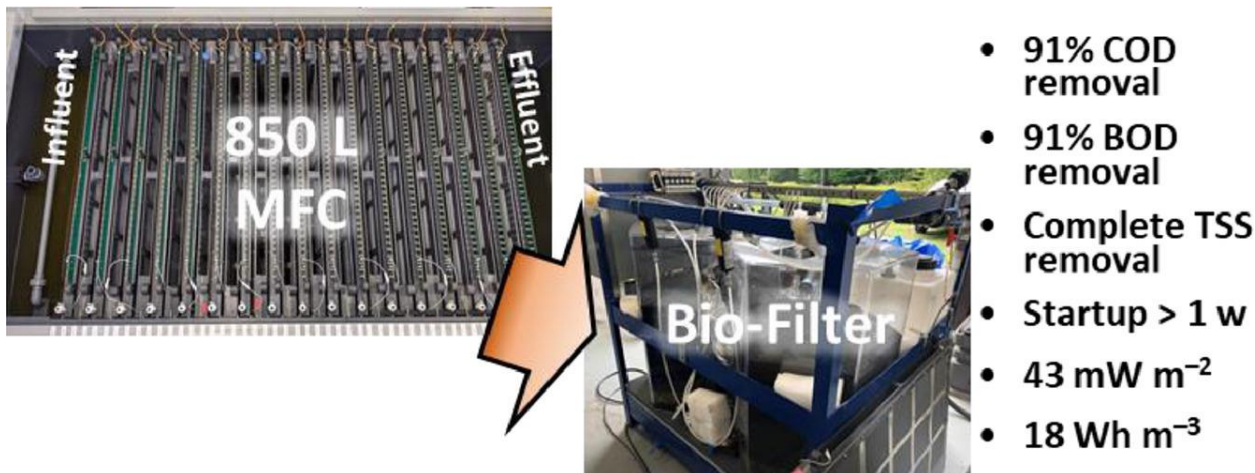
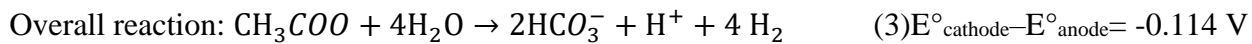
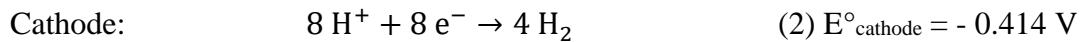
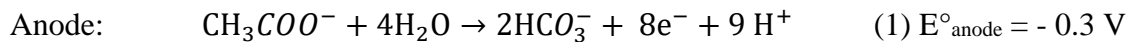


Fig. 2.4. Microbial fuel cell air-cathode pilot plant. Image adapted with permission from Elsevier, water research. Ruggero Rossi et al. (215)118208. 2022.²⁶

Microbial anodes can extract chemical energy from waste streams and convert that energy into useful electricity for power applications. If a small voltage is provided to the cathode, microbial anodes in contact with wastewater can provide electrons to assist the hydrogen evolution at the cathode through an electrolysis process.⁵ Such system is called Microbial electrolysis cells and can convert the chemical energy contained in wastewater into hydrogen which is a valuable-added product.

2.3.Microbial electrolysis cells

Microbial Electrolysis Cell (MEC) are (bio)electrochemical devices that use microorganisms to drive the anodic oxidation of organic matter and generate electrons that are transferred to the cathode for the hydrogen evolution reaction.⁵ MECs (Fig. 2. 5) can utilize different substrates as the source for organics, for example industrial, agro-industrial, and domestic wastewaters. The oxidation of an electron donor at the anode (e.g., acetate) is coupled to the reduction of an electron acceptor with a lower electrode potential at the cathode (H^+/H_2). The global reaction result in a negative cell voltage of - 0.114 V (eq 1 to 3),¹⁰ which theoretically is the applied potential required to drive the electrochemical evolution of hydrogen. In practice, the applied potentials are ≤ 1.2 V, which is still significantly lower than the potential required for conventional water electrolysis (≥ 1.8 V).



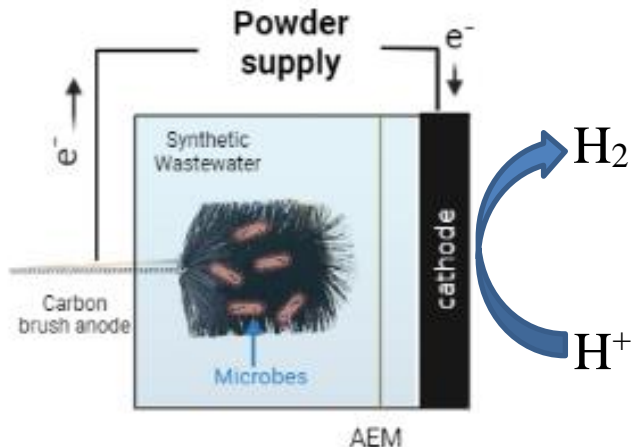


Fig. 2. 5.Schematic representation of a two-chambers Microbial Electrochemical Cell (MEC) separated with an Anion Exchange Membrane (AEM).

This is because the oxidation of organics is thermodynamically favorable. MECs have the potential to play a major role in the deep decarbonization of the energy sector by providing a sustainable pathway to integrate or repurpose conventional energy-consuming wastewater treatment plants into renewable power generators and green hydrogen producers. Consequently, a massive research work has been carried out to address the different aspects needed to achieve the large-scale implementation. For example, the use of different substrates for microbial anodes, different reactor configuration and operation, different cathode materials and electroactivity towards hydrogen evolution reaction (HER).^{7,27-33} Among the multiple challenges addressed in previous studies, the cathode side still hinders the large-scale implementation of MECs.

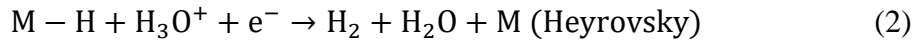
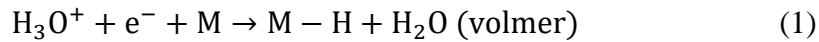
2.3.1. MECs for sustainable hydrogen production

Hydrogen can be extracted from fossil fuels, biomass, water, or a combination of different sources. Nowadays, around 50 million metric tons of hydrogen are produced globally per year, where most of the production is supported by natural gas, which is currently the primary source of hydrogen. Natural gas accounts for around 75% of the annual global dedicated hydrogen

production, using around 205 billion cubic meters of natural gas (6% of the global natural gas usage). Oil and electricity cover the remaining fraction.³⁴ The use of natural gas for producing hydrogen ($t\text{CO}_2/t\text{H}_2$) generates significant CO_2 emissions, around 10 tons of carbon dioxide per ton of hydrogen from natural gas, resulting in an overall contribution of 830 Mt CO_2 /year given by fossil derived hydrogen gas.³⁴ Thus, the future of hydrogen for the chemical industry (e.g., ammonia production) and other end uses cannot be supported by fossil fuel due to the environmental issues associated with carbon emissions. Instead, hydrogen from renewable sources using microbial electrolysis cells is a very attractive option to integrate an energy recovery process into the wastewater treatment infrastructure and enable the future sustainable hydrogen economy. However, the bottle neck of practical applications of MECs is the cathode side. More studies are necessary to be performed to propose an economic-competitive platform to scale up MEC cathodes.

2.3.2. Cathodes for microbial electrolysis cells

The cathode side is one of the most important components in MECs since the hydrogen evolution takes place at the cathode catalysts. Due to the presence of microbes in the systems, the catholyte pH at the cathode should be maintained from neutral to alkaline conditions to prevent any form of anode acidification that might compromise the microbial metabolism and overall cell performance. It is widely accepted that the HER takes place on the surface of the cathode via a multi-step electrochemical process.³⁵ Specifically, in acid conditions, the multi-step electrochemical process occurs via the following reactions:



In the reactions above, the M refers to a vacant surface site of the electrocatalyst, and the M-H refers to the adsorbed hydrogen atoms. In acid solutions, the Volmer reaction (1) involves an initial discharge of the hydronium ion and the formation of hydrogen intermediates (i.e., M-H), and the subsequent formation of H₂ involves the electrochemical Heyrovsky step (2) and/or the Tafel step (3). In alkaline/neutral conditions, the Volmer and Heyrovsky steps involve the hydroxide ion while the Tafel step remains uncharged (4) and (5).



The difference between the acidic conditions and alkaline/neutral conditions is that in the alkaline/neutral conditions the M-H intermediates are formed by dissociation of H₂O.

Pt metal has been the top reference for hydrogen evolution reaction. The Volcano plot (Fig. 2.6) shows the relationship between the experimental J₀ (in log-scale), for hydrogen evolution over different monometallic materials surfaces and the calculated hydrogen chemisorption energy per atom, ΔE_H (top axis, Fig. 2.6) or the energy for hydrogen adsorption, ΔG_{H*}=ΔE_H+0.24 eV (bottom). The active metals are on the left side of the volcano (low coverage of H_{ads}), for example, Pt, Pd, Ni, etc., and the nonactive ones, such as Cu, Ag, and Au are on the right side (high coverage of strongly absorbed hydrogen). It is well recognized that if the intermediates bind too weakly, it

is difficult for the surface to activate them; conversely, if the intermediates bind too strongly, it will occupy all available surface sites and poison the reaction.³⁶ Thus, appropriate binding energies, closer to the Pt position, are required to obtain the best HER performance.

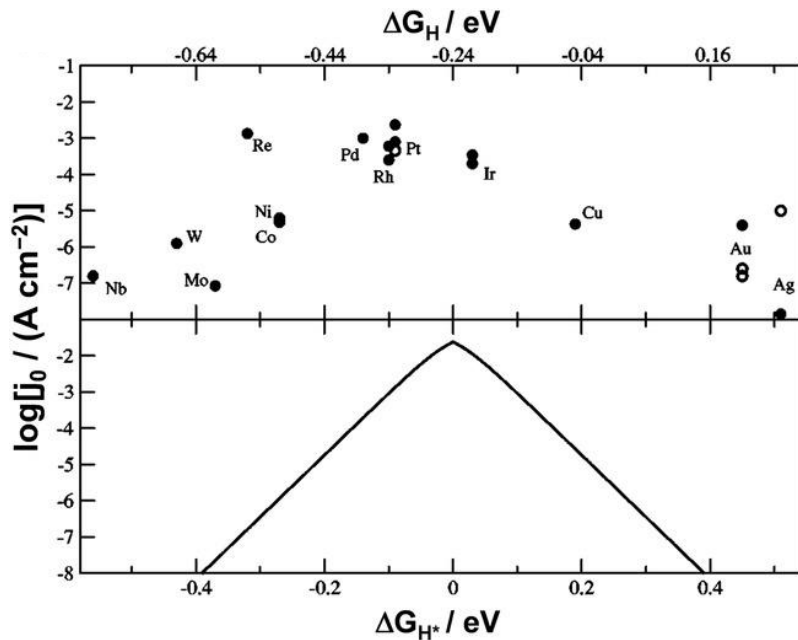


Fig. 2.6. Top: experimentally measured exchange current, $\log(j_0)$, for hydrogen evolution over different metal surfaces plotted as a function of the calculated hydrogen chemisorption energy per atom, ΔE_H (top axis). Single data of crystals are indicated by open symbols. Bottom: The result of the simple kinetic model now plotted as a function of the free energy for hydrogen adsorption, $\Delta G_{H^*} = \Delta E_H + 0.24 \text{ eV}$. Adapted with permission from © 2005 The Electrochemical Society. J. K. Norskov et al. 2005, 152(3)J23-J26.³⁷

Several studies have been focused on the evaluation of different cathode materials such carbon-based cathodes, stainless-steel mesh, nickel-based cathodes, platinum-based cathodes. In addition, different cathode operational parameters have been tested including the use of catholyte

recirculation, and vapor-fed cathodes.^{7,30,31,38} Among the different cathodes, a closely-spaced cathode made of Pt/C and operated with water vapor recirculation, has displayed the record-high sustained current density ($43.1 \pm 0.6 \text{ A/m}^2$) and hydrogen production rates ($72 \pm 2 \text{ L-H}_2/\text{L-d}$) in MECs at a cell voltage of 0.79 V.³¹ Pt/C cathodes are excellent for HER but the downside is that the use of Pt is cost-prohibited for visualizing the large-scale applications.^{30,39,40} Ni-based cathodes have emerged as an excellent option for MECs due to comparable hydrogen production rates than the costly Pt-based cathodes, which have been the top reference for HER activity in the past years.^{7,33,41-44} Despite the promising performances of currently developed Ni cathodes, a breakthrough method of cathode fabrication and operation is still needed to overcome the current barriers for enabling greater hydrogen production rate in MECs with lower cost.

2.3.3. Ni/AC cathodes background

The use of precious metals such as Pt is not practical for microbial electrolysis, and wastewater treatment applications, due to the high capital cost.^{7,39,44-47} Nickel cathodes are economically competitive and display good catalytic activity towards HER. For example, one of the highest H₂ production rates was reported using a commercial Ni foam cathode (50 L-H₂/L-d), and it was attributed to the high specific surface area ($128 \text{ m}^2/\text{m}^2$ projected electrode area),⁴⁵ but the performance of this Ni foam cathode drastically declined over time due to corrosion processes, which consequently increased the cathode overpotential. It is likely that the drop in electroactivity of nickel foam or nickel sheets cannot be restored without considering the fully replacement of the cathode once these are damaged by corrosion processes at some point during the MEC operation.^{32,48} To overcome the drawback related to the stability overtime, nickel cathodes have been produced by mixing nickel salts and activated carbon (AC) powder.⁷ AC itself is not a good

catalyst for HER,⁴⁹ but the AC is an excellent option as a catalyst support, it has a large surface area (~2500 m²/g) available for metal dispersion, good electrical conductivity, and it is inexpensive.⁵⁰ In the previous study, Ni salts were deposited by simple adsorption method onto the AC surface, the resulted nickel-functionalized activated carbon (AC/Ni) cathode showed around 11% higher H₂ production rates than a Pt based cathode used as a control and around 10% higher rates in comparison with a commercialized Ni foam cathode (50 mg-Ni/cm²) used as a blank, even with 82% less amount of Ni used (AC/Ni cathode: 8.8 mg-Ni/cm²).⁷ Moreover, the performance of AC/Ni can be restored in an event of Ni loss, or electroactivity decline, by simple nickel solution re-adsorption process.⁷ The multiple advantages mentioned, in comparison with the other commercial cathodes (Pt and Ni foam), place the AC/Ni cathode as an excellent option for visualizing the large-scale application of MECs.

2.3.4. Cathode operational modes

MEC systems can be divided into two basic configurations, i) single chamber and ii) double or dual chamber MECs. Double chamber MECs are preferred due to the possibility of producing high purity H₂. Several double chamber designs have been developed over almost two decades, from the very first simple double-bottle MEC design to the benchmark square-shaped (or cubic) chambers.^{7,33,43,46,51–55} The other advantage of a two-chamber MEC design is the possibility of controlling the catholyte operational parameters independently from the anode chamber and microbes, for example, operational parameters such as pH range, different buffer solutions, catholyte conductivity, and flow rates for catholyte recirculation can be independently controlled. The previous study showed that the catholyte recirculation reduces the overpotential by improving the gas removal trapped in the surface of the cathode, hence, the catholyte recirculation resulted in

a higher H₂ production rates in comparison with the test in the absence of flow.³⁸ Changing catholyte parameters have been oriented towards the continues operation and hydrogen production. However, the cathode performance can decline overtime, and only one study has addressed the possibility of cathode regeneration after a possible event of performance decline.⁷ Novel MEC cathodes should take into consideration the need for minimizing the maintenance or cathode replacements during operation, and also, minimize or eliminate the need of other components such as polymer binders, which will greatly simplify the manufacture process and reduce the overall cost for large-scale systems.³⁹

2.3.5. Flow electrodes background

Polymer binder adds a very hydrophobic phase to the electrodes that might hinder the diffusion of reactants and products.²⁵ In addition, the polymer binders are generally electrochemically inactive and insulating, which also might restrain the full potential of catalytic materials in electrochemical systems.⁵⁶ Most importantly, it is not clear how the use of binders will impact the performance, the cost of maintenance, replacement, and lifespan of real-world scale cathodes for MECs. Flow electrodes have recently emerged as an attractive option to eliminate the need for binding materials and provide flexibility in the scaling up process of the electrodes, since no electrode fabrication is required to place the electrode into the cell.

Flow electrodes are composed of active particles suspended in a liquid phase (electrolyte) under continues stirring, where the random motion of particles make and break contact with each other and the current collector to form a 3D active electrode volume. When electricity is applied to the cell, electrons are transferred from the current collector to the active suspended particles through a Direct Electron Transfer (DET) mechanism. This charge transfer mechanism allows the

electrode active area to increase with the volume of the reactor rather than the area of the current collector.⁵⁷ A flow-electrode is usually prepared by mixing an electrochemically active material (e.g., AC powder), conductive additives (e.g., carbon black), and a liquid electrolyte in an appropriate ratio.⁵⁸ In addition, flow electrodes display high energy density generation due to electrochemical reaction can take place across the complete three-dimensional volume of the reactor.⁵⁹ Flow-electrodes were initially introduced in 2013 as an innovative approach for seawater desalination through capacitive deionization.⁶⁰ Recently, increasing number of studies have been addressing the improvement on performance, configurations, components and operation^{58,61–66}. Recently, flowable electrodes have been also proposed for electrochemical capacitive energy storage,^{67,68} nutrients and resource recovery from contaminated waters,⁶⁹ selective recovery of phosphate,⁷⁰ and a few additional studies utilizing flow-electrodes for redox reactions such as flow-anodes for hydroxyl radicals (*OH) generation as oxidants for complete degradation of phenol and other organic pollutants,⁷¹ and flowable anolytes for rechargeable energy storage in redox flow batteries.⁷² However, no studies have been conducted on hydrogen evolution reaction utilizing flowable cathodes.

CHAPTER 3.

Impact of activated carbon wettability and polyvinylidene fluoride binder loading on Ni/AC cathodes.

The information in this chapter is adapted from Daniel A. Moreno-Jimenez & Kyoung-Yeol Kim (2022). Enhanced wettability improves catalytic activity of nickel-functionalized activated carbon cathodes for hydrogen production in microbial electrolysis cells. Bioresource technology, 350, 126881. DOI: <https://doi.org/10.1016/j.biortech.2022.126881>. 0960-8524/© 2022 Elsevier Ltd. All rights reserved.

3.1. Introduction

Microbial electrolysis cells (MECs) are electrochemical devices that use microorganisms to drive the anodic oxidation of organic matter and generate electrons that are transferred to the cathode for the hydrogen evolution reaction (HER).⁵ MECs require considerably lower applied potentials (>0.5 V) than the electrochemical water splitting (>1.8 V) in practice to overcome the thermodynamic barrier of the HER. Also, the smaller applied potentials allow obtaining energy yields over 100% based on the electrical input and the energy in the hydrogen produced.^{7,33,38,46,54,73} MECs display high energy yields due to microbial anodes which can recover energy from used-water (previously wastewater) streams containing organic substrates.⁷⁴⁻⁷⁶ There is evidence of pilot-scale MEC reactors ranging from 4 L to 1000 L scales that has provided valuable information for the MEC scale-up.^{52,77-80} Also, these studies raised a few challenges, such as reactor design, cathode materials, and low conductivity of real used-water streams for microbial anodes. These issues have been addressed in recent MEC studies, but the cathode side still hinders the large-scale

applications for hydrogen production from used-water.^{31,79,81} This is partly due to the challenges related to the high cost of cathode materials and the electrochemical stability over time towards HER.^{39,40}

Ni-based cathodes have been emerged as an excellent option for MECs due to comparable or even higher hydrogen production rates than the costly Pt-based cathodes, which have been the top references for HER activity.^{7,32,33,41–44,46} Despite the promising performances of current developed Ni cathodes, a breakthrough method of cathode fabrication is still needed to overcome the current barriers for greater hydrogen production rate in MECs with lower cost. In one study, Ni catalysts were deposited onto the AC by adsorption and the Ni adsorbed AC (AC/Ni) was fixed onto the current collector with a polyvinylidene fluoride (PVDF) binder. The AC/Ni cathodes demonstrated higher hydrogen production rates than Pt/C cathode and comparable hydrogen production rates (1.1 ± 0.1 L-H₂/L-d) to commercialized Ni foam (Ni content: 50 mg-Ni/cm²) even with 82% less amount of Ni used (8.8 mg-Ni/cm²), and Ni catalysts are regenerable through further adsorptions.

⁷ Although AC/Ni cathodes demonstrated promising results, it is still unknown how different surface chemistries (i.e., functional groups on the AC, binder loading, etc.) of AC/Ni could impact HER catalytic activities and consequentially hydrogen production rates in MECs. It is desirable to further improve AC/Ni through better understandings of surface chemistry to achieve higher hydrogen productions in MECs.

AC surface is amenable; thus, it can be modified by simple oxidation using acid solutions. One study reported a wet oxidation method with nitric acid to enrich the surface of AC with oxygen heteroatoms⁶¹. The nitric acid treatment resulted in light oxidation of the AC surface that did not dramatically impact the morphology and the specific surface area, but significantly improved the hydrophilic nature of the AC. The previous studies showed that the treatment with nitric acid

increased the portion (from 8.8 to 18.2 at.%) of oxygen-containing species (such as carboxylic acids, -COOH) on the AC.^{82,83} The nitric acid treatment modified the surface properties, mainly improving the wettability and diffusion rates of reactants on the electrode which also impacted its electrochemical behaviors.⁸² The nitric acid treatment has also demonstrated to increase the content of nitrogen heteroatoms on the AC surface (from 0.5 to 1 at.%).⁸⁴ One study reported that the increased portion of N atoms likely facilitated the Volmer step ($H_{ad} \leftrightarrow H^+ + e^-$) by enhanced electron donation and the sorption of H^+ .⁴⁹ The increased portion of N on the AC (AC_N) in that study demonstrated two times higher hydrogen production rates in MECs than a pristine AC, likely due to the enhanced formation of H_{ad} . However, hydrogen production rates reported in that study were very low (0.003±0.0004 L-H₂/L-d) due to the lack of catalysts like Ni.

The PVDF binder is a key component of the AC/Ni cathode, PVDF forms a polymer network that can hold the catalyst materials onto the current collector and provides microstructural stability and robust mechanical properties without compromising the electrical performance.^{25,85,86} In addition, HER cathodes made with a PVDF binder have displayed excellent catalytic activities when blended with active particles, even when the PVDF binder incorporates a hydrophobic phase to the electrode that might hinder the diffusion of reactants (especially water molecules due to hydrophobicity) to the catalyst surface.^{25,87} Electrochemical properties of electrodes with a PVDF binder (like AC/Ni cathodes) could be varied with the PVDF binder loading, but the impact of PVDF binder loading has not been examined yet.

In this study, it is hypothesized that the nitric acid treatment could improve the HER activities of AC/Ni cathodes by incorporating more oxygen and nitrogen functionalities on the AC surface. Improved interaction at the electrode-electrolyte interface could result in higher hydrogen production rates in MECs. To the best of the authors' knowledge, this is the first study reporting

impacts of acid treatment on AC/Ni cathodes for hydrogen production. A new AC-based cathode was fabricated with nitric acid-treated AC (t-AC/Ni) and characterized using Fourier transform infrared (FT-IR) spectroscopy, X-ray photoelectron spectroscopy (XPS), and X-ray diffraction (XRD). In addition, adsorption capacities (for Ni salts) and wettability of acid-treated AC were examined by adsorption isotherm tests and contact angle measurement to see changes in surface properties. AC/Ni cathodes with acid treatment (t-AC/Ni) and without any treatment (AC/Ni) were examined in MECs to see the impact of acid treatment on hydrogen production rates. AC-Ni cathodes with different PVDF loadings (4.6 and 7.3 mg-PVDF/cm²) were examined as well in MECs to compare electrochemical activities and hydrogen production rates with different binder loadings.

3.2.Materials and methods

3.2.1. Nitric acid treatment of AC powder.

AC (Norit® SX plus CAT, Sigma Aldrich Chemistry USA) powder was treated with a nitric acid solution as previously described.⁸² Briefly, 1 g of AC powder was treated with a 40 mL of HNO₃ solution (65 wt.%, A200-212 certified ACS Plus, Fisher chemical) under continuous stirring for 3 h at room temperature. After that, the acid-treated AC (t-AC) was washed with deionized (DI) water until the pH of the washed DI water reached neutral pH. Finally, the t-AC powder was dried at 100 °C overnight and stored in a desiccator until its use.

3.2.2. AC/Ni cathode fabrication.

A fixed amount (26.5 mg-AC/cm²) of pristine AC or t-AC powder was placed in the beakers (50 mL), then a 5 mL of Ni solution (0.405 M, using NiCl₂·6H₂O salts, VWR, life science, USA)

was added to each AC powder and stirred for 1 h to induce the nickel adsorption. Each Ni adsorbed acid-treated AC (t-AC/Ni) and Ni adsorbed pristine AC (AC/Ni) was placed on a separate membrane disk (pore size: 0.45 μ m, Whatman, Fisher Scientific) and filtered using a vacuum filtration system with additional washes using a DI water to remove impurities and residual nickel salts. Retained t-AC/Ni and AC/Ni powders were dried at 60 °C overnight. For the electrode fabrication, a 0.63 mL of PVDF solution (8% w/v, dissolved in *N,N*-dimethylacetamide, DMAc) was added to each Ni-functionalized AC powder and homogenously mixed to form a paste-like mixture that was spread onto a semi-circular (6.84 cm² area) stainless steel (SS) mesh (type 304, 50 \times 50 mesh McMaster-Carr, USA) current collector. Then mixtures were immediately submerged into a water bath for 1 h to induce phase inversion.²⁵ Finally, the fabricated t-AC/Ni and AC/Ni cathodes were dried in the fume hood overnight. Estimated nickel loadings for t-AC/Ni and AC/Ni are 0.55 mg-Ni/cm² (from adsorption test described in Section 3.2.5). To examine the impact of different PVDF loadings, fixed amounts of Ni (1.4 mg-Ni/cm²) and AC powder (26.5 mg AC/cm²) were mixed in the beakers with DI water (2 mL) and continuously stirred for 30 min to induce adsorption of Ni salts. Then Ni-adsorbed AC powders were dried at 60 °C overnight as previously described.⁷ After that, a fixed volume of 0.63 mL of PVDF solutions with different PVDF concentrations (5% w/v and 8% w/v, dissolved in DMAc) was added to those Ni-functionalized AC powders to produce AC/Ni cathodes with two different PVDF binder loadings: 4.6 mg-PVDF/cm² (AC/Ni-4.6, AC:PVDF, 5.8:1 mass ratio) and 7.3 mg-PVDF/cm² (AC/Ni-7.3, AC:PVDF, 3.63:1, mass ratio). AC, PVDF binder, and Ni catalyst loadings used for this test are based on the previous study where firstly reported Ni-functionalized AC cathodes.⁷

3.2.3. Abiotic electrochemical test.

Electrochemical characterization was carried out at room temperature in a two-chamber cubic cell (anode chamber: 28 mL, cathode chamber: 14 mL) separated by an anion exchange membrane (AEM) (Fumasep® FAB-PPS-130, Fuel Cell Store, USA). A potentiostat/galvanostat (VSP, BioLogic Science Instruments, USA) was used to perform the electrochemical tests in a three-electrode configuration. Cathodes were placed as the working electrode (projected area of 5.54 cm²), SS mesh the counter electrode, and Ag/AgCl (model RE-5B, BASi USA) the reference electrode. A plain phosphate buffer solution (PBS, 50 mM, Na₂HPO₄: 4.58 g/L; NaH₂PO₄: 2.13 g/L) was used for both anode and cathode chambers. The catholyte solution was recirculated during the tests (flow rate: 20 mL/min, 0.7 min hydraulic retention time, HRT) and sparged with a high purity Ar gas (99.999%) before use. Linear sweep voltammetry (LSV) test was carried out using a scan rate of 2 mV/sec in a potential window from -0.4 V to -1.4 V (vs Ag/AgCl). LSV scans were performed in triplicate, there was a 10 min waiting step between scans to allow the system to stabilize before running the next scan. The last LSV scan was used for a Tafel plot analysis. LSV tests were performed on newly fabricated AC/Ni cathodes and used AC/Ni cathodes after being operated in MECs for several cycles (≥ 10 cycles). The used AC/Ni cathodes were retrieved from the MEC reactors and stored at room temperature in a desiccator for 6 months prior to the second LSV test. Electrochemical impedance spectroscopy (EIS) test was performed in a 3-electrode cell using catalytic ink, which was elaborated with 10 mg of catalyst materials (AC/Ni or t-AC/Ni) mixed with 100 μ L of PVDF solution (8% w/v), 50 μ L of DI water, and 50 μ L of isopropyl alcohol that were ultrasonicated for 20 min. The catalytic ink (5 μ L) was deposited onto a glassy carbon electrode (3 mm diameter). Glassy carbon with the dried drop of catalytic ink was used as the working electrode, Pt wire the counter electrode, and Ag/AgCl the reference electrode.

The Ar-sparged plain PBS solution (as described above, 15 mL volume) was used for this test as well.

3.2.4. MEC reactor construction and operation.

Microbial anodes were acclimated over 6 months in single-chamber microbial fuel cells (MFCs) prior to use in this study. Microbial anodes were inoculated with the primary effluent from the Albany County South wastewater treatment plant (70% v/v) and a synthetic used-water (1 g/L acetate in a 50 mM PBS with nutrients, Na₂HPO₄: 4.58 g/L; NaH₂PO₄: 2.13 g/L; KCl: 0.13 g/L; NH₄Cl: 0.31 g/L; trace mineral solution: 12.5 mL; vitamin solution: 5mL).⁸⁸ After the acclimation period, anodes were transferred into the MEC reactors which consist of a two-chamber reactor separated by an AEM. The anodic chamber (28 mL working volume) was operated in fed-batch mode with a synthetic used-water while the cathode chamber (14 mL) was operated with a plain PBS solution (80 mL) with recirculation using a peristaltic pump (Masterflex model 7522-38, USA) at the flow rate of 20 mL/min (0.7 min HRT). The catholyte was sparged with a high purity Ar gas to remove dissolved oxygen before starting each cycle. A glass bottle with a rubber cap was connected to the cathode chamber by a Viton tubing (96412-16, Masterflex). Catholyte recirculation was used since it has demonstrated reduced cathode overpotentials for HER in MECs.^{38,89} Produced hydrogen gases were collected in the headspace of the glass bottle and in a gas collection bag (200 mL, Calibrated Instruments, NY) which is attached to the top of the glass bottle through a rubber stopper. An applied voltage of 0.9 V was used using a DC power supply (BK precision®, model 1621A). After each cycle (24 h), anolyte and catholyte were completely replaced with a fresh solution. The current was monitored using a multimeter (DAQ6510 Keithley, Tektronix company, USA) by measuring the voltage across a 10-ohm resistor.

3.2.5. Analytical methods and calculations.

Collected gases from a gasbag and headspace were analyzed using a gas chromatograph (Model 8610C, SRI Instruments Inc., USA), and the hydrogen production rate was calculated based on the volume of hydrogen produced divided by the reactor working volume (42 mL) per cycle time in days ($L\text{-H}_2/L_{\text{reactor-day}}$). Current density (A/m^2) was calculated as $I_{\text{avg},90}$ (average current density produced when 90% of the total charge has been transferred over the cycle) divided by the projected area of the electrode (5.54 cm^2). $I_{\text{avg},90}$ reflects the time needed to accumulate most of the charge from the organic matter and minimizes the impact of hydrogen recycling in the analysis.⁹⁰ Cathodic hydrogen recovery (r_{cat} , %) and energy yield (η_E , %) were calculated as previously described in the literature⁵. Briefly, the moles of H_2 that could be produced from the current recorded are calculated using $n_{\text{CE}} = \int_0^t Idt/2F$, where I is the current (A), F is the Faraday constant (96485C/mole e^-), and t is the total time (s). Cathodic hydrogen recovery was calculated as $r_{\text{cat}} = n_{\text{H}_2}/n_{\text{CE}}$, where n_{H_2} is the actual moles of hydrogen recovered. Electrical energy consumption (W_E , J) was calculated using $W_E = \sum_{i=1}^n (I_i E_{ps} \Delta t - I_i^2 R_{\text{ext}} \Delta t)$, accounting for the voltage drop caused by the external resistor. Here, E_{ps} is the voltage set up at the power supply (V), R_{ext} is the external resistor (Ω), and Δt is the time interval (s). Energy yield is calculated as $\eta_E = -W_{\text{H}_2}/W_E$, where $W_{\text{H}_2} = n_{\text{H}_2}(\Delta G_{\text{H}_2})$, the energy contained in the moles of hydrogen produced (n_{H_2}) based on the Gibbs free energy of hydrogen ($\Delta G_{\text{H}_2} = -237.1 \text{ kJ/mol}$). LSV data obtained from the abiotic test was used to produce Tafel plots and analyzed using the Tafel equation $\eta = a + b \log(j)$, where η is the overpotential, j is the current density in (A/m^2), b is the Tafel slope (mV/dec) and a is the onset potential. When $\log(j)$ becomes zero, the overpotential becomes the Tafel constant a .⁹¹ XRD for t-AC/Ni and AC/Ni powders was performed in a diffractometer (Bruker D8 Advance) with Cu-K α source using a 2θ range from 20° to 70° , step

size of 0.02° , and a scan rate of $0.12^\circ\text{min}^{-1}$. Diffractograms were analyzed using HighScore plus software (version 4.9, 2020, by PANanalytical B.V., Almelo, The Netherlands). FTIR was performed using a PerkinElmer spectrometer (model spectrum 100, USA) in a region between 4000 and 500 cm^{-1} . X-ray photoelectron spectroscopy (XPS) was performed using a PHI Quantera hybrid instrument employing a $200\text{ }\mu\text{m}$ monochromatic Al $\text{K}\alpha$ X-ray to irradiate the surface of AC/Ni and t-AC/Ni samples. High-resolution spectra were taken at pass energy of 26 eV and with a step size of 0.05 eV. The quantification and peak fitting were carried out using PHI multipak v9.9.0.8., and peak positions were restricted to fit in line with literature values. XPS was performed to probe the chemical state in the C 1s, O 1s, and N 1s regions and determine the degree of incorporation of heteroatoms on the AC/Ni and t-AC/Ni cathodes.

A nickel adsorption test was carried out to compare the adsorption capacities of t-AC and pristine AC powders at different Ni concentrations ranging from 25 ppm to 5869 ppm. Adsorption batches (5 g of AC or t-AC per L of nickel solution) were kept at room temperature under constant shaking (using a VWR, Standard Analog shaker) for 72 hours until reached the adsorption equilibrium. After the adsorption period, nickel solutions were recovered using syringe filters (Target2, Cellulose acetate $0.2\text{ }\mu\text{m}$) and analyzed using an ion chromatograph (930 compact IC Flex, Metrohm). Adsorption data resulted from the batch test were fitted using Langmuir and Freundlich models.⁹² Finally, to study the wettability property, AC and t-AC powders were homogenously mixed with PVDF powder (70:30, AC:PVDF wt.% ratio) and compressed at 4000 lb for 30 min in a manual hydraulic press (Carver, Inc., USA) using a stainless-steel pressing device to form carbon tablets. AC/Ni and t-AC/Ni electrodes were also fabricated. Both tablets and electrodes were tested in a video contact angle system (VCA optima, AST products inc., USA.). AC and t-AC tablets were tested using video recording mode at 31 frames per second

(dynamic contact angle). The first frame showing contact with AC surface was used for statistical analysis, while electrodes were tested in a photo mode (static contact angle). In all cases, random points across the surface area were taken and a student t-test was used to analyze significant differences between data sets.

3.3. Results and discussion

3.3.1. Surface characterization of AC/Ni cathodes using XPS, XRD, and FT-IR.

The XPS spectra, for both catalysts, revealed peaks that were fit by principal compounds at 284.52 eV (C-C), 285.73 eV (C-O), 287.72 eV (C=C) for carbon (C 1s) region; 532 eV (SiO₂) for oxygen (O 1s) region and in the range from 395 to 405 eV for nitrogen (N 1s) region (Fig. 3. 1). The peak corresponding to single (C-C) and double bond (C=C) carbon comprises 37.2% and 7.7% of C 1s photoemission for AC/Ni catalyst (Fig. A 1B), and slightly lower values were observed for t-AC/Ni, where single bond carbon (C-C) comprises 31.9% and double bond carbon (C=C) comprises 6.1% of the photoemission (Fig. A 1A), indicating that the acid treatment etched away a small fraction of the carbon-carbon bonds on the t-AC surface. The peak corresponding to C-O comprises 20.2 at.% for AC/Ni and 22.3 at.% for t-AC/Ni, confirming the light oxidation of t-AC after the acid treatment (Fig. A 1). The scan on the O 1s region revealed the presence of SiO₂ species on the AC surface, which displayed a small fraction (1.1 at.%) integrated during the manufacturing process of the commercial AC. The fraction of SiO₂ increased in the t-AC/Ni surface (from 1.1 to 3.67 at.%), possibly due to the etching of carbon after the acid treatment which might have changed the C/SiO₂ ratio. The XPS analysis revealed an overall increment of 16.9% in the atomic fraction of oxygen-containing species on the t-AC/Ni surface in comparison to the AC/Ni catalyst. In addition, the scan in the N 1s region revealed a small fraction of nitrogen on the

surface, equivalent to 0.25 at.% for AC/Ni and 0.56 at.% for t-AC/Ni, which indicate that nitric acid treatment increased more than two times (124%) the content of nitrogen heteroatoms on the t-AC surface.

XRD patterns for t-AC/Ni and AC/Ni show two main diffraction peaks at 2-theta 20.9 and 26.51 corresponding to crystalline SiO₂, and different peak intensities confirm the change in C/SiO₂ ratio after the acid treatment. FT-IR was performed on the AC and t-AC powders as well. The small increment in the atomic fractions resulted in absorption bands with almost identical positions and shapes suggesting that light oxidation was almost negligible in the FT-IR spectra (Fig. 3. 2).

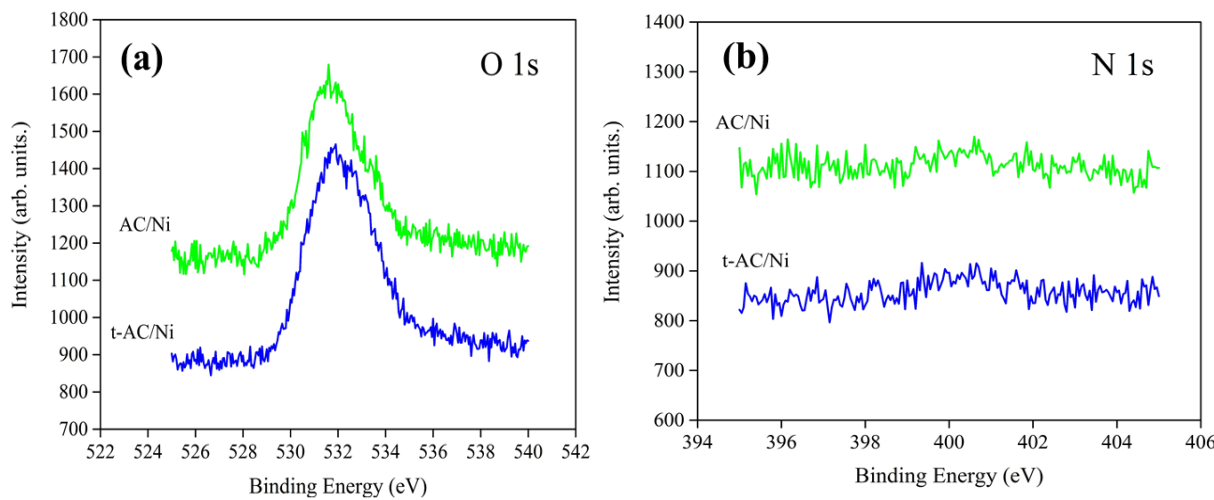


Fig. 3. 1. High-resolution XPS spectra in the a) N 1s, and b) O 1s regions of Ni-adsorbed activated carbon (AC/Ni) and Ni-adsorbed acid-treated activated carbon (t-AC/Ni).

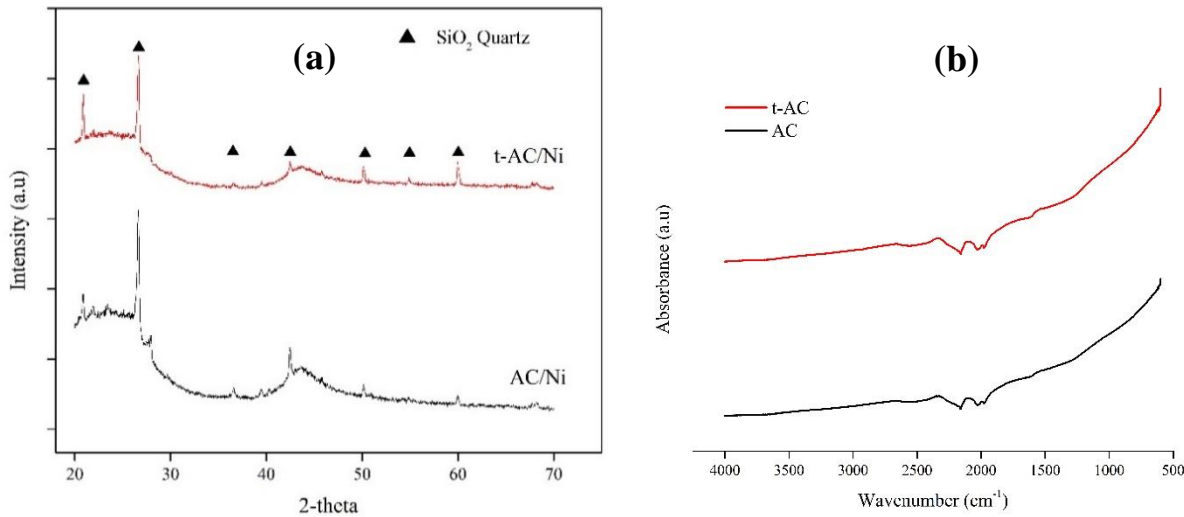


Fig. 3.2. Surface characterization methods, a) XRD patterns for t-AC/Ni and AC/Ni powders with reference peaks matching SiO_2 crystal impurities and b) FT-IR spectra for t-AC (upper red line) and pristine AC (bottom black line) powders.

3.3.2. Wettability and Ni adsorption capacity of AC powder.

Median contact angle values of $48 \pm 3^\circ$ for t-AC powder and $60 \pm 5^\circ$ for pristine AC powder were obtained from the dynamic contact angle analysis (Fig. 3.3), showing significantly different contact angle values (student t-test, $p < 0.05$) after acid treatment (Fig. 3.4a). The decreased contact angle for t-AC represents an overall improvement of 21% on its wettability. Wettability of the electrodes is a crucial property for electrochemical reactions since better wettability allows the electrolyte to diffuse quickly inside the micropores of the carbon material.

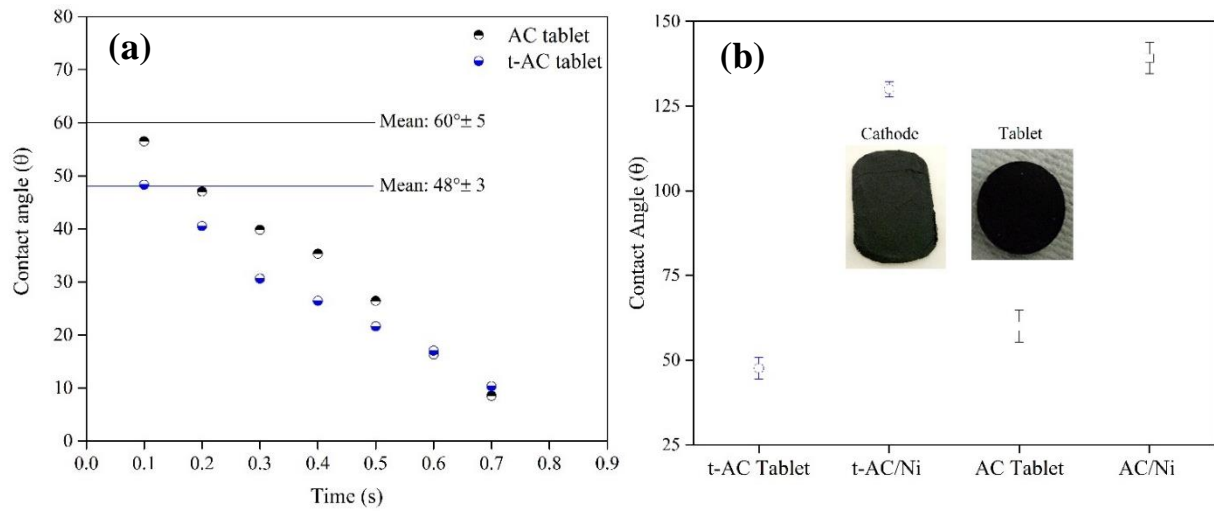


Fig. 3. 3. Comparison of contact angles, a) selected dynamic contact angle plot (1 of 5 data sets) for AC and t-AC tablets, and b) mean values for tablets and electrodes. Error bars indicate mean \pm standard deviation ($n \geq 5$) from testing random points across the surface.

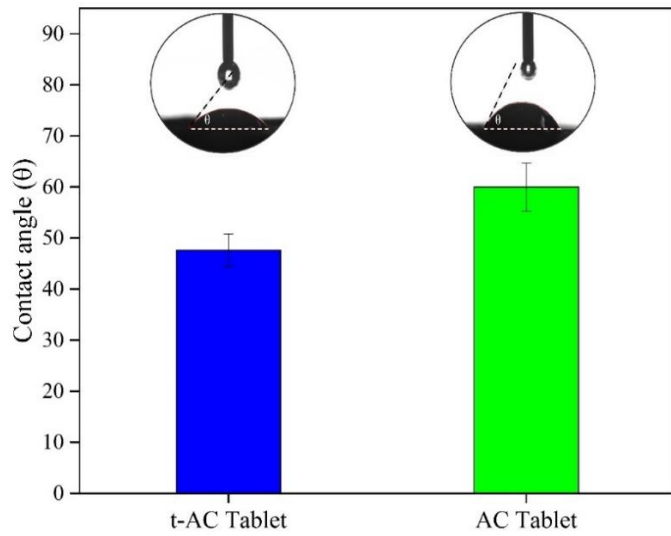


Fig. 3. 4. Contact angle for acid-treated AC (t-AC) and pristine AC tablets. Error bars indicate mean \pm standard deviation ($n \geq 5$) from testing different points across the surface.

The better wettability of the electrodes likely results in better ion transport and overall reduction of the internal resistance of the system.⁹³ The wettability of AC/Ni cathodes was enhanced in this study likely due to the introduction of oxygen atoms after the acid treatment. Oxygen atoms can modify the electrostatic field at the carbon surface, inducing certain polarity, which likely promotes the interaction between water molecules and carbon material.⁹⁴ An additional contact angle test was carried out to see the impact of the PVDF binder on the wettability of AC electrodes. Significantly different ($p < 0.05$) median contact angle values of $130 \pm 2^\circ$ for t-AC/Ni and $139 \pm 5^\circ$ for AC/Ni were obtained (Fig. 3. 3b), which represent an overall improvement of 6.5% on the wettability of the electrode. This result indicates that the increased wettability of the t-AC support significantly improves the wettability of electrodes, the enhanced wettability lasts even after electrode fabrication by phase inversion with a PVDF binder which creates a very hydrophobic surface layer.

Pristine AC and t-AC powder displayed similar adsorption capacities for Ni salts (Fig. A2A) and there are no significant differences ($p > 0.05$) in adsorption coefficients obtained from Langmuir (Fig. A2B) and Freundlich (Fig. A2C) isotherm models. For example, Ni adsorption coefficients of K_f (Freundlich isotherm) for t-AC was $0.14 \text{ (mg/g)(L/mg)}^{1/n}$ and $0.13 \text{ (mg/g)(L/mg)}^{1/n}$ for pristine AC, and q_m (Langmuir isotherm) for t-AC was 3.31 mg/g and 5.24 mg/g for pristine AC (Table A 1). This result suggests that the acid treatment did not significantly impact the adsorption capacity of AC powders.

3.3.3. Abiotic electrochemical test for catalytic activity towards HER.

The t-AC/Ni cathode showed the highest electrochemical activity towards HER (in the Tafel plot) among all other cathodes tested in this study (Fig. 3. 5). A significantly lower slope (136

mV/dec) and more positive onset potential (-0.725 V vs. Ag/AgCl) were obtained from Tafel plots for t-AC/Ni in comparison with AC/Ni, which showed a Tafel slope of 147 mV/dec and more negative onset potential of -0.742 V (vs. Ag/AgCl). In addition, the EIS test showed that t-AC/Ni had lower ohmic resistance ($R_{\text{ohmic}} = 249.3 \Omega$) and charge transfer resistance ($R_{\text{ct}} = 189.6 \Omega$) than those of AC/Ni ($R_{\text{ohmic}} = 267.3 \Omega$ and $R_{\text{ct}} = 284.1 \Omega$) (Fig. 3. 6), representing a slight reduction in the ohmic resistance (6.7%) accompanied with a significant reduction in the charge transfer resistance (33.3%) for the t-AC/Ni cathode. These abiotic test results suggest that the improved wettability of t-AC/Ni likely enhanced the catalytic activity towards HER by improving the charge transfer at the electrode surface and ion transport at the interface of electrode-electrolyte. Similar conclusions were made in previous studies where examined AC-based electrodes as supercapacitors.⁹³ In that study, improvements in the wettability of the AC electrodes facilitated the ion transport through the micropores and it enhanced the electrical conductivity by decreasing the equivalent series of resistance of the cell.

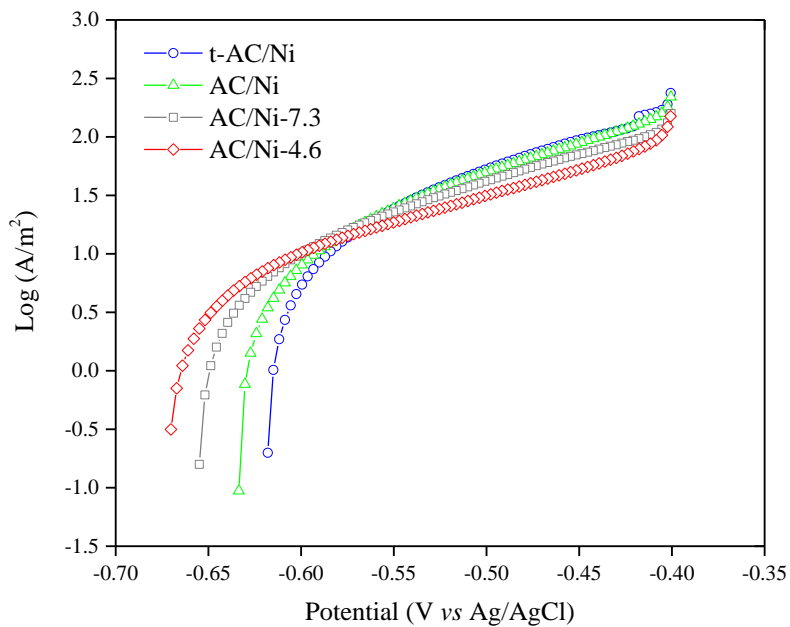


Fig. 3. 5. Tafel polarization curves for electrochemical activity analyses of different nickel-functionalized AC cathodes.

Different PVDF loadings impacted the catalytic activities of AC/Ni electrodes as well. The AC/Ni cathode with a PVDF loading of 7.3 mg-PVDF/cm² (AC/Ni-7.3) demonstrated better electrochemical activities (Fig. 3. 5) in comparison with the electrode fabricated with a PVDF loading of 4.6 mg-PVDF/cm² (Ni/AC-4.6). For instance, the AC/Ni-7.3 cathode displayed a lower Tafel slope (166 mV/dec) and slightly more positive onset potential (-0.764 V vs. Ag/AgCl) than the AC/Ni with a lower PVDF loading (AC/Ni-4.7) that produced a Tafel slope of 190 mV/dec and an onset potential of -0.784 V vs. Ag/AgCl. In the previous study for carbon-based electrodes in Li batteries, lower electrochemical activities were found with lower PVDF loadings (10 wt.%) due to the insufficient binder content to connect all the components in the electrode. When the PVDF content increased from 10 to 30 wt.% in the electrode, the electrochemical performance increased, which was attributed to a better physical contact.⁹⁵ AC/Ni electrodes with different PVDF loadings displayed a similar trend, showing higher electrochemical activities with a higher PVDF binder loading.

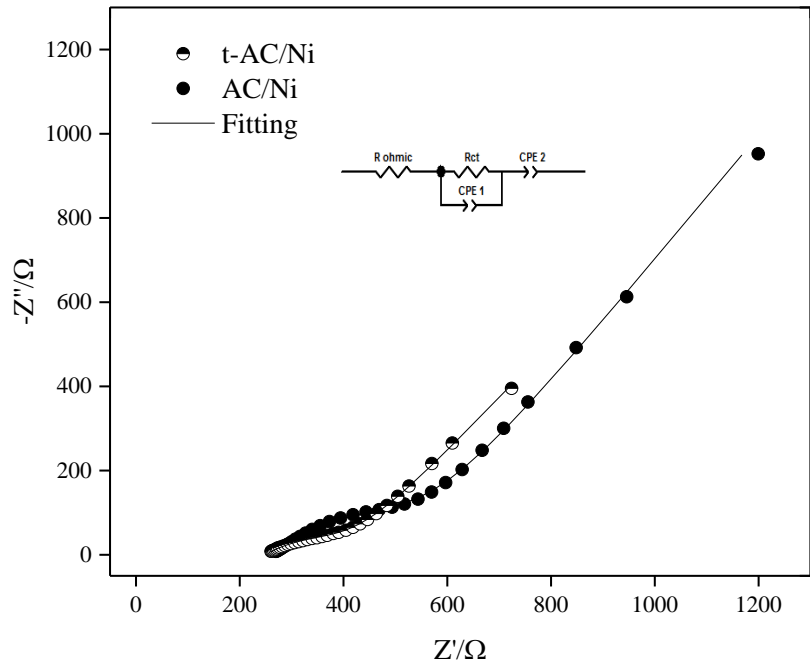


Fig. 3. 6. Nyquist plots for t-AC/Ni and AC/Ni catalysts by EIS analyses. The inserted figure is the equivalent circuit used for fitting the spectra through the fit and simulation method.

3.3.4. Hydrogen production rates in MECs.

Higher hydrogen production rates were obtained from the MEC with t-AC/Ni than the MEC with AC/Ni (Fig. 3. 7). For example, t-AC/Ni produced a median value of 0.35 ± 0.02 L-H₂/L-d and AC/Ni cathode produced a median value of 0.19 ± 0.01 L-H₂/L-d. The hydrogen production rate was 84% higher in the MEC with t-AC/Ni cathode than the MEC with AC/Ni. This result corresponds with the higher catalytic activity observed in the abiotic test resulting from the improved wettability. Hydrogen production rates were increased with a higher PVDF loading, AC/Ni-7.3 produced 0.22 ± 0.02 L-H₂/L-d which were 47% higher production rates than AC/Ni-4.6 (0.15 ± 0.01 L-H₂/L-d) (Fig. 3. 7). This result corresponds with the greater electrochemical activities observed from the Tafel analysis when increasing the PVDF loading.

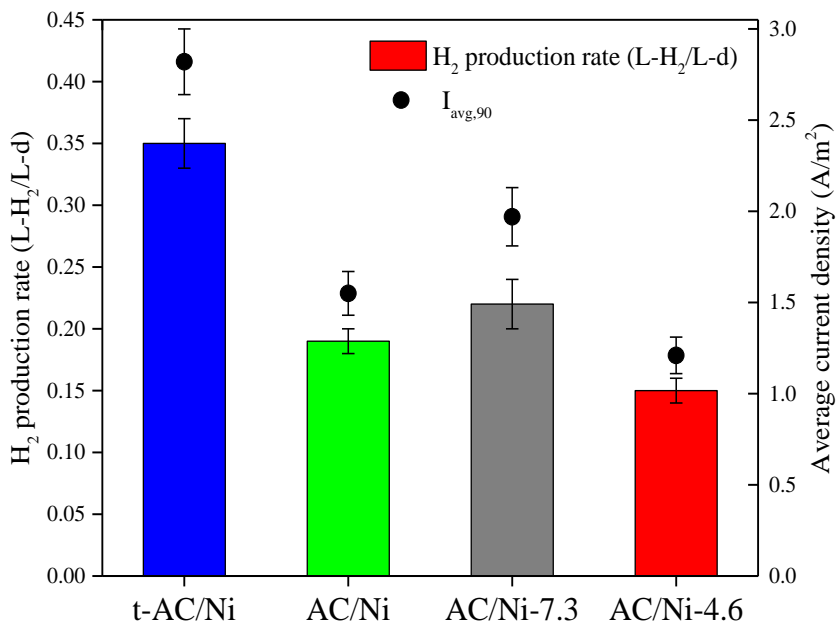


Fig. 3. 7. Hydrogen production rates normalized by the reactor volume and cycle time ($L-H_2/L\text{-day}$) and average current densities represented as $I_{avg,90}$. Error bars indicate mean \pm standard deviation ($n \geq 10$).

AC/Ni and t-AC/Ni had comparable Ni catalyst loading but t-AC/Ni showed the highest hydrogen production rate among all other cathodes tested. This result further emphasizes the strong impact of improved wettability of the cathode which is attributed to the increment (16.9%) in oxygen-containing species on the surface of AC (t-AC).^{82,87} Also, a higher portion of N heteroatoms (124% increased) likely accelerated the sorption of H^+ on the surface of t-AC promoting the Volmer step ($H_{ad} \leftrightarrow H^+ + e^-$) which can enhance the hydrogen production rate in MECs.⁴⁹

The hydrogen production rate using AC/Ni was 13.6% lower than the obtained using the AC/Ni-7.3 cathode. This is likely due to differences in Ni catalyst loadings, AC/Ni contained less amount of Ni catalyst loaded ($0.55 \pm 0.02 \text{ mg-Ni/cm}^2$) than AC/Ni-7.3 (1.4 mg-Ni/cm^2). The

previous study reported a similar hydrogen production trend in MECs, AC/Ni with less Ni loadings showed lower hydrogen production rates.⁷ Higher hydrogen production rates were obtained from t-AC/Ni cathode in this study (0.35 ± 0.02 L-H₂/L-d) in comparison to the previous study where the AC/Ni cathode (with 8.8 mg Ni/cm² catalyst loading) without acid treatment produced 0.30 ± 0.02 L-H₂/L-d.⁷ Higher hydrogen production rates in this study are attributed to the improved wettability and electroactivity of the t-AC/Ni cathode. Slightly lower hydrogen production rates were obtained in this study in comparison to the other previous study where cathodes were fabricated using Ni metal particles blended with AC power which produced 0.38 L-H₂/L-d (using 4.8 mg-Ni/cm²).⁴⁶ The higher hydrogen production rate was likely due to a different type of nickel precursor (Ni210 powder, Alfa-Aesar, MA) and much higher Ni loadings (from 4 to 46 mg-Ni/cm²) used in that study. The other study examined a similar AC/Ni cathode with a PVDF binder (4.8 mg-Ni/cm² catalyst loading) and reported 1.56 L-H₂/L-d of hydrogen production rate, which is 4.5 times higher than that in this study. The higher hydrogen production rate in the previous study is due to the different MEC reactor configurations. The previous study used a single-chamber MEC design which produces usually higher current densities and hydrogen production rates due to a lower internal resistance with a lack of the membrane separator.^{18,96}

3.3.5. Average current densities, energy yields, and cathodic hydrogen recoveries.

All tested cathodes showed a maintained current density production over the entire duration of this study (≥ 10 cycles) (Fig. 3.8). The current density production achieved peak values at the beginning of each cycle (first 5 hours) and slowly decreased over time due to substrate depletion. The current density ($I_{avg,90}$) was 82% higher in the MEC with t-AC/Ni (2.8 ± 0.2 A/m²) in comparison with that produced by the MEC with AC/Ni (1.6 ± 0.2 A/m²) (Fig. 3. 7). As the PVDF

loading increased from 4.6 to 7.3 mg-PVDF/cm², the current density ($I_{avg,90}$) increased by 63% (from 1.2 ± 0.1 A/m² to 2.0 ± 0.2 A/m²). t-AC/Ni showed an average energy yield (ηE) of $129\pm8\%$ and cathodic hydrogen recovery (r_{cat}) of $93\pm6\%$ (Fig. 3.9). Slightly lower energy yield and cathodic hydrogen recovery were obtained with AC/Ni, which showed $\eta E = 124\pm9\%$ and $r_{cat} = 90\pm6\%$. Interestingly, significantly lower energy yield and cathodic hydrogen recovery values ($p < 0.05$) were obtained with AC/Ni-7.3 ($\eta E = 111\pm9\%$ and $r_{cat} = 80\pm6\%$) than those obtained with AC/Ni-4.6 with a lower PVDF binder loading ($\eta E = 124\pm11\%$ and $r_{cat} = 90\pm8\%$) even with 47% more hydrogen productions in MECs (Fig. 3.7). This result suggests different scenarios including a slightly lower selectivity of the cathode in terms of reduction of the target reactants,⁴⁹ the impact of slightly lower exchange current density with AC/Ni-7.3 ($\text{Log } (A/\text{m}^2) = 0.39$) than with AC/Ni-4.6 ($\text{Log } (A/\text{m}^2) = 0.44$) (Fig. 3.5), or a certain degree of hindrances due to the increase in PVDF loading. Slightly lower energy yield and hydrogen recovery of AC/Ni-7.3 did not severely impact the hydrogen production rate since this cathode produced more hydrogen than AC/Ni-4.6 over the cycles. Energy yields (ηE , %) were greater than 100% in all MECs (Fig. 3.9) indicating that the amount of energy contained in the hydrogen recovered was greater than the electrical energy input from the power supply in all cases.

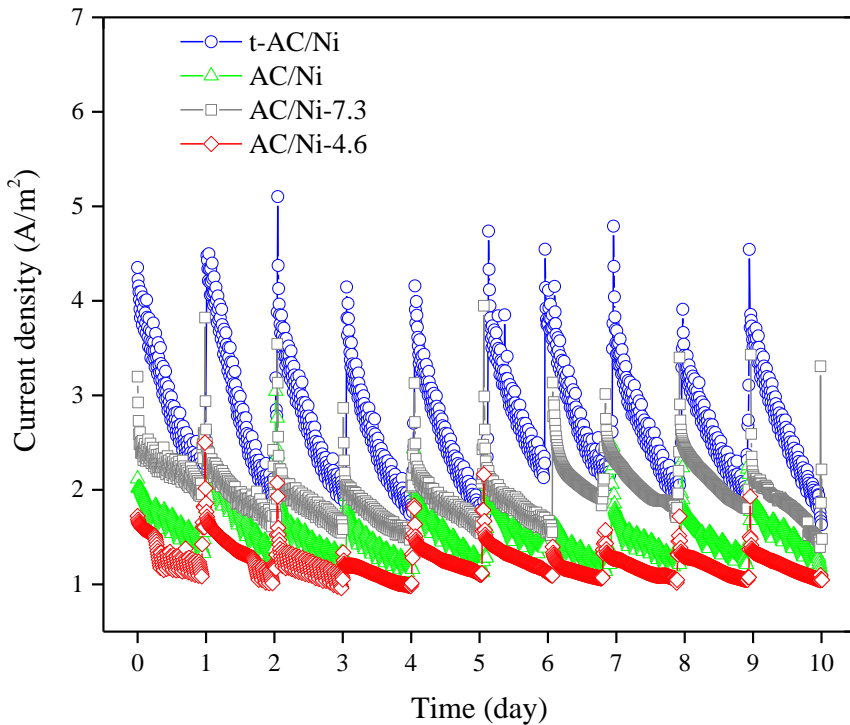


Fig. 3.8. Current density productions over 10 days for MECs with different AC/Ni cathodes.

To further examine the catalytic activities and stability after a prolonged period, the tested AC/Ni cathodes were retrieved from MECs and analyzed using LSV scans after 6 months of storage outside of the solution. The Tafel plot analysis for used-AC/Ni electrodes showed a slight shift to more negative onset potentials (t-AC/Ni showed an onset potential of -0.792 V, -0.797 V for AC/Ni, -0.783 V for AC/Ni-7.3, and -0.808 V for AC/Ni-4.6). Although no decreases in current densities and hydrogen production rates were observed during 10 day-operation (Fig. 3.8), LSV results for used AC/Ni electrodes suggest a small loss in catalytic activities ($< 9.2\%$). This might be due to the dryness of the used-AC/Ni cathodes that have been stored outside of the solution for 6 months, which can adversely impact on physicochemical properties of AC/Ni cathodes. In a previous study, AC/Ni cathodes demonstrated no performance decrease over 30

days of operation.⁷ Even with small losses in catalytic activities of AC/Ni cathodes, the catalytic performance can be easily restored by an additional adsorption step using a nickel solution.⁷

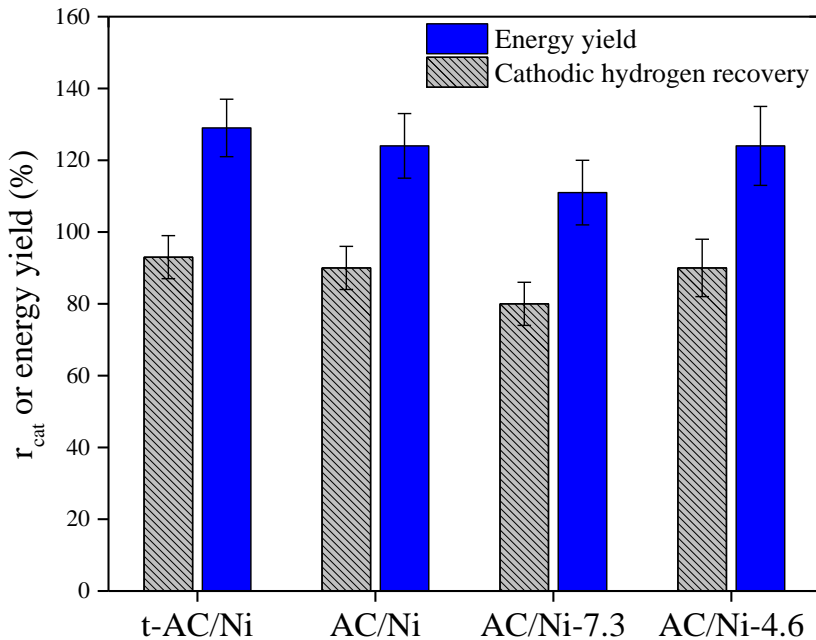


Fig. 3.9. Cathodic hydrogen recovery (% , r_{cat}) and energy yield (% , η_E) in MECs with different cathodes tested. Error bars indicate mean \pm standard deviation ($n \geq 10$).

3.4. Conclusions

The hydrogen production rate in MECs using Ni-functionalized AC (AC/Ni) cathode was improved (84%) by enhancing wettability (21% increment) of the AC through oxidation with nitric acid. Enhanced wettability was attributed to an increment in oxygen-containing species, and this better wettability prevails even after the formation of the PVDF network. Increased content of N on the acid-treated AC likely promotes the Volmer step in the HER. AC/Ni with higher PVDF loading displayed a higher hydrogen production rate (47%), likely the increased PVDF loading

maintain the electrode structure and promoted a better connection between AC/Ni particles and the SS mesh.

CHAPTER 4.

Flowable Ni-loaded AC cathodes for hydrogen production and operational optimization.

The information in this chapter is adapted from Daniel A. Moreno-Jimenez, Yamini Kumaran, Harry Efstathiadis, Moon-Hyun Hwang, Byong-Hun Jeon, and Kyoung-Yeol Kim (2023). Flowable nickel-loaded activated carbon cathodes for hydrogen production in microbial electrolysis cells. *Manuscript submitted.*

4.1. Introduction

Microbial electrolysis cells (MECs) can produce high-purity hydrogen at the cathode by oxidizing organic matter in waste streams with small energy input.⁵ Although MECs are excellent options to implement energy recovery while treating wastewater, the cathode side has been a major bottleneck for the practical application of MECs at a larger scale.⁹⁷ Platinum (Pt) is known as the best catalyst for hydrogen evolution reaction (HER), but the use of Pt in MECs is not practical due to the high capital cost.^{7,39,44-47}

Nickel (Ni) based cathodes have shown great potential to fully replace Pt in MECs. In an earlier stage of studies, the MEC with a Ni foam cathode demonstrated hydrogen production rates of 50 L-H₂/L_{reactor-d}, but the Ni foam cathode deteriorated over time due to corrosion.⁴⁵ To overcome this drawback, instead of using Ni foam or metal sheets, Ni salts or particles can be chemically combined or blended with robust carbon substrates such as activated carbon (AC).⁴⁶ AC itself is not a good catalyst for HER,⁴⁹ but AC is inexpensive and it can provide a very large surface area ($\sim 2500\text{ m}^2/\text{g}$) to metal catalysts which is beneficial to promote catalytic activities.⁵⁰ One study reported a new solid-type activated carbon (AC) cathode loaded with Ni catalysts for MECs.⁴⁶ The

solid-type Ni-loaded AC (Ni/AC) cathode produced 11% higher hydrogen production rates than the Pt control and 10% higher H₂ production rates than a commercialized Ni foam cathode even with 82% less amount of Ni content.⁷ The other study further improved the HER catalytic activities (by 84%) of the solid Ni/AC by enhancing wettability on the cathode surface, and also reported the potential adverse impacts of the binder on the catalytic activities.⁸ Although the solid-type Ni/AC cathode has shown great performances in MECs to date, cathode manufacturing steps for large-scale and mass production could be complicated and the cathode performance at large scale would not be reliable over time due to potential structural changes that are usually observed in solid-type electrodes.^{25,96,98–101}

Flow (or slurry) electrode has been proposed to eliminate the need for manufacturing processes and binders while it can promote electrochemical performances by maximizing the active surface area and reducing saturation near the electrode.^{59,102} Flow electrodes are composed of conductive powder or particles suspended in an electrolyte under continuous stirring or recirculation.⁵⁷ Random motion of conductive particles makes and breaks contacts with each other and the current collector to form a 3-dimensional electrode active area.^{57,59} AC-based flow electrodes were initially applied for capacitive deionization (CDI) to desalt seawater.⁶⁰ The flow CDI (fCDI) can be running continuously with replenishment of AC particles outside of the cell and demonstrated great potential to be easily scaled up by only increasing AC loadings.^{60–66,70} AC flow electrodes have been also studied for resource recovery from waste streams. One study reported high recovery efficiencies (> 80%) for nitrogen and phosphorus ion species in wastewater with 5–15 wt.% AC flow electrode loadings.¹⁰³ The other study achieved P recovery efficiencies of 62% over 96 h continuous operation using AC flow electrodes.⁷⁰ A few more recent studies examined flow electrodes involving redox reactions to enhance the oxidation of contaminants and

desalination.^{71,104,105} However, no study has examined AC-based flow electrodes for catalytic reactions such as HER in MECs.

In this study, we examined a new Ni/AC flow cathode suspended in a buffering solution (catholyte) for enhancing HER electroactivity in MECs. Inexpensive Ni/AC powders were suspended in the catholyte with no cathode fabrication and recirculated in a closed loop to facilitate the continuous production of hydrogen. To understand the impacts of Ni/AC powder and Ni content loadings, different Ni/AC powder loadings (0.125, 0.25, 1, and 5 wt.%) and Ni/AC powders with different Ni atomic loadings (2 and 4 Ni-at.%) were tested in both abiotic cells and MECs. The electrochemical activity and hydrogen production rates of the Ni/AC flow cathodes were compared to those of the Pt control and blank (only current collector without powder). Carbon blank (CB) was blended with the Ni/AC flow cathode at different loadings to see if conductive additives could further improve the electroactivity of the flow cathodes.

4.2. Materials and methods

4.2.1. Ni loading on AC particles.

Ni/AC powders were synthesized with two different methods based on the previous studies.^{7,8,85} With the Ni adsorption method, a fixed amount of AC powder (4 g, Norit® SX plus CAT, Sigma Aldrich Chemistry, USA) was mixed with 1 g of NiCl₂·6H₂O (VWR, USA) in a glass beaker. The mixture of AC and Ni salts was stirred in deionized (DI) water (100 mL) for 30 min to induce the adsorption of Ni salts onto the AC surface. The prepared Ni/AC slurry was poured on a membrane disk filter (pore size: 0.45 µm, Whatman, Fisher Scientific, USA) and washed with DI water using a vacuum filtration system to remove residuals. Then, the retained Ni/AC was dried at 60 °C overnight.

A hydrothermal method was used to load more Ni catalysts onto the AC surface. The AC powder (1 g) was added to the glass beaker containing nickel salt solution (100 mL, 1 M $\text{Ni}(\text{NO}_3)_2 \cdot 6\text{H}_2\text{O}$) and mixed with continuous stirring for 30 min. The prepared slurry was ultrasonicated for 10 min and then transferred to an autoclave reactor and maintained at 150 °C for 18 hours to further induce the Ni loading onto the AC surface. The Ni/AC slurry was poured on the membrane disk filter, then washed and dried at 60 °C overnight. The amount of Ni loaded on the AC was calculated using X-ray photoelectron spectroscopy (XPS) analyses and the Ni contents were determined by Ni atomic ratios (Ni, at.%) on the AC surface. Hereafter, the Ni/AC flow cathode with a 2 at.% of Ni content (prepared by the adsorption method) will be denoted as Ni_2/AC and the Ni/AC flow cathode with a 4 at.% Ni content (prepared by the hydrothermal method) as Ni_4/AC .

4.2.2. Ni/AC flow cathode experiment.

To examine the prepared Ni/AC flow cathodes, different amounts of Ni_2/AC powders (0.05, 0.1, 0.4, and 2 g) were added to a catholyte (40 mL) to produce 0.125 ($\text{Ni}_2/\text{AC}_{0.125}$), 0.25 ($\text{Ni}_2/\text{AC}_{0.25}$), 1 (Ni_2/AC_1), and 5 (Ni_2/AC_5) concentrations (weight of AC powder/volume of the catholyte, wt%) of Ni_2/AC flow cathodes. In addition, Ni_4/AC powders (0.05 g) with higher Ni loading (4 Ni-at.%) were used to attain the flow cathode with 0.125 wt.% ($\text{Ni}_4/\text{AC}_{0.125}$). The catholyte was a 50 mM plain phosphate buffer solution (PBS, Na_2HPO_4 : 4.58 g/L; NaH_2PO_4 : 2.13 g/L, pH = 7.3, 5.6 mS/cm). A semicircular (6.84 cm²) stainless steel (SS) mesh (type 304, 50×50 mesh, McMaster-Carr, USA) was used as a current collector in the MEC with flow cathode (Fig. 4.1). The abiotic and MEC experiments were also tested without Ni/AC powders (only with a SS mesh current collector, blank test) since SS itself is also active for HER.³⁸ A solid Pt cathode (Pt

control, 0.5 mg-Pt/cm² loading) was prepared as previously described.^{7,43,106} Briefly, Platinum on carbon (Pt/C) powder (10% Pt on carbon Vulcan XC-72, Fuel Cell Store, USA), was mixed with deionized water (28.4 µL), isopropyl alcohol (113.9 µL), and Nafion® solution (228.1 µL, 5 wt.%, Sigma Aldrich, USA). The Pt/C slurry was spread onto a semicircular SS mesh (6.84 cm²) by brush painting and dried overnight in the fume hood. Finally, to study the impact of conductive additives (i.e., carbon black), the Ni₂/AC_{0.125} flow cathode was amended with the addition of 0.025, 0.05, and 0.1 g of carbon black (CB, Vulcan XC-72, Cabot corporation, USA) to attain 0.06 (Ni₂/AC_{0.125}/CB_{0.06}), 0.13 (Ni₂/AC_{0.125}/CB_{0.13}), and 0.25 wt.% of CB (Ni₂/AC_{0.125}/CB_{0.25}) in the catholyte.

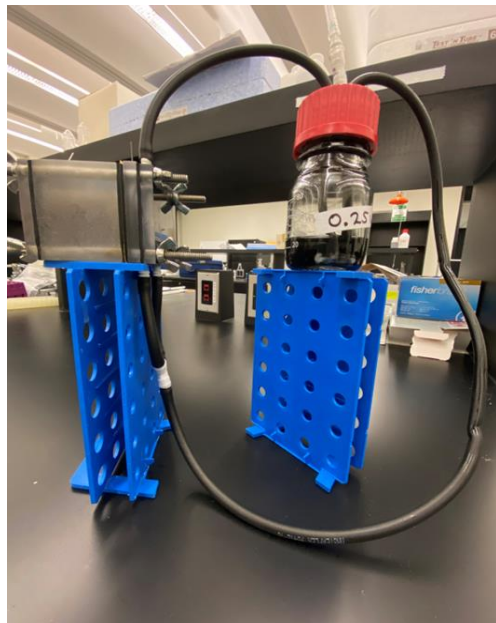


Fig. 4.1. Photo of the flow electrode MEC setup used in this study. Closed-loop connection from the glass-bottle reservoir to the cathode chamber for flow cathode recirculation.

4.2.3. Abiotic electrochemical test.

Electrochemical characterization was conducted in a two-chamber polycarbonate cell (consisting of two cubic chambers with a 3 cm diameter hole, 2 cm long, and a 14 mL working volume in each chamber) separated by an anion exchange membrane (AEM) (Fumasep® Fuel Cell Store, USA) having a projected surface of 7 cm². A potentiostat (VSP, BioLogic Science Instruments, USA) was used to perform linear sweep voltammetry (LSV) and galvanostatic electrochemical impedance spectroscopy (GEIS) tests in a 3-electrode configuration using different working electrodes (Ni/AC flowable cathodes, SS mesh, and Pt cathode), Ag/AgCl reference electrode (model RE-5B, BASi, IN), and a SS mesh counter electrode. The LSV scans were recorded using a scan rate of 5 mV/sec from the open circuit potential (OCP) to -1.4 V vs. Ag/AgCl. After triplicate LSV scans, the 3rd scan was taken for comparison with other working electrodes. Cyclic voltammetry (CV) was conducted in a potential range from -0.4 V to -0.8 V vs. Ag/AgCl using a scan rate of 5 mV/sec. In the working electrode chamber, 40 mL of the Ni/AC flow cathodes with different Ni and Ni/AC loadings, or only 40 mL of 50 mM plain PBS (for SS mesh blank and Pt control) were recirculated. In the anode chamber, a 50 mM plain PBS (80 mL) was used. The pH of the catholyte was adjusted to 7 by adding a small volume (<1.5 mL) of hydrochloric acid solution (1 M HCl) and sparged with Ar gas to remove dissolved oxygen prior to each test. Each anodic and cathodic chamber was connected to an external gas-tight glass bottle (150 mL) via Viton tubing (HV-96412-16, Cole Parmer, USA), and the anolyte and catholyte were recirculated at a constant flow rate of 20 mL/min using a peristaltic pump (EW-07522-30, Cole Parmer, USA). GEIS was performed using a current bias of -40 mA in the abiotic cell and a signal amplitude of 1 mA in a frequency range from 4 kHz to 1 Hz. An additional CV test from -0.8 to

0.8 V vs. Ag/AgCl was performed as previously described (see section 3.2.3) using Ni/AC catalytic ink in a 3-electrode cell to measure the redox potential of the Ni²⁺/Ni pair.

4.2.4. MEC reactor setup and operation.

Microbial anodes were acclimated for over 6 months in a microbial fuel cell and other MECs prior to this study.⁸ The MEC was a two-chamber reactor separated by the AEM. The cathode chamber (0.6 cm long, 3 cm diameter hole, with a working volume of 4.2 mL) was connected via Viton tubing to an external gas-tight glass reservoir containing 40 mL of Ni/AC flow cathodes or 40 mL of 50 mM plain PBS without Ni/AC powder for blank and control tests. Catholytes were recirculated at a flow rate of 20 mL/min (hydraulic retention time, HRT = 12.6 sec in the cathode chamber) using a peristaltic pump. The hydrogen gases produced in the cathode chamber were dragged from the chamber to the bottle with the liquid flow and collected in the headspace and in a gas collection bag (Calibrated Instruments, NY) attached to the top of the glass bottle through a rubber cap (Fig. 4.1). Synthetic wastewater containing (in 1 L DI water, sodium acetate: 1 g/L; Na₂HPO₄: 4.58 g/L; NaH₂PO₄: 2.13 g/L; KCl: 0.13 g/L; NH₄Cl: 0.31 g/L; and amended with trace mineral solution: 12.5 mL; and vitamin solution: 5 mL) was continuously recirculated at 2 mL/min (HRT = 14 min) in the anodic chamber (28 mL). The anolyte recirculation flow rate was kept low to avoid potential anodic biofilm wash-off. MEC tests were performed over 4 h or 24 h cycles to examine hydrogen production rates at the peak of the current densities (usually for the first 5 hours of the MEC operation).⁸ Before each cycle, the catholyte pH was adjusted to 7 using 1 M HCl solution and sparged with Ar gas to remove dissolved oxygen. The anolyte was completely replenished with fresh synthetic wastewater (150 mL) before starting each cycle.

4.2.5. Analytical methods and calculations.

Hydrogen gases collected in both the gas collection bag and the headspace of the glass reservoir were analyzed using a gas chromatograph (Model 8610C, SRI Instruments Inc., USA). Hydrogen production rates were calculated based on the volume of hydrogen produced divided by the total reactor working volume (32.2 mL) per cycle time in days ($L\text{-H}_2/L_{\text{reactor-day}}$). Current densities (A/m^2) were calculated as $I_{\text{avg},90}$ (see Chapter 3).⁹⁰ Cathodic hydrogen recovery ($r_{\text{cat}}, \%$) and energy yield ($\eta_E, \%$) were calculated using previously developed methods for MECs (see Chapter 3).⁵ To examine the electrochemical behavior of different Ni/AC powder loadings, the pseudo-capacitance (C, F/g) was calculated at -0.6 V (vs. Ag/AgCl) using $C = (I_a - I_c)/(2v \times m)$, where I_a and I_c are anodic and cathodic currents, respectively, v the scan rate (V/sec), and m the mass of Ni/AC.¹⁰⁷ GEIS was analyzed using the equivalent circuit R-ohmic in series with a constant phase element (CPE) and the charge transfer resistance (Rct) (Rohmic+CPE/Rct) and the fit and simulation method in Zfit (EC-Lab, version 10.23). XPS was performed using a PHI Quantera hybrid instrument employing a $200\ \mu\text{m}$ monochromatic Al K α X-ray to irradiate the surface of Ni/AC. High-resolution spectra were taken at pass energy of 26 eV and with a step size of 0.05 eV between 880 eV and 840 eV binding energy intervals. The quantification and peak fitting were carried out using CasaXPS (version 2.3.25) and peak positions were restricted to fit in line with literature values (NIST XPS database) for Ni $2p_{3/4}$ region.¹⁰⁸

4.3. Results and discussion

4.3.1. Characterization of Ni/AC flow electrodes.

For the Ni/AC flow cathodes prepared with different Ni deposition methods (i.e., adsorption and hydrothermal methods), the XPS spectra showed a nickel peak at 860.4 eV (Ni $2p_{3/2}$ region)

that can be convoluted to different nickel oxidation states (Fig. 4.2). The peak at position 858 eV, and 863 eV corresponds to Ni^{3+} oxidation state and the distinct peaks at positions 852 eV and 860 eV are attributed to the Ni^{2+} oxidation state. Ni salts used ($\text{NiCl}_2 \cdot 6\text{H}_2\text{O}$ or $\text{Ni}(\text{NO}_3)_2 \cdot 6\text{H}_2\text{O}$) are mainly composed by Ni^{2+} ions, which usually result in a larger content of Ni^{2+} on the carbon support rather than other oxidation states when using adsorption (room temperature) or hydrothermal synthesis (~ 150 °C) of nickel.¹⁰⁹ Ni^{3+} ions ($\text{Ni}_{1-\delta}\text{O}$) are likely to appear at higher temperatures (>400 °C) and under oxygen conditions during the thermal decomposition of nickel salts.¹¹⁰ Thus, the atomic concentration of nickel here is likely comprised by Ni^{2+} ions on the AC, which was determined to be 2 at.% (or 8.4 wt.%) on the Ni/AC flow cathode synthesized by the adsorption method (Ni₂/AC) and 4 at.% (or 13 wt.%) synthesized by the hydrothermal method (Ni₄/AC).

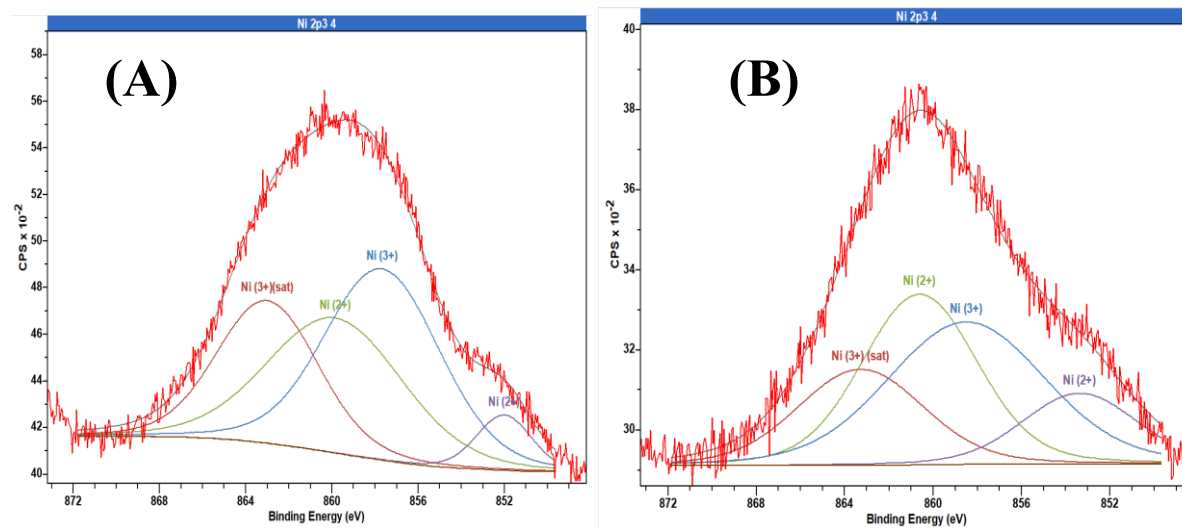


Fig. 4.2. X-ray photoelectron spectroscopy spectra fitting for (A) Ni₄/AC synthesized by hydrothermal method and (B) Ni₂/AC synthesized by adsorption method.

4.3.2. Abiotic electrochemical performances with different Ni/AC loadings.

Ni₂/AC flow cathodes displayed higher catalytic activities with the smaller Ni/AC loadings. For example, Ni₂/AC_{0.125} produced the most positive HER potential of -0.97 V vs. Ag/AgCl at -10 A/m², followed by Ni₂/AC_{0.25} (-1.02 V vs. Ag/AgCl), and similar HER potentials were recorded with Ni₂/AC₅ (-1.06 V vs. Ag/AgCl), and Ni₂/AC₁ (-1.07 V vs. Ag/AgCl) (Fig. 4.3a). These results indicate that the Ni/AC concentration is crucial on HER catalytic activities of Ni/AC flow cathodes, likely showing more positive HER potentials at lower Ni/AC loadings. The Ni/AC loading of Ni₂/AC_{0.125} (or 1.25 g-Ni₂/AC/L) is significantly lower (40 to 80 times) than the AC loadings (5-10 AC-wt.%) usually used in previous fCDI studies.^{61,66,71}

The Ni₂/AC_{0.125} flow cathode also displayed the highest specific current densities (mA/g) in comparison with other Ni₂/AC powder loadings (Fig. 4.3b). The Ni/AC flow cathodes showed a suppressed current density as the concentration of Ni/AC powder increases (Fig. 4.3b). As a result, Ni₂/AC_{0.125} flow cathode showed higher pseudo-capacitive behavior (0.4 F/g) than other Ni/AC concentrations (Ni₂/AC_{0.25}: 0.2 F/g; Ni₂/AC₁: 0.02 F/g; and Ni_{0.5}/AC₅: 0.008 F/g). In comparison to the SS mesh blank, the addition of the smallest Ni₂/AC_{0.125} loading triggered a high specific current density (mA/g) (Fig. 4.4), likely due to the enhanced Faradaic reactions by the Ni catalysts dispersed on the AC. Previous studies showed that Ni catalysts dispersed on carbon materials trigger Faradaic reactions that increase the specific pseudo-capacitances (F/g) and current densities in electrochemical capacitors.¹¹¹⁻¹¹³

We further examined ohmic resistances of Ni/AC flow cathodes under different concentrations. As result, the ohmic resistances of the Ni₂/AC flow cathodes significantly increased (43%, from 0.3 to 0.43 ohms) as the Ni₂/AC concentrations increased from 0.25 (Ni₂/AC_{0.25}) to 1 wt.% (Ni₂/AC₁) (Fig. 4.5). This result indicates that the Ni/AC overloading (>

0.25 wt.%) could outweigh the catalytic effect of Ni catalysts on the AC surface by increasing the ohmic resistances and making the system more resistive as observed in the CV results (Fig. 4.3b). The increment in ohmic resistances at high Ni/AC concentrations could also be attributed to the stagnant Ni/AC powder around the current collector which creates poor particle-particle contact and particle settling.⁶⁸ Also, those stagnant regions in the cathodic chamber could impact the percolating network of AC particles and the diffusive-convective charge transport caused by the Brownian motion of Ni/AC particles.^{114–116} Previous fCDI studies also reported the importance of hydrodynamic behaviors of AC powders, concluding that higher AC powder concentrations will not necessarily promote charge transfer due to the impact of high viscosity.⁶⁶ Ni/AC powder concentrations below 0.125 wt.% were not suitable for recirculation in our system because most of the particles remained attached to the reactor walls and tubing. Pt was used as a benchmark cathode (control) in this study and displayed the highest current densities (Fig. 4.4), likely due to better kinetics towards HER than Ni, but the Pt cathode is costly and not practical for MEC applications at large scales.^{7,117}

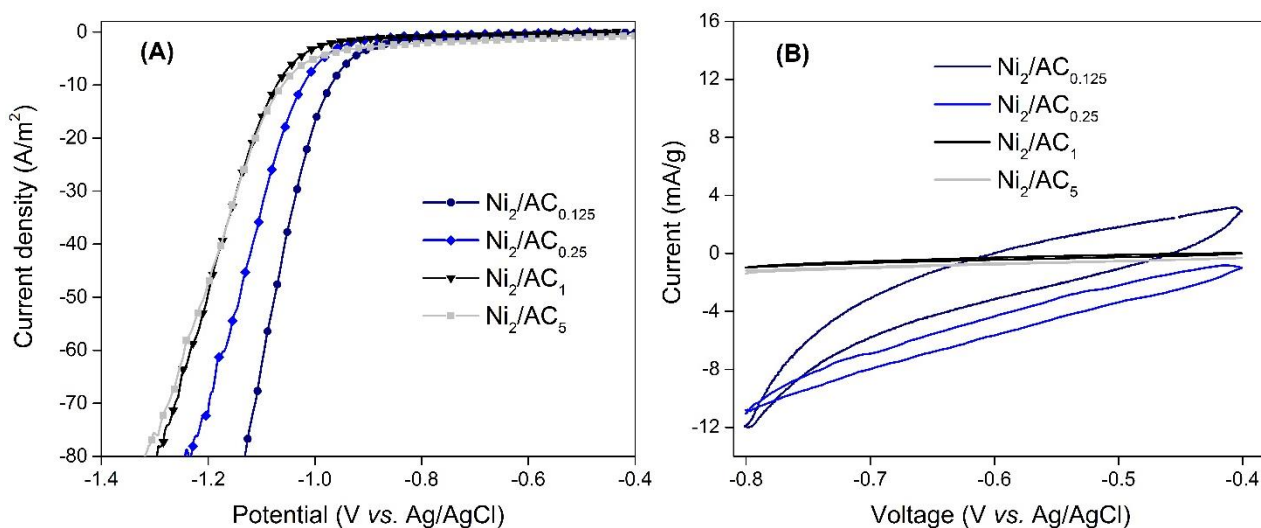


Fig. 4.3. Current-potential curves of Ni/AC flow cathodes at different Ni/AC powder loadings by (A) LSV and (B) CV tests.

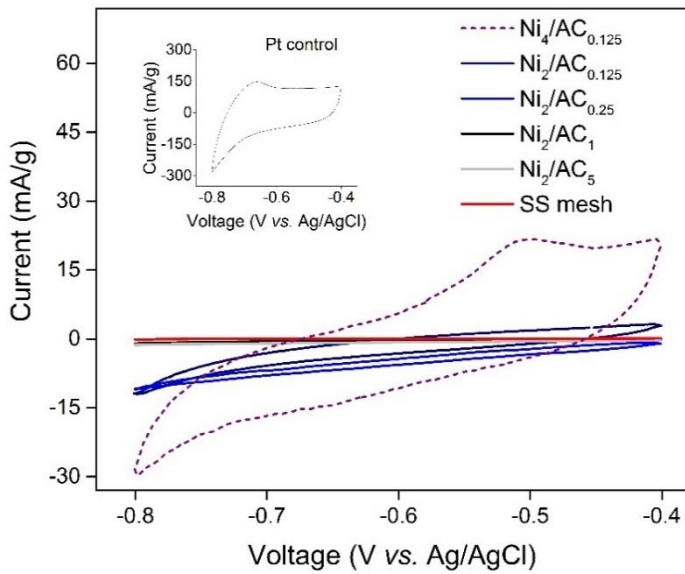


Fig. 4.4. Current-potential curves for Ni/AC flow cathodes, stainless-steel (SS) mesh blank, and Pt control by cyclic voltammetry tests.

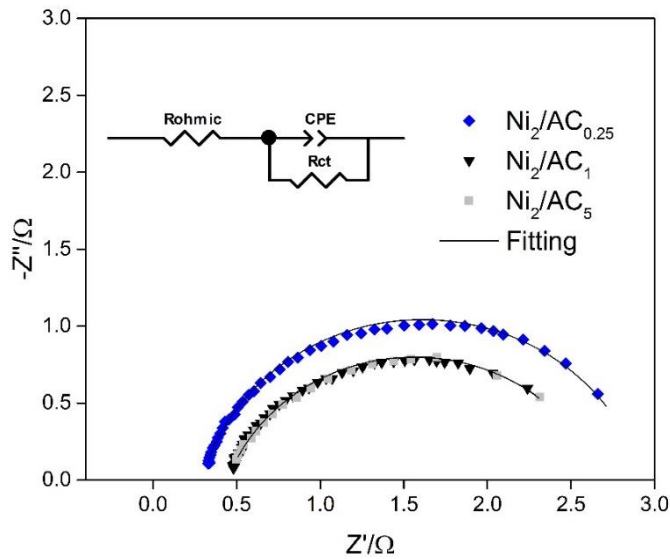


Fig. 4.5. GEIS test for Ni/AC flow cathodes with different Ni₂/AC powders loadings (≥ 0.25 wt.%). The insert figure represents the equivalent circuit model used to fit the spectra.

4.3.3. Impact of different Ni loadings on Ni/AC flow cathode.

The Ni/AC flow cathode with increased Ni content (4 at.%, Ni₄/AC_{0.125}) produced a more positive potential at all current densities in comparison with that with a lower Ni content (2 at.%, Ni₂/AC_{0.125}) under the same Ni/AC concentration (Fig. 4.6a). For example, Ni₄/AC_{0.125} showed -0.86 V vs. Ag/AgCl at -10 A/m², followed by Ni₂/AC_{0.125} (-0.97 V vs. Ag/AgCl) and the SS mesh blank (-0.98 V vs. Ag/AgCl). As expected, the Pt control displayed the most positive HER potentials at -10 A/m² (-0.64 V vs. Ag/AgCl). These results indicate that increasing Ni content on the AC surface can improve catalytic activities towards HER, or Faradaic reactions of Ni/AC flow cathodes. GEIS spectra showed 31% lower charge transfer resistances (R_{ct}) for the Ni₄/AC_{0.125} flow cathode (R_{ct} = 1.8 Ω) in comparison with Ni₂/AC_{0.125} (R_{ct} = 2.6 Ω) (Fig. 4.6b). Similarly, the ohmic resistance was reduced from 0.38 Ω (Ni₂/AC_{0.125}) to 0.25 Ω (Ni₄/AC_{0.125}). Thus, the improved HER catalytic activities of Ni/AC flow cathodes with greater Ni content are likely attributed to significant reductions in charge transfer (31%) and ohmic resistances (34%) of the Ni/AC flow cathode. In addition, the R_{ct} of the Pt control (R_{ct} = 1.8 Ω) is comparable to that of the Ni₄/AC_{0.125}, suggesting a comparable charge transfer kinetics of Ni/AC cathodes to Pt control. The SS mesh blank displayed an ohmic resistance of 0.41 Ω, and charge transfer resistance of 2.1 Ω, which are higher than those of the Ni₄/AC_{0.125} flow cathode, indicating the addition of Ni₄/AC_{0.125} powders has promoted the electrochemical activities on the cathode side. Ni₄/AC_{0.125} displayed significantly higher current densities than the SS mesh blank and other flow cathodes, which produced a peak value of pseudo-capacitance (1.6 F/g) (Fig. 4.4).

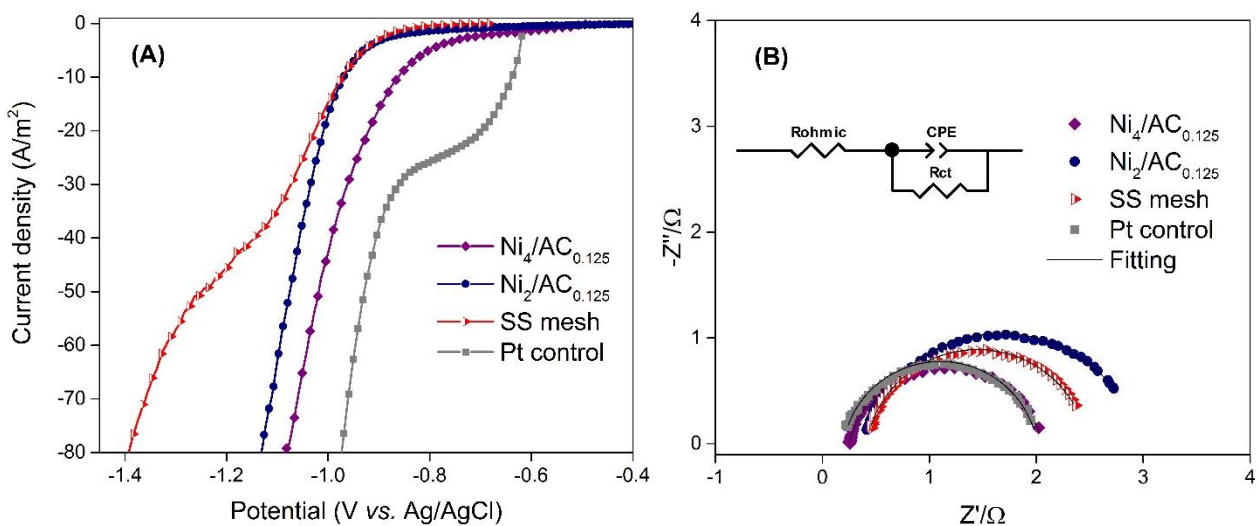


Fig. 4.6. Abiotic electrochemical characterization of Ni/AC flow cathodes with different Ni content (2 and 4 Ni-at.%), compared to SS mesh blank and Pt control. (A) current-potential curve by LSV and (B) GEIS tests, the inserted figure represents the equivalent circuit model used to fit the spectra.

Ni/AC catalyst displayed an oxidation peak occurring at 0.06 V coupled with a reduction peak at -0.24 V (vs. Ag/AgCl) (Fig. A 3). This redox pair is likely attributed to the complete oxidation of Ni (II)/Ni and the reversible Ni/Ni (II) reaction since other oxidation states (i.e., Ni^{3+}) have been observed at much higher oxidation potentials (~ 1.67 V vs. Ag/AgCl for oxidation pair Ni (II)/Ni (III)).¹¹⁸ The reduced nickel particles likely precipitate in the catholyte and result in Ni losses from the AC surface. Similar Ni losses have been previously examined in Ni/AC solid-type cathodes to be around 4.4% of the cathode weight over several cycles, which eventually results in the need for cathode replacement. However, in the flow cathode system, this nickel detachment from the AC surface might not be critical since AC and Ni particles are continuously recirculated in the system and detached nickel particles can still participate in the reaction during random collisions with the current collector and other AC particles.

4.3.4. MEC performances with Ni/AC flow cathodes at 4 h cycle.

Based on the abiotic electrochemical test results, a Ni/AC loading of 0.125 wt.% was selected for MEC tests. The Ni₄/AC_{0.125} flow cathode displayed hydrogen production rates of 1.62±0.15 L-H₂/L-d, which were 26% higher than the MEC with Ni₂/AC_{0.125} (1.29±0.06 L-H₂/L-d) with lower Ni loading (Fig. 4.7a). The MEC with Ni₄/AC_{0.125} produced comparable hydrogen production rates to the Pt control cathode (1.64±0.09 L-H₂/L-d) with no significant differences (student *t*-test: *p* > 0.05), and 40% higher hydrogen production rates than SS mesh blank (1.29±0.02 L-H₂/L-d, without Ni/AC powders). The MEC with Ni₄/AC_{0.125} produced higher average current densities ($I_{avg,90}$, 7.7±0.8 A/m²) than the MEC with Ni₂/AC_{0.125} (6.6±0.8 A/m²) (Fig. 4.7a). Ni₄/AC_{0.125} produced slightly lower average current densities than the Pt control (8.3±0.4 A/m²), likely due to the lower ohmic resistance (20%) of the Pt than Ni₄/AC_{0.125} (Fig. 4.6b). The hydrogen production rates achieved here with the Ni₄/AC_{0.125} flow cathode were 5 times higher than those previously reported with solid-type Ni/AC cathodes (0.35±0.02 L-H₂/L) in a similar two-chamber MEC configuration,^{3,11} but lower than those obtained in a different MEC configuration with a vapor catholyte and a Pt/C cathode (72±2 L-H₂/L-d).³¹ Although the recent MEC study produced record-high hydrogen production rates in MECs, the use of Pt catalyst is not practical and running vapor catholyte in a larger-scale reactor is still unclear.

Higher hydrogen production rates by Ni₄/AC_{0.125} with greater Ni content are consistent with the abiotic test results, showing lower overpotential, lower ohmic (34%), and charge transfer resistances (31%) with a greater Ni loading. The greater amount of Ni catalysts on the AC surface implies a greater AC surface coverage that likely helps to improve the direct electron transfer (DET) from the current collector to the suspended Ni/AC particles. In the Ni/AC flow cathode system, Ni/AC particles are not bonded to the current collector. Thus, the catalysts connection

relies on the random collision of the Ni/AC particles with the current collector and Ni/AC particles themselves. This characteristic is intrinsically different from the one in typical solid-type electrodes, such as the Pt control, where the catalyst particles are fixed to the current collector, likely resulting in lower ohmic resistances. $\text{Ni}_4/\text{AC}_{0.125}$ flow cathode and Pt control displayed comparable charge transfer resistances (Pt control, $R_{\text{ct}} = 1.8 \Omega$, $\text{Ni}_4/\text{AC}_{0.125}$, $R_{\text{ct}} = 1.8 \Omega$), indicating that electrons are being transferred towards HER at comparable rates, even with greater HER catalytic activities of Pt than Ni/AC (Fig. 4.6a). The direct electron transfer mechanisms in flow electrodes allow the electroactive surface area to be expanded across the reactor volume rather than limited to the size of the current collector.⁵⁷ Thus, it is suggested that comparable hydrogen production rates by $\text{Ni}_4/\text{AC}_{0.125}$ to the Pt control are likely due to an extended electroactive area across the cathode chamber volume. The impacts of current collectors (materials, shapes, surface areas, etc.) on the catalytic activities of Ni/AC flow cathodes are beyond the scope of this study. However, it is believed that the intrinsic charge transfer resistance between the given current collector and Ni/AC powders and the electrical conductivity of the current collector material could play an important role in the electron transfer mechanism in Ni/AC flow cathodes.

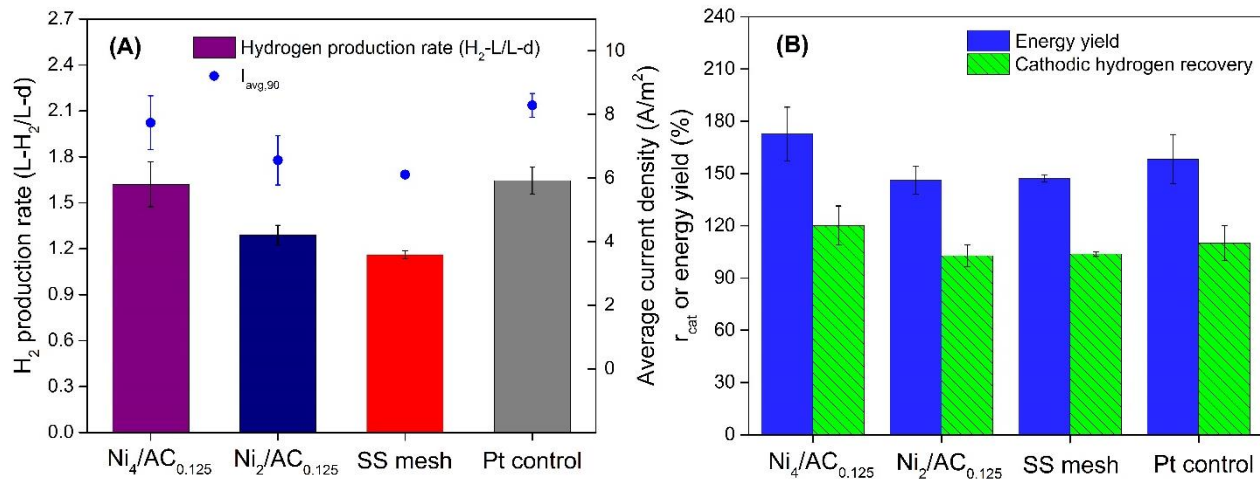


Fig. 4.7. MEC test results with Ni/AC flow cathodes, compared to SS mesh blank and Pt control at 4 h cycles. (A) Hydrogen production rates normalized by the reactor volume and cycle time (L-H₂/L-day) and average current densities represented as I_{avg,90}. (B) Cathodic hydrogen recovery (%), r_{cat}) and energy yield (%), ηE). Error bars indicate mean ± standard deviation (n ≥ 3).

The MEC with Ni₄/AC_{0.125} showed the highest average energy yield (ηE , 173±15%) among all other cathodes tested at 4 h cycle, followed by Pt control (158±14%), SS mesh blank (147±2%), and Ni₂/AC_{0.125} (146±8%) (Fig. 4.7b). Cathodic hydrogen recoveries (r_{cat}) were nearly 100% for all cathodes tested, (120±11% for Ni₄/AC_{0.125}, 110±10% for Pt control, 104±1% for SS mesh blank, and 103±6% for Ni₂/AC_{0.125}) (Fig. 4.7b). These results indicate that cathodic recoveries were approaching to 100% in all cathodes.⁷

4.3.5. MEC performances with Ni/AC flow cathodes at 24 h cycle.

All MECs with tested cathodes operated at 24 h cycle demonstrated lower hydrogen production rates than those at a shorter (4 h) cycle time. For example, the hydrogen production rates were 0.96±0.08 L-H₂/L-d for Ni₄/AC_{0.125}, 0.70±0.09 L-H₂/L-d for Ni₂/AC_{0.125}, 0.41±0.11 L-H₂/L-d for SS mesh blank, and 1.09±0.1 L-H₂/L-d for the Pt control (Fig. 4.8a), which were 41% for Ni₄/AC_{0.125}, 34% for Pt control, 46% for Ni₂/AC_{0.125}, and 65% for SS mesh lower than those at 4 h cycle. The prolonged operation also impacted the average current densities, which decreased by 36% for Ni₄/AC_{0.125} (4.9±0.5 A/m²), 23% for the Pt control (6.4±0.5 A/m²), 27% for Ni₂/AC_{0.125} (4.9±0.3 A/m²), and 43% for the SS mesh blank (3.5±0.1 A/m²) in comparison with the shorter 4h cycles. Current densities with Ni₄/AC_{0.125} and Ni₂/AC_{0.125} remained higher than with the SS mesh blank until the end of the cycles, and Ni₄/AC_{0.125} produced comparable current densities to Pt after

peak values until the end of the cycle (Fig. 4.9c). Previous MEC studies where tested in a semi-batch mode have reported peak values of current density in the first 5 h of operation and decreasing over time (24 h), likely associated with the anodic substrate depletion and changes in catholyte pH.^{7,8} However, the impact of substrate depletion in this study was not crucial since the synthetic wastewater with a high substrate concentration and volume (1 g/L sodium acetate in 50 mM PBS in a closed-loop batch, 150 mL) was recirculated to minimize the impacts by anodic reactions.

The catholyte pH values of 12 were measured at the end of the 24 h cycles for Ni₄/AC_{0.125}, Ni₂/AC_{0.125}, and Pt control, while slightly lower catholyte pH values (11.4±0.1) were measured for the SS mesh blank. The catholyte pH increases over time due to a continuous proton (H⁺) consumption by HER.⁷ Previous HER studies have suggested that the H-binding energy largely increases (resulting in lower HER) under alkaline conditions due to the OH⁻ adsorption on the HER catalytic active sites.^{119–121} With Ni/AC flow cathodes, it is still unclear how to obtain Tafel slopes without the interference or dominant contribution of the current collector, but other studies using solid-type Ni/AC cathodes obtained Tafel slope values (136 mV/dec) which have suggested a Volmer-Heyrovsky HER mechanism on Ni/AC catalysts.⁸ The increase in catholyte pH likely promotes an unbalanced Volmer step relative to the Heyrovsky step with greater hydrogen surface coverage that might have resulted in a reduction in current densities (and HER catalytic activities) with Ni₄/AC_{0.125} over 24 cycles.^{8,35} However, the current densities with Ni₄/AC_{0.125} remained comparable to those with Pt until the end of the cycle, indicating Ni/AC flow cathodes were less impacted by the changes in catholyte pH than other electrodes.

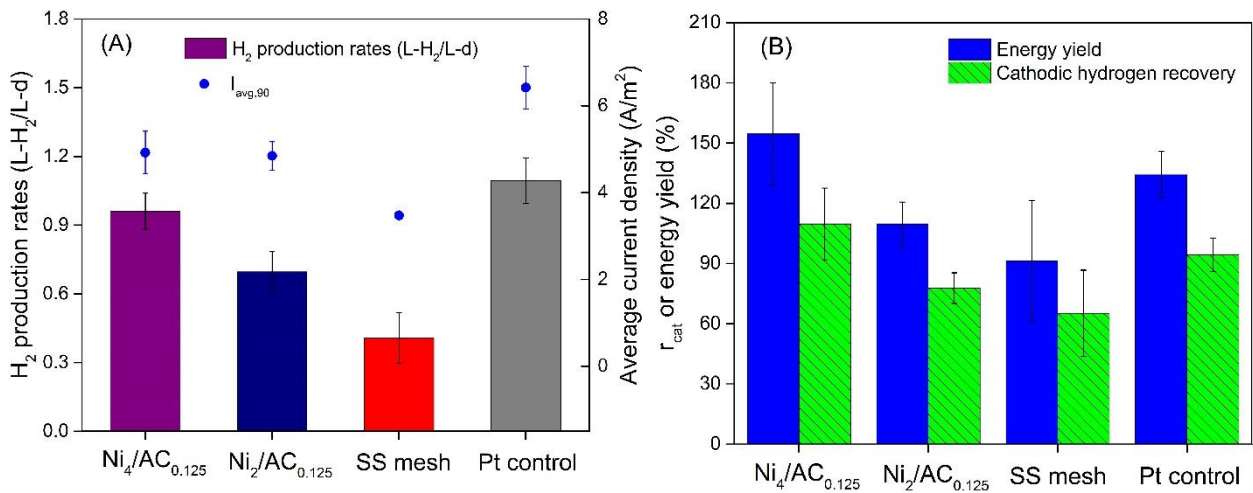


Fig. 4.8. MEC test results with Ni/AC flow cathodes, compared to SS mesh blank and Pt control at 24 h cycles. (A) Hydrogen production rates normalized by the reactor volume and cycle time ($L\text{-}H_2/L\text{-day}$) and average current densities represented as $I_{avg,90}$. (B) Cathodic hydrogen recovery (%, r_{cat}) and energy yield (%, ηE). Error bars indicate mean \pm standard deviation ($n \geq 3$).

$Ni_4/AC_{0.125}$ flow-cathodes displayed higher energy yields (ηE : $155 \pm 25\%$), and cathodic hydrogen recoveries (r_{cat} : $110 \pm 18\%$) than the $Ni_2/AC_{0.125}$ (ηE : $110 \pm 11\%$; r_{cat} : $78 \pm 8\%$), Pt control (ηE : $134 \pm 12\%$; r_{cat} : $94 \pm 8\%$), and SS mesh blank (ηE : $91 \pm 30\%$; r_{cat} : $65 \pm 21\%$) (Fig. 4.8). These values were lower than those obtained at 4 h cycle. However, the results still show that the presence of AC powder with increased content of Ni helps to sustain the hydrogen production over a prolonged operational condition (24 h).

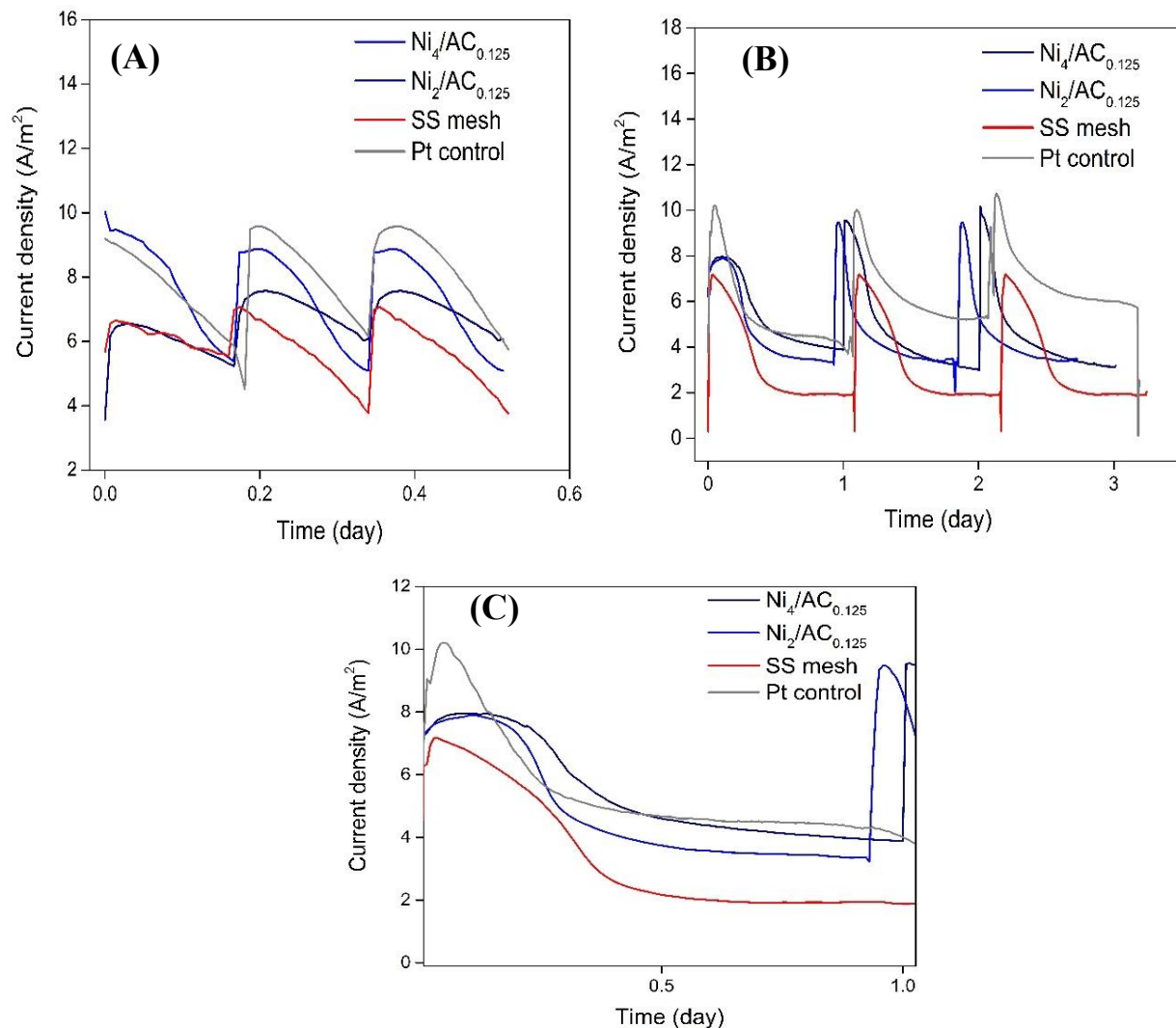


Fig. 4.9. Current generations over the cycles in MECs with Ni/AC flow cathodes, SS mesh blank, and Pt control. (A) current generations at 4 h cycle, (B) current generations at 24 h cycle, and (C) current generations for a single cycle over 24 h.

4.3.6. Impact of carbon black on the Ni/AC flow cathode.

The Ni/AC flow cathodes ($\text{Ni}_2/\text{AC}_{0.125}$) amended with CB concentrations of 0.06 wt.% ($\text{Ni}_2/\text{AC}_{0.125}/\text{CB}_{0.06}$) and 0.25 wt.% ($\text{Ni}_2/\text{AC}_{0.125}/\text{CB}_{0.25}$) showed slightly more negative potential

values (-0.98 V vs. Ag/AgCl for $\text{Ni}_2/\text{AC}_{0.125}/\text{CB}_{0.06}$, and -1 V vs. Ag/AgCl for $\text{Ni}_{0.5}/\text{AC}_{0.125}/\text{CB}_{0.25}$) at -10 A/m^2 than the Ni/AC flow cathode without CB (-0.97 V vs. Ag/AgCl for $\text{Ni}_2/\text{AC}_{0.125}$) (Fig. 4.11). In MECs, $\text{Ni}_2/\text{AC}_{0.125}/\text{CB}_{0.06}$ produced 10% higher H_2 production rates ($1.42 \pm 0.01 \text{ L-H}_2/\text{L-d}$) than $\text{Ni}_2/\text{AC}_{0.125}$ ($1.29 \pm 0.06 \text{ L-H}_2/\text{L-d}$). However, H_2 production rates were decreased as CB loadings increased from 0.13 to 0.25 wt.% (Fig. 4.10a). The average current densities were not significantly affected by CB blending but CB blending higher than 0.13 wt.% adversely impacted on cathodic hydrogen recoveries and energy yields corresponding with the lower hydrogen production rates (Fig. 4.10b).

CB itself is not a good catalyst for HER, but CB blending with flowable electrodes usually enhances the charge transport efficiency (e.g., in fCDI) by improving the frequency of collisions between active particles and the electron transfer kinetics between AC flowable particles and the current collector.^{58,70,71} The lowest concentration of CB (0.06 wt.%) likely promoted the random Brownian motion in the flowable electrode and enhanced the particle-particle interactions,^{66,71} resulting in slightly higher H_2 production rates than the flow cathode without CB ($\text{Ni}_2/\text{AC}_{0.125}$). However, CB overloading (>0.13 wt.%) to the Ni/AC flow cathode led to stagnant powders and particle settling, which likely yielded a resistive behavior that was also observed with Ni/AC overloading. Consequently, HER potentials were shifted to more negative values (Fig. 4.11) and resulted in the reduction of hydrogen production rates (Fig. 4.10a). Other factors might have contributed to the lower performance at higher CB loadings, including a parasitic mechanism such as electron transfer to the CB electrical double layer rather than towards HER.

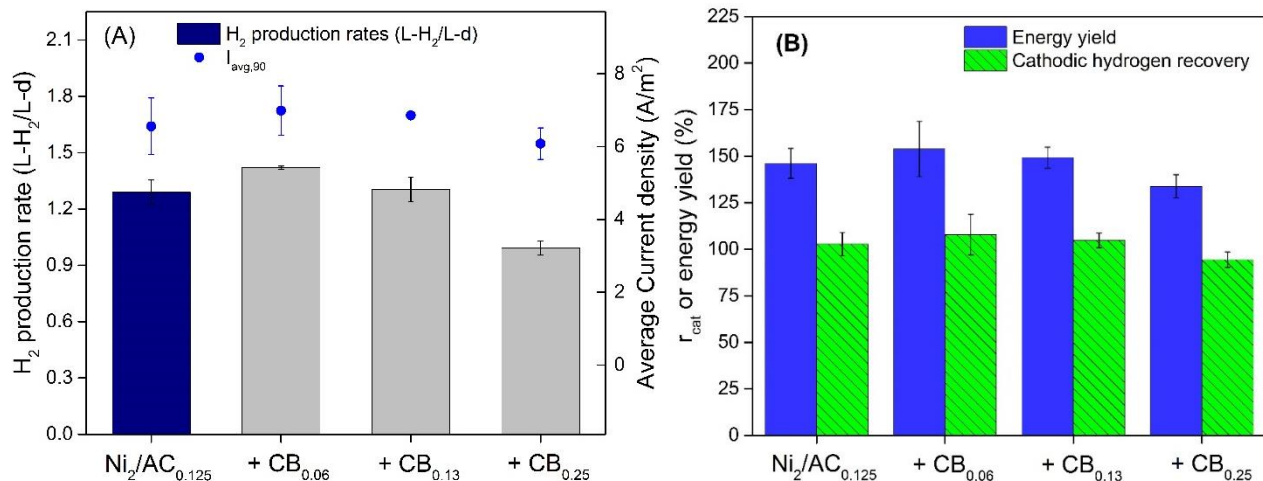


Fig. 4.10. Impact of carbon blank as an additive in flow cathodes at 4 h cycles. (A) Hydrogen production rates normalized by the reactor volume and cycle time ($L-H_2/L\text{-day}$) and average current densities represented as $I_{avg,90}$. (B) Cathodic hydrogen recovery (%), r_{cat} and energy yield (%). Error bars indicate mean \pm standard deviation ($n \geq 3$).

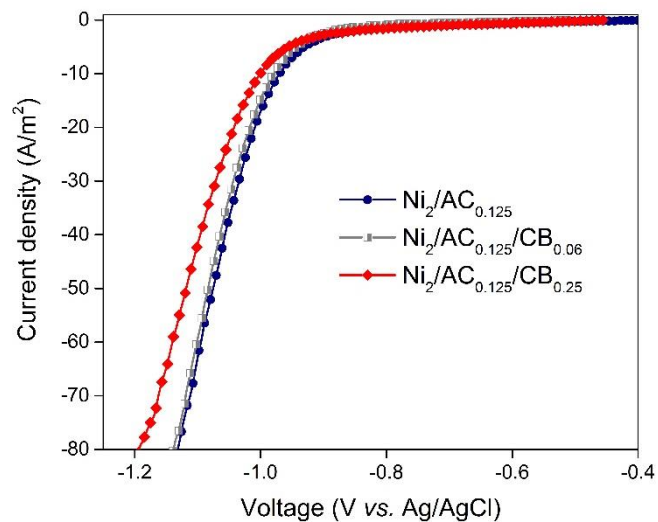


Fig. 4.11. Abiotic electrochemical characterization of $Ni_2/AC_{0.125}$ flow cathodes amended with carbon black by LSV.

4.4.Perspectives on the Ni/AC flow cathode application in MECs for hydrogen production.

Ni/AC flow cathodes offer more benefits in electrochemical activities than conventional solid-type cathodes by providing a larger catalytic surface area by dispersing Ni/AC particles. Ni/AC flow cathodes demonstrated 5 times higher hydrogen production rates than previous solid-type Ni/AC cathodes and comparable to Pt control under the same conditions.^{7,8} The result suggests the potential improvement in catalytic activities by applying flow-type cathodes with optimized Ni catalyst loadings and Ni/AC concentrations. Although our present study demonstrated the highest HER performances with the lowest Ni/AC loadings (i.e., 0.125 wt.%), the adverse impacts of Ni/AC or CB overloading might be able to overcome by increasing Ni loadings on AC that resulted in improved HER activities in this study. Also, in terms of economical perspectives, manufacturing steps and replacement are not required for Ni/AC flow cathodes which will be beneficial to reducing mass production and maintenance costs. Since one of the biggest challenges for the practical application of MECs lies in scale-up, such advantages of Ni/AC flow cathode will leverage to break through the current barriers.

More future flowable electrode studies for HER are still required to fully understand the underlying electron transfer mechanisms and optimize the operational parameters. For example, one previous study suggested that the electrochemical performance of flow electrodes for capacitive deionization is affected by the flow dynamics of the suspended AC particles and the composition of the supporting catholyte.⁶⁶ In addition, Ni/AC flow cathodes demonstrated reduced hydrogen production rates over a prolonged operation (24 h) due to the increased catholyte pH over time. Therefore, suitable cathode chamber designs to promote the flow dynamics and new catalyst designs with potential adaptability at different pHs should be addressed in future flow cathode studies. For example, bifunctional catalysts such as NiMo could be used to overcome the

sluggish kinetics of HER in alkaline media.¹⁰⁹ Finally, the role of the current collector (shapes and materials) in the direct electron transfer mechanism across the flow cathode system for HER needs to be explored although different current collector materials have been previously examined for anodic oxidation with flow electrodes.⁷¹

CHAPTER 5.

Flowable Ni-loaded activated carbon cathode coupled with different current collectors

The information in this chapter is adapted from Daniel A. Moreno-Jimenez, and Kyoung-Yeol Kim (2023). Impact of different current collectors on a nickel-loaded activated carbon flow cathode for hydrogen production in microbial electrolysis cells. *Manuscript in preparation.*

5.1. Introduction

Microbial electrolysis Cells (MECs) are electrochemical devices that can oxidize organic matter using bioanodes and generate electrons to assist the hydrogen evolution reaction (HER) at the cathode.⁵ MECs require lower applied potentials (<1.2 V) to overcome the thermodynamic barrier of the HER compared to the conventional water electrolysis (>1.8 V), due to the possible utilization of the embedded energy in organic substrates. Although MECs are highly attractive to integrate the hydrogen economy into the next generation of wastewater treatment and resource recovery facilities, still there are challenges for the applications of MECs at large scale, mainly related to the cathodes side. Pt is the top reference for HER electroactivity and commonly used in MEC cathodes, however, it is not practical for applications in MECs at all scales.

In pioneer studies, a nickel (Ni) foam cathode enabled high hydrogen production rates in MECs, although the performance declined over time, it demonstrated the feasibility of using nickel as an economic-competitive option to fully replace Pt in MECs.⁴⁵ More recent studies were focused on resolving nickel metal stability issues. For example, instead of Ni foam, nickel powders were bonded with Nafion® binder on a current collector.⁴⁴ The resulted Ni powder stationary cathode

produced comparable hydrogen production rates than a Pt cathode, but the use of Ni powders led to metal dissolution in the catholyte, suggesting a catalyst mass loss, which could result in a detrimental performance over time. A more recent study addressed this issue by loading nickel salts on activated carbon (AC) through a simple adsorption method.⁷ AC is not active for HER but it provides an excellent supporting-conductive phase and a very large surface area ($2500\text{ m}^2/\text{g}$), which is beneficial to disperse Ni salts.⁵⁰ The Ni-functionalized AC (Ni/AC) powders were bonded with polyvinylidene fluoride (PVDF) binder onto a current collector (stainless-steel mesh), followed by a phase inversion fabrication process. The new Ni/AC stationary cathode demonstrated higher hydrogen production rates than Pt/C cathode and comparable hydrogen production rates ($1.1 \pm 0.1\text{ L-H}_2/\text{L-d}$) to commercialized Ni foam (Ni content: 50 mg-Ni/cm^2) even with 82% less amount of Ni used (8.8 mg-Ni/cm^2). Thus, other studies have been focused on improving the performance of Ni/AC stationary cathode. For example, the AC surface was acid-treated (t-AC) to enhance its wettability properties and then used to manufacture the Ni/AC cathode. The resulted t-AC/Ni, with enhanced surface wettability, produced 84% higher hydrogen production rates than the blank (Ni/AC fabricated with pristine AC).⁸ Although the study suggested that variations in the binder loading impact significantly the performance of Ni/AC stationary cathodes. Thus, it is concerning how binder agents will restrain the performance of cathodes at a large scale. To overcome this drawback, our recent study (CHAPTER 4) introduced a Ni/AC flow electrode as a novel binder-free cathode, which is easy to fabricate and flexible to integrate in MECs at all scales. Ni/AC powders were suspended in a supporting catholyte (plain phosphate buffer solution) and used as cathode without any further cathode manufacturing methods. The novel flow cathode demonstrated to produce comparable hydrogen production rates

(1.62 ± 0.15 L-H₂/L_{reactor-d}) than the Pt cathode (1.64 ± 0.09 L-H₂/L-d), and almost 5 times higher hydrogen production rates than pioneer Ni/AC stationary cathodes.^{7,8}

To optimize the performance of novel flow cathodes, a greater understanding is needed regarding the contribution of the flowable powders on the HER activity and the role of the current collector as a coupled non-stationary system. Flowable electrodes consist of active particles suspended in a supporting electrolyte, where a dynamic percolating three-dimensional network is formed to transport electric charge between the current collector and the flowable particles.^{122,123}. Even when the collector is a crucial component, the interfacial engineering between current collectors and the flowable electrode is often neglected and only a few studies have examined the impact of different collector materials.¹²⁴ For example, the recent study utilized an anodic flow electrode based on Ti_xO_{2x-1} and carbon black particles coupled with different current collectors (IrRu, IrTa, Pt and Ti) to generate hydroxyl radicals (OH·). The study demonstrate that the use of different current collector change the direct electron transfer (DET) rate in the flow electrode system, which were dependent on the intrinsic resistance to the charge transfer of the different materials.⁷¹ In addition, the chemical stability of the current collector is important to maintain the reaction rate over time. The current collector shape and area plays an important role in the flow electrode. In a previous study, the surface area of the current collector was reduced by 23% by covering the collector with an insulation layer, the reduced collector area resulted in a relative drop in the slurry conductivity.¹²⁵ Thus, enlarging the collector contact area likely enhances the charge transfer by improving the contact time of particles with the charge feeder or collector material, as well as increasing the number of collisions with the flowable network.¹²⁶ It has been suggested that the potential drops with the distance from the current collector to the bulk flow electrode.¹²⁷ This effect will likely induce different potentials with the distance from the working electrode,

which might result in different reaction rates across complete network volume of suspended particles.¹²⁸ Thus, it is crucial to elucidate the impact of different current collectors in the voltage drop across the flow cathode and the contribution of different surface-collector properties, such as resistivity and catalytic activities toward HER to decide which is likely the best coupling material to enhance the overall hydrogen production rates in MEC using the novel flow cathodes.

In the study, flow cathodes were prepared with Ni/AC powders and coupled with different current collectors (nickel foam, nickel mesh, stainless-steel mesh, and titanium). The abiotic electrochemical characterization was conducted in plain phosphate buffer solution (blank) and with flow cathodes added to elucidate the individual contribution of collector materials and flowable powders in the charge transferred toward HER. The voltage drop across the bulk catholyte was measured using a probe 2 cm far from the collector surface to examine if different collector materials induce different potentials in the flowable network and without flow cathode (blank tests). Finally, the hydrogen production rates, current densities, energy yields and cathodic hydrogen recoveries were examined in MECs using flow cathodes coupled with Ti and Ni foam current collectors.

5.2. Materials and methods

5.2.1. Ni loaded on AC particles.

Ni/AC catalyst powders were synthesized by hydrothermal method using a similar procedure previously described in chapter 4. The amount of Ni loaded on the AC was calculated using X-ray photoelectron spectroscopy (XPS) analysis. The resulted Ni content is expressed as Ni atomic ratio (Ni, at.%) on the AC surface. Ni/AC catalysts powders contained 4% Ni atomic ratio on the AC surface (see CHAPTER 4).

5.2.2. Ni/AC flow cathode preparation.

The prepared Ni/AC catalyst powders (0.05 g) were added to a 40 mL supporting catholyte composed by plain PBS. A semicircular pieces (6.84 cm^2) of stainless-steel mesh (type 304, 50×50 mesh, 30% open area, 0.23 mm wire diameter, McMaster-Carr, USA), Ni cloth (400 nickel cloth, 50×50 mesh, 30% open area, 0.23 mm wire diameter, McMaster-Carr, USA), titanium sheet (ultra-corrosion resistant grade 2, 0.5 mm thickness, McMaster-Carr, USA), and Ni foam ($128\text{ m}^2/\text{m}^2$ projected area,⁴⁵ 0.3 mm thickness, MTI corporation, CA, USA.) were used as cathodic current collectors.

5.2.3. Abiotic electrochemical tests.

The electrochemical characterization was conducted in a two-chamber polycarbonate cell separated by an anion exchange membrane (AEM, Fumasep® Fuel Cell Store, USA). A potentiostat (VSP, Biologic science instruments, USA) was used to perform linear sweep voltammetry (LSV), and chronoamperometry (CA) tests in a 3-electrode cell configuration with the working electrode tip connected to the cathodic current collector (SS mesh, Ti, Ni mesh or Ni foam), Ag/AgCl was used as a reference electrode (model RE-5B, BASi, IN, USA), and SS mesh as a counter electrode. In addition, to measure the voltage induced to the bulk catholyte, the open circuit potential (OCP) was measured between a Ti probe located at 1 cm from the reference electrode and 2 cm from the working electrode (Fig. 5.1) while simultaneously running a CA test at different working electrode potentials (-0.7 , -0.8 , -0.9 , -1 , and -1.1 V vs. Ag/AgCl) using 5 min voltage steps. The ohmic resistance with different correct collectors in the assembled abiotic cell was measured using a 3-electrode configuration and electrochemical impedance spectroscopy (EIS) performed at OCP using a frequency range between 30 kHz to 5 Hz and a 5 mV signal amplitude. In all cases, the working electrode was connected to the different current collectors (Ni

foam, Ni mesh, SS mesh, or Ti) in contact with plain PBS. The LSV tests were recorded using a scan rate of 5 mV/sec from OCP to -1.4 V vs. Ag/AgCl. After triplicate LSV scans, the 3rd scan was taken for comparison with other working electrodes. In the working electrode chamber, 40 mL of the Ni/AC flow cathode or 40 mL of plain 50 mM PBS (no powders added) were recirculated at 20 mL/min (hydraulic retention time, HRT=42 sec), which was the minimum flow rate found to maintain the Ni/AC particles continuously recirculating in the closed-loop system without severe accumulation in the cathodic chamber. Although much higher flow rates were not tested, those might not be beneficial since the particle collision frequency is affected by the particle velocity in a flow through parallel configuration.¹²³ In the anode chamber, a 50 mM PBS (80 mL) was used and operated as previously described (see CHAPTER 4).

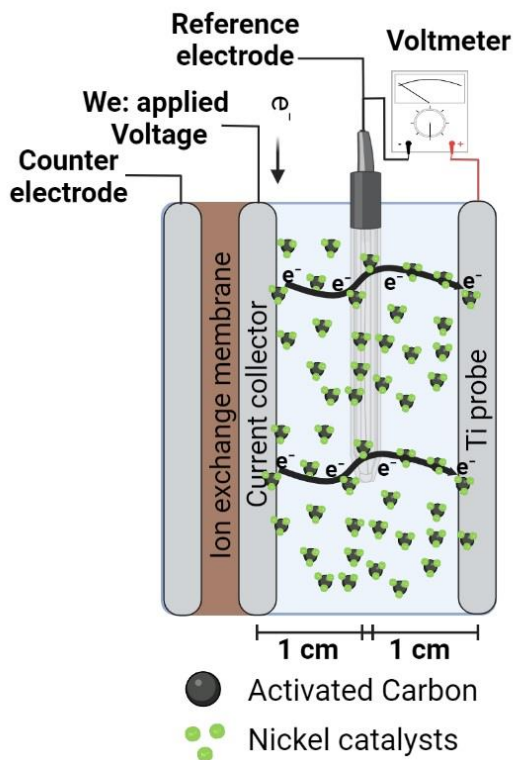


Fig. 5.1. Schematic representation of the abiotic cell used for electrochemical characterization. The working electrode (We) is connected to the different current collectors tested (SS mesh, Ni mesh, Ti or Ni foam).

5.2.4. MEC reactor setup and operation.

MECs were assembled as previously (see chapter 4). In the cathodic chamber, flow cathodes were in contact with the current collector (Ti or Ni foam) and under continuous recirculation (20 mL/min, HRT=12.6 sec) forced by the peristaltic pump. The hydrogen gas produced was dragged out from the cathodic chamber by the liquid flow and stored in the glass reservoir headspace and in a gas collection bag (Fig. 5.2). In the anodic chamber (4 cm long, 3 cm diameter, 28 mL working volume), synthetic wastewater (containing in 1 L DI water, sodium acetate: 1 g/L; Na₂HPO₄: 4.58 g/L; NaH₂PO₄: 2.13 g/L; KCl: 0.13 g/L; NH₄Cl: 0.31 g/L; and amended with trace mineral solution: 12.5 mL; and vitamin solution: 5 mL) was continuously recirculated at 2 mL/min (HRT=14 min), and MECs were running over 4 h cycles, in a triplicate test, to examine hydrogen production rates at the peak of current densities, which usually are stable over the first 5 hours of the MEC operation.⁸ Before each cycle, the anolyte reservoir was replenished with fresh synthetic wastewater (150 mL) the pH of the flow cathode was adjusted to 7 using HCl (1M) solution added dropwise. The dissolved oxygen in the catholyte solution (flow cathode) was removed using an Ar gas sparging needle.

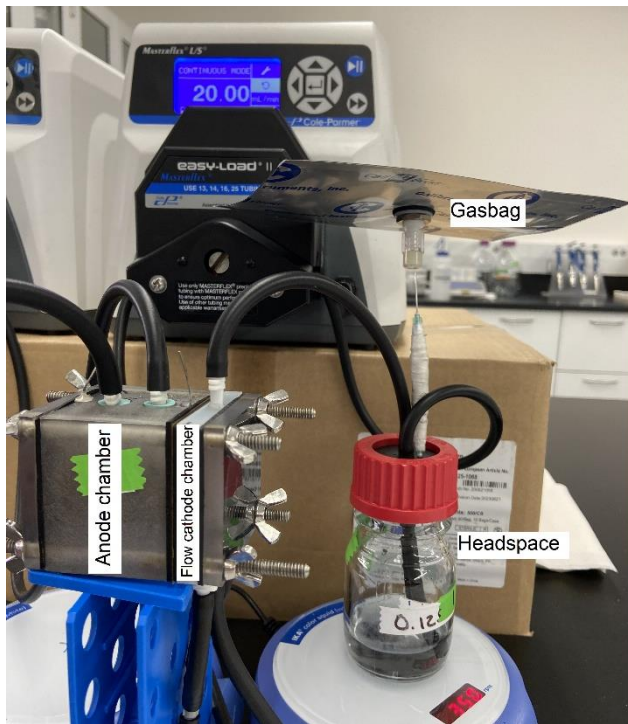


Fig. 5.2. MEC reactor and experimental setup.

5.2.5. Analytical methods and calculation.

The charge transferred toward HER was calculated from the abiotic LSV scans (using the third scan in a triplicate test) with different current collectors in contact with plain PBS (blank, no powders added), and in contact with the flow cathode, by integrating the current over time within the potential window from OCP to -1 V (vs. Ag/AgCl) ($Q = \int_0^t at^{-1}V idt$). It is assumed that the fraction of charge transferred to the flowable powders ($Q_{t\text{-flow}} = (Q_{\text{flow+CC}} - Q_{\text{blank}})/Q_{\text{flow+CC}}$) is the relative difference between the charge produced by the flow cathode coupled with the current collector ($Q_{\text{flow+CC}}$) and the charge produced by the current collector (blank) itself (Q_{blank}). The ohmic resistances of the different current collectors were calculated utilizing the intercept of the high-frequency impedance with the real axis. The ohmic resistance values were normalized by the

electrode projected area (5.54 cm^2). Hydrogen gases collected in both the gas collection bag and the headspace of the glass reservoir were analyzed using a gas chromatograph (Model 8610C, SRI Instruments Inc., USA). Hydrogen production rates, average current densities, cathodic hydrogen recovery, energy yield and XPS were calculated as previously described in CHAPTER 4.

5.3. Results and discussion.

5.3.1. Characterization of Ni/AC catalyst powders.

Ni/AC catalysts prepared using a hydrothermal method showed a nickel peak at 859.6 eV ($\text{Ni } 2\text{p}_{3/2}$ region) in the XPS spectrum that was deconvoluted to different nickel oxidation states (Fig. 4.2a). The peaks at positions 863 eV and 857.9 eV correspond to Ni^{3+} oxidation state and the different peaks at positions 852 eV and 860 eV correspond to the Ni^{2+} oxidation state. The overall atomic concentration of nickel comprises 4 atomic percent (at.%) (or 13 wt.%) of nickel loaded on the AC powders.

5.3.2. Electrochemical activity of the flow cathode with different current collectors.

Current collectors displayed different onset potentials in plain PBS (blank tests) indicating that the intrinsic electroactivity of the interphase current collector-electrolyte depends on the specific materials. For example, Ni foam blank produced the most positive HER potential of -0.88 vs. Ag/AgCl at -10 A/m^2 (Fig. 5.3A), followed by Ni mesh blank (-0.96 V vs. Ag/AgCl), SS mesh blank (-0.97 V vs. Ag/AgCl), and Ti blank (-1.3 V vs. Ag/AgCl). Unlike other current collectors, Ti is poorly active for HER, yet it showed decent electrical conductivity comparable to the other collectors tested as blanks (no flow cathode added) in the assembled cell (Ti: $0.08\text{ m}\Omega\text{m}^2$, followed by Ni foam: $0.12\text{ m}\Omega\text{m}^2$, Ni mesh: $0.14\text{ m}\Omega\text{m}^2$, and SS mesh: $0.2\text{ m}\Omega\text{m}^2$) (Fig. 5.4). Ni/AC flow

cathode demonstrated to shift the HER potentials to more positive values with all current collectors. For example, Ni/AC flow cathode with Ni mesh current collector produced the most positive HER potential of -0.77 vs. Ag/AgCl at -10 A/m 2 (Fig. 5.3B), which is a relative shift of 20% in comparison with the blank, followed by Ni/AC flow cathode with Ni foam (-0.82 vs. Ag/AgCl, 7% relative shift), Ni/AC flow cathode with SS mesh (-0.86 vs. Ag/AgCl, 11% relative shift), and Ni/AC flow cathode coupled with Ti (-0.94 vs. Ag/AgCl, 28% relative shift). These results indicate that the overall electroactivity of the flow cathode is strongly dependent on the current collector material, likely an active current collector coupled with the flow cathode creates a synergistic effect to promote lower HER overpotentials than the collector (or stationary electrode) itself.

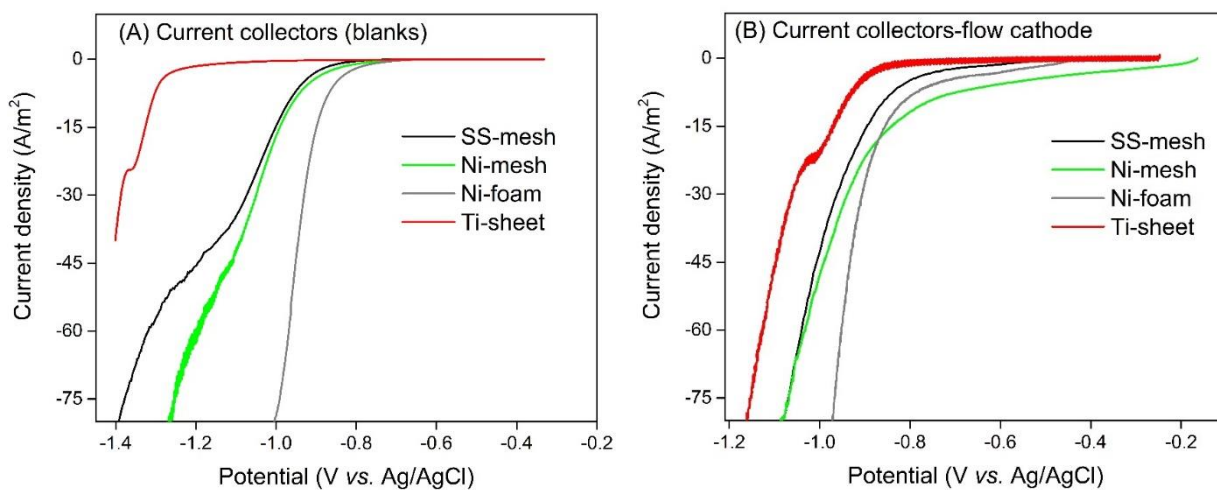


Fig. 5.3. Current-potential curves. A) Current collector in plain PBS for blank test, B) Ni/AC flow cathode coupled with different current collectors.

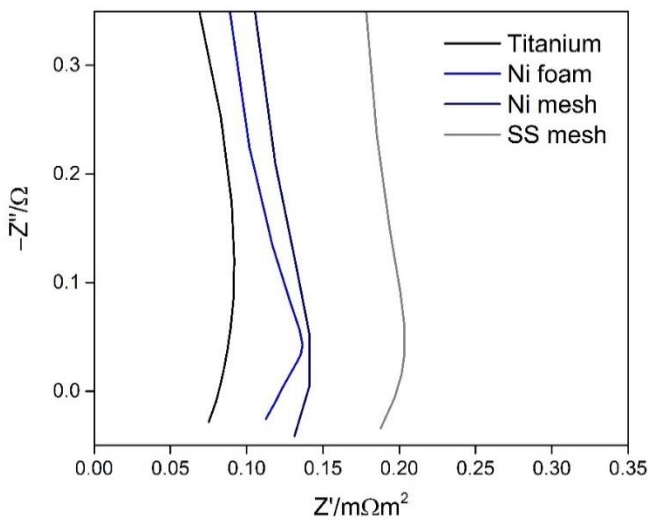


Fig. 5.4. Potentiostatic EIS for different current collectors in plain PBS (blank test).

The charge transferred toward HER was calculated by numerical integration of the current over time. The flow cathode coupled with Ni foam demonstrated to produce the highest amount of charge for HER (1C) within the potential window tested (OCP to $-1V$ vs. Ag/AgCl), with a relative contribution of 42% of charge transferred to the flowable catalyst powders (Fig. 5.5A). Flow cathodes coupled with Ni mesh produced 0.88C, with a relative contribution of 85% of the charge transferred to the flowable catalyst powders, followed by the flow cathode coupled with SS mesh (0.48C), with a relative flow cathode contribution of 79%, and flow cathode coupled with Ti, which showed 0.16C, with 95% of this charge attributed to the flow cathode. Ti itself is not active for HER, within the potential window tested. Thus, it produced the lowest charge for HER, yet the good conductivity of the Ti material allows most of the electricity to be transferred from the Ti surface to the flowable catalyst powders. The contribution of the metal collector surface activity plays a crucial role in the overall charge transfer toward HER, as the collector surface

became more active ($\text{Ni foam} > \text{Ni mesh} > \text{SS mesh} > \text{Ti}$), the overall charge transfer increased. In addition, the high surface area of Ni foam ($128 \text{ m}^2/\text{m}^2$),⁴⁵ versus other collectors, might also promoted the greater charge transferred toward HER. Interestingly, Ni mesh showed a slightly lower electroactivity toward HER in the blank test than Ni foam (Fig. 5.3A), yet it triggered the peak of charge from the flow cathode (0.75C) (Fig. 5.5A). Likely the moderate surface activity of Ni mesh promotes a synergistic effect with the flow cathode.

A simplified charge transfer model is proposed in Fig. 5.5B. The model describes three proposed electrochemical interactions at the current collector interphase, 1) HER taking place at the current collector interphase with the plain PBS, 2) HER at Ni/AC clusters closer to the current collector, and 3) direct electron transfer (DET) from the metal collector to the flowable cathode.

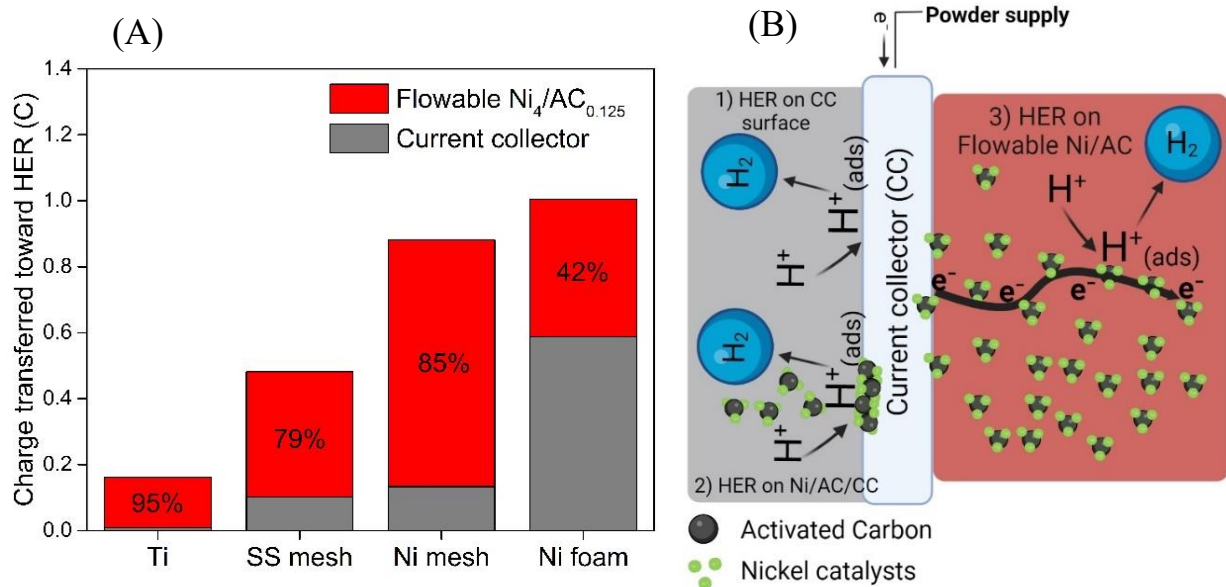


Fig. 5.5. Flow cathode coupled with different current collectors. A) charge transferred toward HER, B) simplified model of the current collector interphase phenomena 1) HER at the current collector interphase with PBS, 2) HER at Ni/AC clusters attached to the current collector (left, color grey) and, 3) direct electron transfer to the flowable catalyst powders (right, color red).

In the simplified model, the DET charges the flowable active network, which likely induces a voltage across the bulk flow cathode. The voltage drop across the electrolyte during the electrolysis could be significant at different distances from the working electrode (We).¹²⁸ Due to the resistances given by the intermittent connection in the flowable network and the liquid catholyte phase, it is expected that the voltage applied to the current collector drops in the flowable network with the distance. The induced voltage in the bulk catholyte is an indicator of the electronic conductivity of the flowable network since the charge transfer dynamics is mainly governed by the potential difference between flowable particles and the current collector.¹²⁹ A Ti probe was located 2 cm far from the current collector and the voltage drop was measured in the bulk plain PBS catholyte (for blank tests) and in the flow cathode using the different current collectors. The voltage induced in the bulk solution was significantly higher (≥ 148 mV at We: -0.7 V vs. Ag/AgCl) in the presence of flow cathodes than in the plain PBS for Ti, Ni mesh and SS mesh but remained low (≤ 23 mV at We: -0.7 V vs. Ag/AgCl) for Ni foam (Fig. 5.6) in both solutions. For example, a working electrode potential of -0.7 V (vs. Ag/AgCl) was applied to the Ti current collector and it induced a voltage of 210 mV at the probe located in the bulk flow cathode (Fig. 5.7), Ni mesh induced 153 mV, SS mesh induced 148 mV, and Ni foam induced 13 mV (vs. Ag/AgCl), which is the largest voltage drop across the bulk flow cathode.

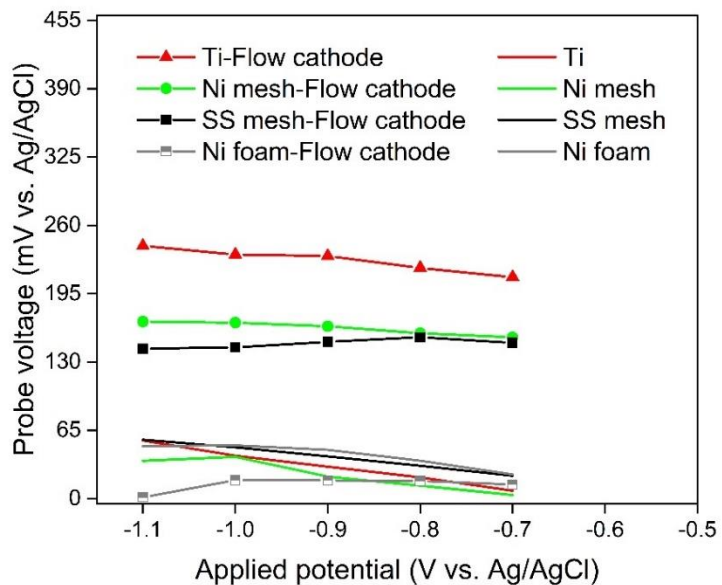


Fig. 5.6. Voltage induced at the probe at different working electrode potentials.

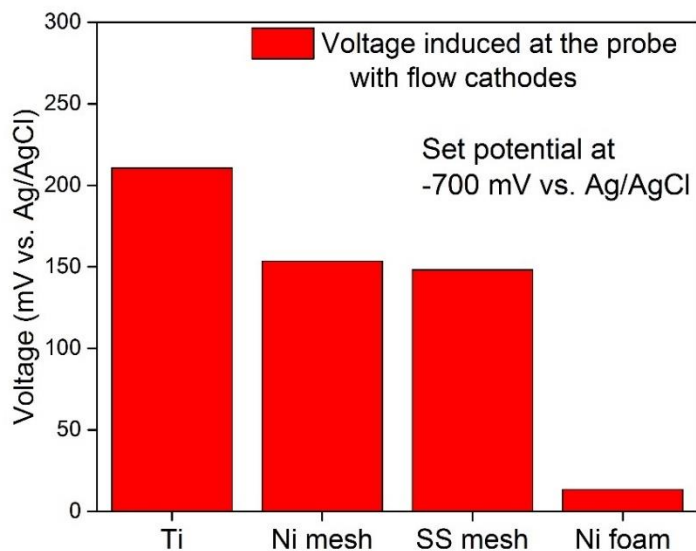


Fig. 5.7. Voltage induced at the probe (2 cm far from the current collector) using flow cathode coupled with different current collectors.

A recent study suggested that the aspect current collector area to flow electrode impacts the extension of the percolation network, with a higher collector area resulting in an strengthen flowable network.¹³⁰ Here, the flat SS and Ni meshes had a large open area (30%), which likely reduced the effective extension of the percolation network toward the bulk flow cathode and might contributed to the voltage drop, showing slightly lower induced voltages at the probe than the Ti sheet (no open area). However, Ni foam, which has a large projected area ($128\text{m}^2/\text{m}^2$),⁴⁵ did not show a higher induced voltage at the probe. This is likely due to the much higher intrinsic electroactivity of Ni foam toward HER, which utilizes most of the electric charge at the electrode surface rather than in the flowable network. In addition, the voltage drop across the flow electrodes suggests the underutilization of the flowable network, which likely resulted in lower ratio of charge attributed to the flow cathode coupled with Ni foam.¹²⁹ Nevertheless, the synergistic effect between the active current collector surface and the flowable cathode demonstrated to produce the highest amount of charge for HER. In addition, the voltage induced at the probe slightly increased with higher applied potential at the current collector (Fig. 5.6), likely indicating that the charge transfer to the flow cathode could be further enhanced by higher applied potentials. During the particle/particle and particle/current collector collision, only a partial charge is transferred from the current collector to the flowable particles and from one particle to another due to the contact and electrolyte electrical resistances associate within every collision.¹³¹ The sum of resistances in the flow cathode could result in the lower induced voltage at the probe compared to the applied potential at the current collector. In addition, the high fraction of charge (Fig. 5.5A) utilized at the active Ni foam collector surface likely further reduced the partial charge transferred to the flowable powder resulting in a much lower induced voltage at the probe for Ni foam collector. It might be possible to modify the induced voltages response by increasing the powder loading (flow cathode

concentration) but we found an adverse impact of higher loadings (above 0.125wt.% Ni/AC, for powders containing low nickel loading \leq 4-at.%) due to the exacerbated capacitive behavior and impact of stagnant powders in the cathode chamber (see CHAPTER 4), thus, a high powder loading approach might not be beneficial, even at high concentrations, not all particles in the flow electrode contribute to the charge transfer process, and the adverse impact of viscosity in pumping power might poses additional challenges at concentrations above 15wt.% (threshold observed in other capacitive systems).^{129,132}

5.3.3. MEC performance with different current collectors.

Based on the abiotic electrochemical tests, the two current collectors that yielded the lowest and highest amount of charge transferred toward HER (Ni foam and Ti) were tested in MECs to compare the impact of different flow cathode charge contribution. The Ni/AC flow cathode coupled with Ni foam displayed hydrogen production rates of 2.33 ± 0.25 L-H₂/L-d, which were 48% higher than the MEC with Ni/AC flow cathode coupled with Ti (1.57 ± 0.14 L-H₂/L-d) (Fig. 5.8), likely due to the higher sustained current densities produced by the flow cathode coupled with Ni foam (9.6 ± 0.5 A/m²) in comparison to the flow cathode coupled with Ti current collector (7.1 ± 0.3 A/m²) under the same conditions (Fig. 5.8 and Fig. 5.9). The better performance of Ni foam is likely due to the synergistic effect of an active collector surface coupled with the flow cathode, which resulted in an overall higher charge transferred toward HER. Also, the porous structure of nickel foam provided a large surface area which likely increased the volume of particles in contact with the current collector compared to a thin two-dimensional sheet structure.^{126,129} Although Ti can induce higher voltages in the bulk flowable active network, the lack of intrinsic HER activity resulted in an overall low charge produced by HER, mostly attributed to the intrinsic Ni/AC flow catalyst activity, which seems to be the underlaying factor to achieve

greater performance using a non-active collector interphase, such as the Ti for HER. Nevertheless, the hydrogen production rates achieved with the flow cathode coupled with Ni foam were 133% higher than those previously reported in a two-chamber MEC with a Ni foam cathode under catholyte recirculation (1.0 ± 0.1 L-H₂/L-d).⁷ Ni/AC flow cathode coupled with Ti also demonstrated outstanding performances compared to previously reported MECs using stationary Ni/AC cathodes. For example, Ni/AC flow cathode coupled with Ti current collector produced 43% and 349% higher hydrogen production rates than previous stationary Ni/AC cathodes (1.1 ± 0.1 L-H₂/L-d for an AC-Ni8.8 cathode and 0.35 ± 0.02 L-H₂/L-d for an AC-Ni acid-treated cathode) using polymer binders.^{7,8} Those results suggest that the flow cathode concept breakthrough the current performance barriers encountered with solid-type or stationary Ni/AC electrodes. The flow cathodes in the present study produced lower hydrogen production rates than the recent MEC study which used a vapor-fed catholyte and a nickel-molybdenum stationary cathode (81 ± 3 L-H₂/L-d) in a membrane electrode assembly (MEA).¹⁰⁹ In the study, the MEA with a zero-gap carbon felt anode, drastically reduced the anodic ohmic resistance (1.4 mΩm²) compared to the previously reported values for graphite brush anodes (10.6 mΩm²),¹³³ such as the one used in this study. Likely the reduced anodic resistance and the different reactor configuration (vapor-fed cathode) resulted in the higher hydrogen production rates compared to this study, yet the use of vapor catholytes at the large scale is unclear.

The MEC with a flow cathode coupled with Ni foam showed the highest average energy yield (ηE , $186 \pm 13\%$) in comparison with the flow cathode coupled with Ti ($168 \pm 9\%$) over the 4 h cycles (Fig. 5.8). Slightly higher than 100% cathodic hydrogen recoveries (r_{cat}) were obtained for both MECs with different current collectors ($128 \pm 9\%$ for flow cathode-Ni foam and $118 \pm 6\%$ for flow

cathode-Ti). Cathodic hydrogen recovery rates should not be greater than 100%, and thus these values likely just are indicating that cathodic recoveries were ~100% for both cathodes.

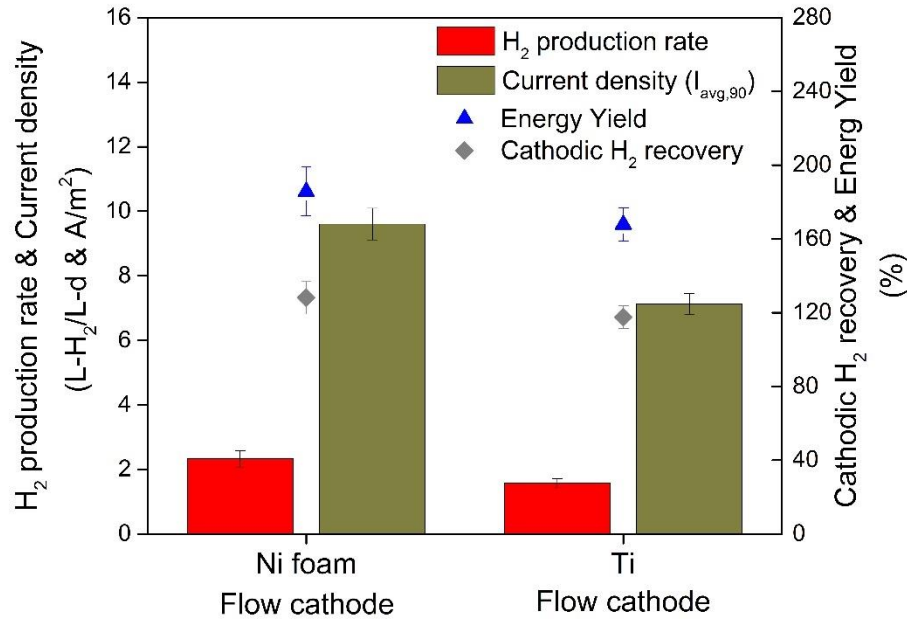


Fig. 5.8 .Comparison of MEC performances (hydrogen production rate, current density, cathodic hydrogen recovery, and energy yield) using flow cathodes coupled with Ni foam and Ti.

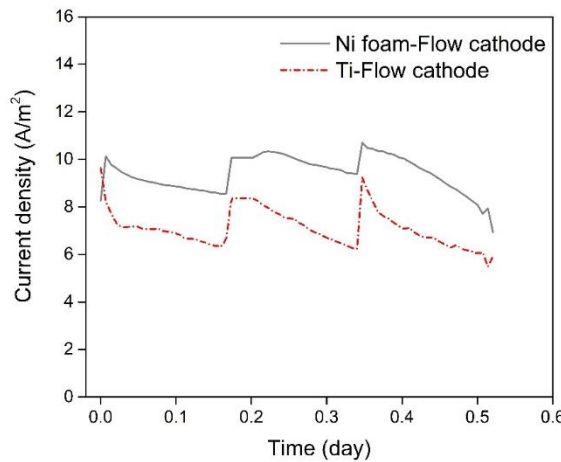


Fig. 5.9. Current generation over the 4 h cycles in MECs with flow cathodes coupled with Ni foam and Titanium (Ti) current collectors.

5.4.Conclusion.

Current collectors showed different intrinsic electroactivities toward HER in the abiotic blank tests, with the most positive potentials displayed by Ni foam, followed by Ni mesh and SS mesh. Ti was poorly active for HER in the blank tests, but it provided good electrical conductivity in the assembled cell comparable to other collector materials. Flow cathodes coupled with the different current collectors displayed a shift to more positive potentials, confirming the key role of flowable powders in decreasing the HER overpotentials. The current collectors coupled with the flow cathode displayed different total charge transferred toward HER. Ni foam coupled with the flow cathode triggered the greater amount of charge, followed by Ni mesh coupled with the flow cathode, SS mesh and Ti. Ti was not active for HER at the potential window tested (OCP to -1V), thus, nearly 95% of the charge produced in the Ti flow cathode was attributed to the flowable powders. As a result, voltage induced at the probe with Ni foam coupled flow cathode were significantly lower than the Ti, Ni mesh and SS mesh, suggesting that the voltage drop across the flowable bulk cathode is greater when introducing a highly active collector surface due to the partial charge transfer toward the flowable network, which might suggest underutilization of the powders. Nevertheless, the flowable powers reacting near the active collector surface coupled with the highly reactive reaction at the Ni foam collector interphase likely creates a synergistic effect to promote the high overall charge transfer. As result, higher hydrogen production rates were obtained with Ni foam than Ti. The current collector plays a crucial role on the overall electricity of flow cathodes, and hydrogen production rate. The approach of enhancing the performance of flow cathodes should consider the integration of the collector surface electroactivity with a conductive and highly active flowable cathode network.

CHAPTER 6.

Recommendations for future studies

A simple nitric acid treatment incorporated higher fractions of nitrogen and oxygen functionalities on the AC surface and significantly enhanced the wettability property. This wettability prevails even after electrode fabrication. The enhanced wettability ultimately improves the hydrogen production rates in MEC. Although this wet acid treatment method was effective in improving the performance of Ni/AC stationary cathodes, it is unclear if the positive impact of the light oxidation prevails in the long term. To ensure long term positive impacts, other treatment methods should be proposed to strongly bind functional groups on the AC surface or further increase the content of those functionalities with stability over time.

The electrochemical performance of Ni/AC cathodes was increased by increasing the Ni loading on the AC surface from 2 at.% to 4 at.%. Although, this was a 50% increment in nickel loading, other deposition methods should be explored to further increase the Ni loading and optimize the catalytic properties of the active powders in the flow cathode.

Ni/AC flow cathodes were susceptible to the pH variation over multiple MEC cycles. It is recommended to explore new catalysts mixtures that integrate a more stable interphase capable of maintaining high electroactivity in a wide pH range toward more alkaline conditions. This approach will ensure the continuous operation of MEC at different cycle durations and with the minimum expenses given by the pH compensation agents.

Different current collectors triggered different amount of charge toward HER. It is believed that this charge contribution is given by three electrochemical mechanisms at the electrode-electrolyte interphase. A simplified model was proposed, where HER reaction could take place at 1) the

interphase with the current collector and plain PBS, 2) the surface of Ni/AC clusters attached to the collector, and 3) different distances from the current collector in the flow cathode. The individual contribution of the last two mechanisms is beyond the scope of this dissertation. It is recommended to explore in future studies new electrochemical or optical methods to elucidate the individual contributions, along with changes in the current collector surface chemistry, microstructure, and catalytic properties before and after exposure to the flow cathodes.

Flow cathode recovery and recycling is desirable. It is recommended to develop a method to recover flow cathodes and examine the performance of the recovered powders.

The voltage drop was measured in the bulk flow cathode placing a probe 2 cm far from the current collector. Due to this voltage drop, it is very likely that the hydrogen evolution reaction takes place closer to the current collector rather than in the distant bulk flow cathode. Measuring the distance of this boundary layer, where the suspended particles are active is an important indicator of the flowable network (or volume) utilization. It is recommended to measure the flow cathode boundary layer theoretically and experimentally. Flowable network utilization (FNU), which might be the ratio between the truly active flow electrode volume (V_{active}) and the reactor chamber volume ($V_{chamber}$) ($FNU = V_{active}/V_{chamber} \%$). To measure the active flowable network, a set of millimetric probes could be placed at different distances from the current collector and the distance of the boundary flowable layer could be calculated using a linear regression approach. The resulted variation of voltage with distance can be correlated with the catalyst specific onset potential, which is the minimum potential needed for HER to occur. Direct observation of the boundary flowable layer is also recommended to validate those experimental calculations, along with computational simulation methods to establish a theoretical model of the flow cathode system for HER.

APPENDIX A

Supplementary information

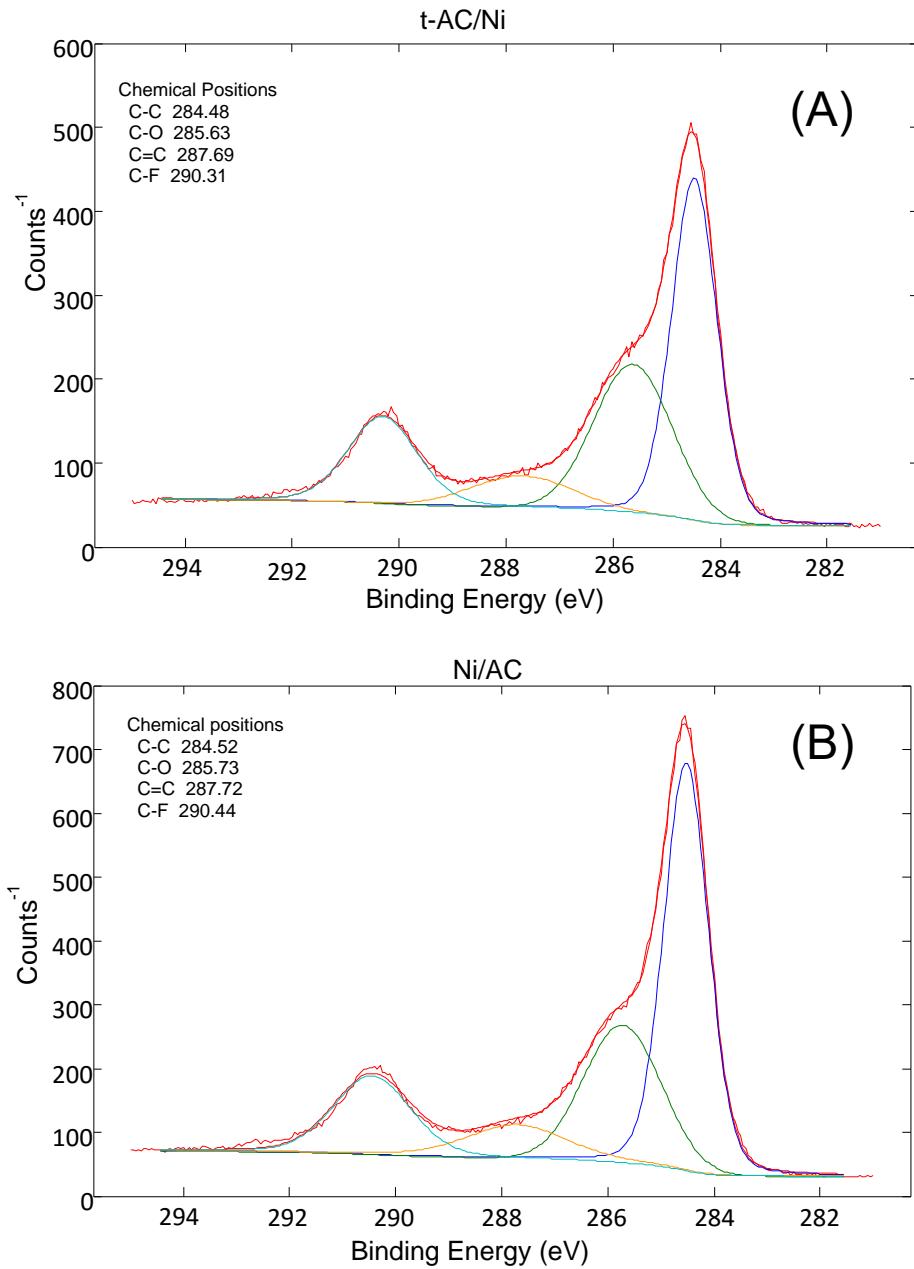


Fig. A 1. High-resolution XPS spectra in the C 1s regions of (A) Ni-adsorbed acid-treated activated carbon (t-AC/Ni) and (B) Ni-adsorbed activated carbon (AC/Ni).

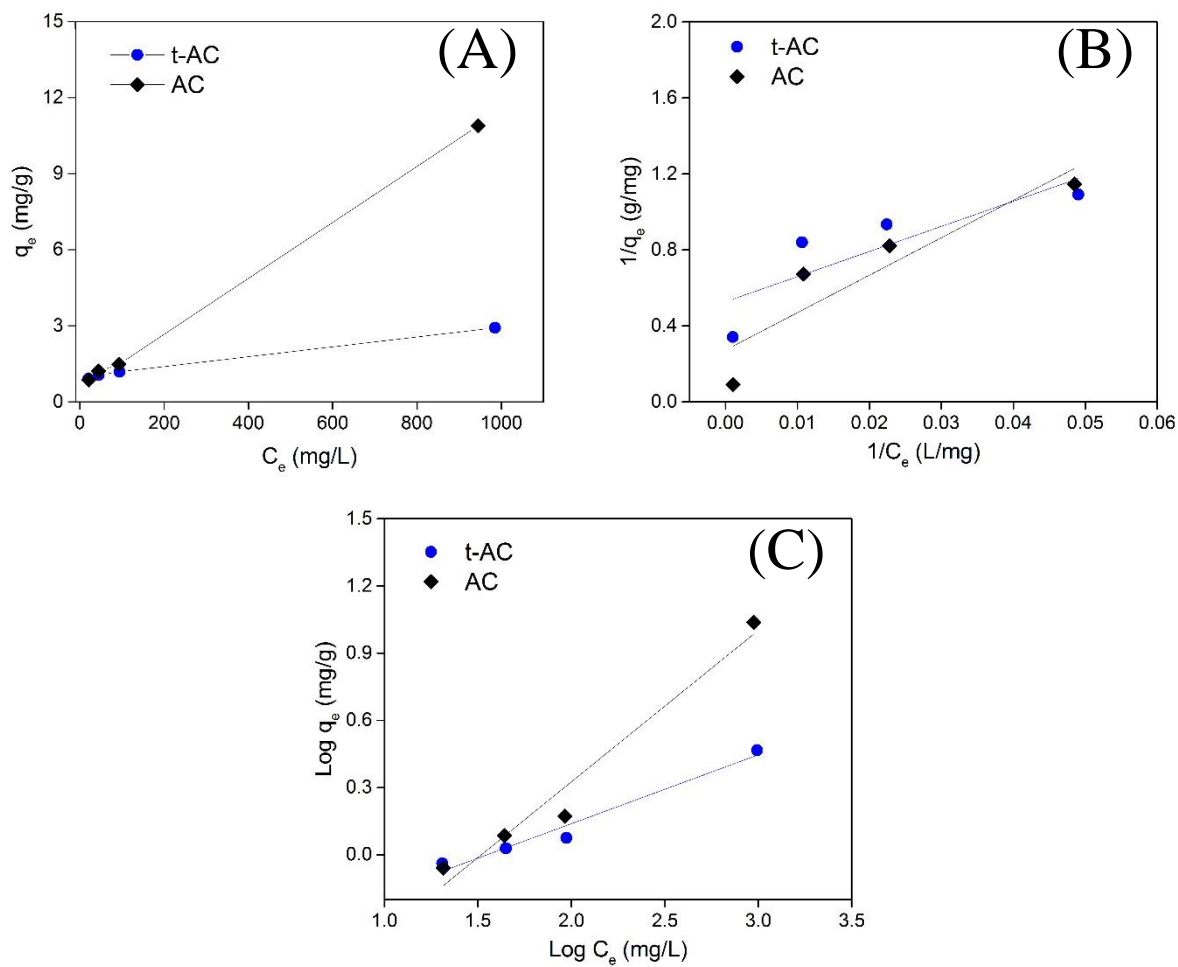


Fig. A2. Nickel adsorption on AC and t-AC (A) experimental equilibrium isotherm data of AC/Ni and t-AC/Ni, (B) Langmuir isotherm model and, (C) Freundlich isotherm model.

Table A 1. Nickel adsorption test parameters resulted from fitting the data set using Freundlich and Langmuir isotherm models.

Sample	Freundlich			Langmuir		
	1/n	K_f (mg/g)(L/mg) $^{1/n}$	R^2	b	q_e (mg/g)	R^2
t-AC	0.54	0.14	0.89	0.016	3.31	0.72
AC	0.59	0.13	0.97	0.009	5.24	0.87

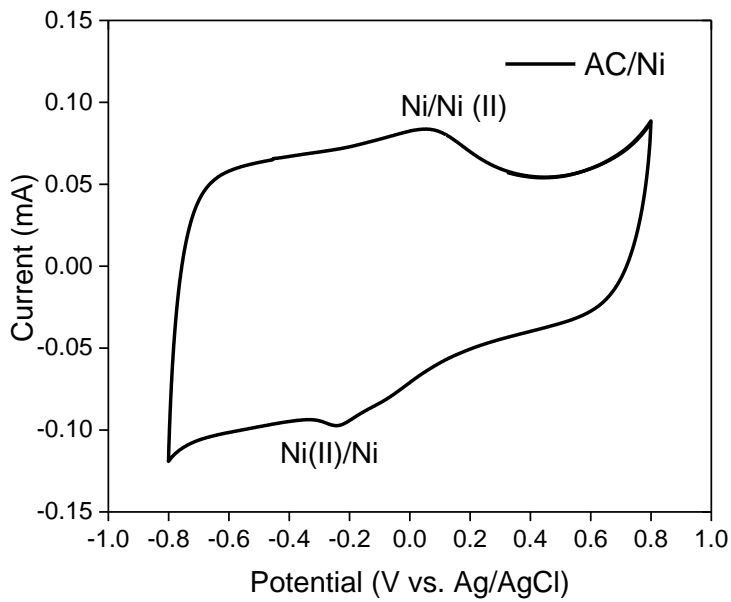


Fig. A 3. Nickel redox potentials determined by cyclic voltammetry test for Ni/AC catalysts in a 3-electrode cell using catalytic ink.

APPENDIX B

Formal permission for the published paper and figures

B.1. Permission for adapted CHAPTER 3.

ELSEVIER LICENSE TERMS AND CONDITIONS

Apr 19, 2023

This Agreement between Mr. Daniel Moreno Jimenez ("You") and Elsevier ("Elsevier") consists of your license details and the terms and conditions provided by Elsevier and Copyright Clearance Center.

License Number	5532670406550
License date	Apr 19, 2023
Licensed Content Publisher	Elsevier
Licensed Content Publication	Bioresource Technology
Licensed Content Title	Enhanced wettability improves catalytic activity of nickel-functionalized activated carbon cathode for hydrogen production in microbial electrolysis cells
Licensed Content Author	Daniel A. Moreno-Jimenez,Kyoung-Yeol Kim
Licensed Content Date	Apr 1, 2022
Licensed Content Volume	350
Licensed Content Issue	n/a
Licensed Content Pages	1
Start Page	126881
End Page	
Type of Use	reuse in a thesis/dissertation
Portion	full article
Circulation	1
Format	electronic
Are you the author of this Elsevier article?	Yes
Will you be translating?	No
Title	NOVEL NICKEL-LOADED ACTIVATED CARBON CATHODES FOR HYDROGEN PRODUCTION IN MICROBIAL ELECTROLYSIS CELLS
Institution name	University at Albany, State University of New York
Expected presentation date	Apr 2023
Order reference number	1
Requestor Location	Mr. Daniel Moreno Jimenez 1400 Washington Avenue
Publisher Tax ID	ALBANY, NY 12222 United States Attn: Mr. Daniel A. Moreno Jimenez 98-0397604
Billing Type	Invoice
Billing Address	Mr. Daniel Moreno Jimenez 1400 Washington Avenue
Total	ALBANY, NY 12222 United States Attn: Mr. Daniel A. Moreno Jimenez 0.00 USD

B.2. Permission for the adapted figure 2.3 in CHAPTER 2. Literature review.

18/4/23, 16:24

Rightslink® by Copyright Clearance Center

The screenshot shows a web page from CCC RightsLink. At the top, there is a navigation bar with icons for Home, Help, Live Chat, and a user profile for Daniel Moreno Jimenez. The main content area displays a journal article titled "Microbial Fuel Cells: Methodology and Technology" by Bruce E. Logan, Bert Hamelers, René Rozendal, et al., published in Environmental Science & Technology from the American Chemical Society on Sep 1, 2006. The ACS Publications logo is visible. Below the article details, a section titled "PERMISSION/LICENSE IS GRANTED FOR YOUR ORDER AT NO CHARGE" contains instructions for credit and usage. At the bottom of the page are "BACK" and "CLOSE WINDOW" buttons.

Microbial Fuel Cells: Methodology and Technology

Author: Bruce E. Logan, Bert Hamelers, René Rozendal, et al

Publication: Environmental Science & Technology

Publisher: American Chemical Society

Date: Sep 1, 2006

Copyright © 2006, American Chemical Society

PERMISSION/LICENSE IS GRANTED FOR YOUR ORDER AT NO CHARGE

This type of permission/license, instead of the standard Terms and Conditions, is sent to you because no fee is being charged for your order. Please note the following:

- Permission is granted for your request in both print and electronic formats, and translations.
- If figures and/or tables were requested, they may be adapted or used in part.
- Please print this page for your records and send a copy of it to your publisher/graduate school.
- Appropriate credit for the requested material should be given as follows: "Reprinted (adapted) with permission from {COMPLETE REFERENCE CITATION}. Copyright {YEAR} American Chemical Society." Insert appropriate information in place of the capitalized words.
- One-time permission is granted only for the use specified in your RightsLink request. No additional uses are granted (such as derivative works or other editions). For any uses, please submit a new request.

If credit is given to another source for the material you requested from RightsLink, permission must be obtained from that source.

BACK CLOSE WINDOW

B.3. Permission for the adapted figure 2.4 in CHAPTER 2. Literature review.

18/4/23, 16:40

RightsLink Printable License

ELSEVIER LICENSE TERMS AND CONDITIONS

Apr 18, 2023

This Agreement between Mr. Daniel Moreno Jimenez ("You") and Elsevier ("Elsevier") consists of your license details and the terms and conditions provided by Elsevier and Copyright Clearance Center.

License Number	5532110114179
License date	Apr 18, 2023
Licensed Content Publisher	Elsevier
Licensed Content Publication	Water Research
Licensed Content Title	Pilot scale microbial fuel cells using air cathodes for producing electricity while treating wastewater
Licensed Content Author	Ruggero Rossi,Andy Y. Hur,Martin A. Page,Amalia O'Brien Thomas,Joseph J. Butkiewicz,David W. Jones,Gahyun Baek,Pascal E. Saikaly,Donald M. Croke,Bruce E. Logan
Licensed Content Date	May 15, 2022
Licensed Content Volume	215
Licensed Content Issue	n/a
Licensed Content Pages	1
Start Page	118208
End Page	0

Type of Use	reuse in a thesis/dissertation
Portion	figures/tables/illustrations
Number of figures/tables/illustrations	1
Format	electronic
Are you the author of this Elsevier article?	No
Will you be translating?	No
Title	NOVEL NICKEL-LOADED ACTIVATED CARBON CATHODES FOR HYDROGEN PRODUCTION IN MICROBIAL ELECTROLYSIS CELLS
Institution name	University at Albany, State University of New York
Expected presentation date	Apr 2023
Order reference number	1
Portions	Graphical abstract
Requestor Location	Mr. Daniel Moreno Jimenez 1400 Washington Avenue ALBANY, NY 12222 United States Attn: Mr. Daniel A. Moreno Jimenez
Publisher Tax ID	98-0397604
Total	0.00 USD

B.4. Permission for the adapted figure 2.6 in CHAPTER 2. Literature review.



This is a License Agreement between Daniel A. Moreno Jimenez, University at Albany, SUNY. ("User") and Copyright Clearance Center, Inc. ("CCC") on behalf of the Rightsholder identified in the order details below. The license consists of the order details, the Marketplace Permissions General Terms and Conditions below, and any Rightsholder Terms and Conditions which are included below.

All payments must be made in full to CCC in accordance with the Marketplace Permissions General Terms and Conditions below.

Order Date	18-Apr-2023	Type of Use	Republish in a thesis/dissertation
Order License ID	1346332-1	Publisher	IOP Publishing
ISSN	1945-7111	Portion	Image/photo/illustration
LICENSED CONTENT			
Publication Title	Journal of the Electrochemical Society	Country	United States of America
Author/Editor	Electrochemical Society.	Rightsholder	IOP Publishing, Ltd
Date	01/01/1948	Publication Type	e-Journal
Language	English	URL	http://www.scitation.org/JE
REQUEST DETAILS			
Portion Type	Image/photo/illustration	Distribution	United States
Number of Images / Photos / Illustrations	1	Translation	Original language of publication
Format (select all that apply)	Electronic	Copies for the Disabled?	No
Who Will Republish the Content?	Academic institution	Minor Editing Privileges?	No
Duration of Use	Life of current edition	Incidental Promotional Use?	No
Lifetime Unit Quantity	Up to 499	Currency	USD
Rights Requested	Main product		
NEW WORK DETAILS			
Title	NOVEL NICKEL-LOADED ACTIVATED CARBON CATHODES FOR HYDROGEN PRODUCTION IN MICROBIAL ELECTROLYSIS CELLS	Institution Name	University at Albany, State University of New York
		Expected Presentation Date	2023-04-24
Instructor Name	Daniel A. Moreno Jimenez		
ADDITIONAL DETAILS			
Order Reference Number	1	The Requesting Person/Organization to Appear on the License	Daniel A. Moreno Jimenez. University at Albany, SUNY.
REQUESTED CONTENT DETAILS			
Title, Description or Numeric Reference of the Portion(s)	Figure 1	Title of the Article/Chapter the Portion Is From	Trends in the Exchange Current for Hydrogen Evolution
Editor of Portion(s)	N/A	Author of Portion(s)	Electrochemical Society.
Volume of Serial or Monograph	N/A	Issue, if Republishing an Article From a Serial	N/A
Page or Page Range of Portion	J24	Publication Date of Portion	1948-01-01

References

- (1) Energy, D. of. Hydrogen Strategy: Enabling A Low-Carbon Economy. Off. Foss. Energy 2020, 24.
- (2) USDRIVE, driving research and innovation for vehicle efficiency and energy sustainability. Hydrogen Production Technical Team Roadmap; 2017.
- (3) Office of energy efficiency and renewable energy. Hydrogen Production, the U.S. Department of Energy (DOE). <https://www.energy.gov/eere/fuelcells/hydrogen-production> (accessed 2022-10-21).
- (4) IRENA. Green Hydrogen Cost Reduction: Scaling up Electrolysers to Meet the 1.5°C Climate Goal; 2020.
- (5) Logan, B. E.; Call, D.; Cheng, S.; Hamelers, H. V. M.; Sleutels, T. H. J. A.; Jeremiassie, A. W.; Rozendal, R. A. Microbial Electrolysis Cells for High Yield Hydrogen Gas Production from Organic Matter. *Environ. Sci. Technol.* 2008, 42 (23), 8630–8640. <https://doi.org/10.1021/es801553z>.
- (6) Logan, B. E.; Rabaey, K. Conversion of Wastes into Bioelectricity and Chemicals by Using Microbial Electrochemical Technologies. *Science* (80-.). 2012, 337 (6095), 686–690. <https://doi.org/10.1126/science.1217412>.
- (7) Kim, K.-Y.; Yang, W.; Logan, B. E. Regenerable Nickel-Functionalized Activated Carbon Cathodes Enhanced by Metal Adsorption to Improve Hydrogen Production in Microbial Electrolysis Cells. *Environ. Sci. Technol.* 2018, 52 (12), 7131–7137. <https://doi.org/10.1021/acs.est.7b06005>.
- (8) Moreno-Jimenez, D. A.; Kim, K.-Y. Enhanced Wettability Improves Catalytic Activity of Nickel-Functionalized Activated Carbon Cathode for Hydrogen Production in Microbial Electrolysis Cells. *Bioresour. Technol.* 2022, 350, 126881. <https://doi.org/10.1016/j.biortech.2022.126881>.
- (9) Yang, J.; Jang, M. J.; Ženg, X.; Park, Y. S.; Lee, J.; Choi, S. M.; Yin, Y. Non-Precious Electrocatalysts for Oxygen Evolution Reaction in Anion Exchange Membrane Water Electrolysis: A Mini Review. *Electrochem. commun.* 2021, 131, 107118. <https://doi.org/10.1016/j.elecom.2021.107118>.
- (10) Yang, E.; Omar Mohamed, H.; Park, S.-G.; Obaid, M.; Al-Qaradawi, S. Y.; Castaño, P.; Chon, K.; Chae, K.-J. A Review on Self-Sustainable Microbial Electrolysis Cells for Electro-Biohydrogen Production via Coupling with Carbon-Neutral Renewable Energy Technologies. *Bioresour. Technol.* 2021, 320, 124363. <https://doi.org/10.1016/j.biortech.2020.124363>.
- (11) Department of Energy. Wastewater Infrastructure. State and community energy programs. <https://www.energy.gov/scep/slsc/wastewater-infrastructure> (accessed 2023-04-13).
- (12) McCarty, P. L.; Bae, J.; Kim, J. Domestic Wastewater Treatment as a Net Energy Producer—Can This Be Achieved? *Environ. Sci. Technol.* 2011, 45 (17), 7100–7106. https://doi.org/10.1021/ES2014264/ASSET/IMAGES/LARGE/ES-2011-014264_0001.JPG.
- (13) Gandiglio, M.; Lanzini, A.; Soto, A.; Leone, P.; Santarelli, M. Enhancing the Energy Efficiency of Wastewater Treatment Plants through Co-Digestion and Fuel Cell Systems. *Front. Environ. Sci.* 2017, 5, 70. <https://doi.org/10.3389/fenvs.2017.00070>.
- (14) Cantwell, J.; Erickson, B.; Fillmore, L.; Kottwitz, J.; Levy, M.; Rickert, M. Energy Data Management Manual for the Wastewater Treatment Sector. Better Build. U.S. Dep. energy 2017.
- (15) Rani, A.; Snyder, S. W.; Kim, H.; Lei, Z.; Pan, S.-Y. Pathways to a Net-Zero-Carbon Water Sector through Energy-Extracting Wastewater Technologies. *npj Clean Water* 2022, 5 (1), 49. <https://doi.org/10.1038/s41545-022-00197-8>.
- (16) Holliger, C.; Fruteau de Laclos, H.; Hack, G. Methane Production of Full-Scale Anaerobic Digestion Plants Calculated from Substrate's Biomethane Potentials Compares Well with

- the One Measured On-Site. *Front. Energy Res.* 2017, 5 (JUN), 12. <https://doi.org/10.3389/fenrg.2017.00012>.
- (17) Schwarzenbeck, N.; Bomball, E.; Pfeiffer, W. Can a Wastewater Treatment Plant Be a Powerplant? A Case Study. *Water Sci. Technol.* 2008, 57 (10), 1555–1561. <https://doi.org/10.2166/WST.2008.215>.
- (18) Logan, B. E. Scaling up Microbial Fuel Cells and Other Bioelectrochemical Systems. *Appl. Microbiol. Biotechnol.* 2010, 85 (6), 1665–1671. <https://doi.org/10.1007/s00253-009-2378-9>.
- (19) Rabaey, K.; Clauwaert, P.; Aelterman, P.; Verstraete, W. Tubular Microbial Fuel Cells for Efficient Electricity Generation. *Environ. Sci. Technol.* 2005, 39 (20), 8077–8082. <https://doi.org/10.1021/ES050986I/ASSET/IMAGES/LARGE/ES050986IF00005.JPG>.
- (20) He, Z.; Minteer, S. D.; Angenent, L. T. Electricity Generation from Artificial Wastewater Using an Upflow Microbial Fuel Cell. *Environ. Sci. Technol.* 2005, 39 (14), 5262–5267. <https://doi.org/10.1021/ES0502876/ASSET/IMAGES/LARGE/ES0502876F00006.JPG>.
- (21) Min, B.; Logan, B. E. Continuous Electricity Generation from Domestic Wastewater and Organic Substrates in a Flat Plate Microbial Fuel Cell. *Environ. Sci. Technol.* 2004, 38 (21), 5809–5814. <https://doi.org/10.1021/ES0491026/ASSET/IMAGES/LARGE/ES0491026F00006.JPG>.
- (22) Liu, H.; Ramnarayanan, R.; Logan, B. E. Production of Electricity during Wastewater Treatment Using a Single Chamber Microbial Fuel Cell. *Environ. Sci. Technol.* 2004, 38 (7), 2281–2285. <https://doi.org/10.1021/ES034923G/ASSET/IMAGES/LARGE/ES034923GF00006.JPG>
- (23) Aelterman, P.; Rabaey, K.; Pham, H. T.; Boon, N.; Verstraete, W. Continuous Electricity Generation at High Voltages and Currents Using Stacked Microbial Fuel Cells. *Environ. Sci. Technol.* 2006, 40 (10), 3388–3394. https://doi.org/10.1021/ES0525511/SUPPL_FILE/ES0525511SI20060314_011817.PDF.
- (24) Logan, B. E.; Hamelers, B.; Rozendal, R.; Schröder, U.; Keller, J.; Freguia, S.; Aelterman, P.; Verstraete, W.; Rabaey, K. Microbial Fuel Cells: Methodology and Technology. *Environ. Sci. Technol.* 2006, 40 (17), 5181–5192. <https://doi.org/10.1021/es0605016>.
- (25) Yang, W.; He, W.; Zhang, F.; Hickner, M. A.; Logan, B. E. Single-Step Fabrication Using a Phase Inversion Method of Poly(Vinylidene Fluoride) (PVDF) Activated Carbon Air Cathodes for Microbial Fuel Cells. *Environ. Sci. Technol. Lett.* 2014, 1 (10), 416–420. <https://doi.org/10.1021/ez5002769>.
- (26) Rossi, R.; Hur, A. Y.; Page, M. A.; Thomas, A. O. B.; Butkiewicz, J. J.; Jones, D. W.; Baek, G.; Saikaly, P. E.; Cropek, D. M.; Logan, B. E. Pilot Scale Microbial Fuel Cells Using Air Cathodes for Producing Electricity While Treating Wastewater. *Water Res.* 2022, 215, 118208. <https://doi.org/10.1016/j.watres.2022.118208>.
- (27) Kadier, A.; Simayi, Y.; Kalil, M. S.; Abdeshahian, P.; Hamid, A. A. A Review of the Substrates Used in Microbial Electrolysis Cells (MECs) for Producing Sustainable and Clean Hydrogen Gas. *Renew. Energy* 2014, 71, 466–472. <https://doi.org/10.1016/J.RENENE.2014.05.052>.
- (28) Tang, J. H. A Review of Suitable Substrates for Hydrogen Production in Microbial Electrolysis Cells. *IOP Conf. Ser. Earth Environ. Sci.* 2021, 621 (1), 012145. <https://doi.org/10.1088/1755-1315/621/1/012145>.
- (29) Shao, Q.; Li, J.; Yang, S.; Sun, H. Effects of Different Substrates on Microbial Electrolysis Cell (MEC) Anodic Membrane: Biodiversity and Hydrogen Production Performance. *Water Sci. Technol.* 2019, 79 (6), 1123–1133. <https://doi.org/10.2166/WST.2019.107>.
- (30) Muddasar, M.; Liaquat, R.; Aslam, A.; Ur Rahman, M. Z.; Abdullah, A.; Khoja, A. H.; Latif, K.; Bahadar, A. Performance Efficiency Comparison of Microbial Electrolysis Cells for Sustainable Production of Biohydrogen—A Comprehensive Review. *Int. J. Energy Res.* 2022, 46 (5), 5625–5645. <https://doi.org/10.1002/er.7606>.
- (31) Rossi, R.; Baek, G.; Logan, B. E. Vapor-Fed Cathode Microbial Electrolysis Cells with Closely Spaced Electrodes Enables Greatly Improved Performance. *Environ. Sci. Technol.*

- 2022, 56 (2), 1211–1220. <https://doi.org/10.1021/acs.est.1c06769>.
- (32) Selembo, P. A.; Merrill, M. D.; Logan, B. E. The Use of Stainless Steel and Nickel Alloys as Low-Cost Cathodes in Microbial Electrolysis Cells. *J. Power Sources* 2009, 190 (2), 271–278. [https://doi.org/https://doi.org/10.1016/j.jpowsour.2008.12.144](https://doi.org/10.1016/j.jpowsour.2008.12.144).
- (33) Kim, K.-Y.; Habas, S. E.; Schaidle, J. A.; Logan, B. E. Application of Phase-Pure Nickel Phosphide Nanoparticles as Cathode Catalysts for Hydrogen Production in Microbial Electrolysis Cells. *Bioresour. Technol.* 2019, 293, 122067. <https://doi.org/10.1016/j.biortech.2019.122067>.
- (34) International energy agency (IEA). The Future of Hydrogen. Rep. Prep. by IEA G20, Japan. 2019.
- (35) Bao, F.; Kemppainen, E.; Dorbandt, I.; Bors, R.; Xi, F.; Schlatmann, R.; Krol, R.; Calnan, S. Understanding the Hydrogen Evolution Reaction Kinetics of Electrodeposited Nickel-Molybdenum in Acidic, Near-Neutral, and Alkaline Conditions. *ChemElectroChem* 2021, 8 (1), 195–208. <https://doi.org/10.1002/celc.202001436>.
- (36) Inocêncio, C. V. M.; Holade, Y.; Morais, C.; Kokoh, K. B.; Napporn, T. W. Electrochemical Hydrogen Generation Technology: Challenges in Electrodes Materials for a Sustainable Energy. *Electrochem. Sci. Adv.* 2022, e2100206. <https://doi.org/10.1002/elsa.202100206>.
- (37) Nørskov, J. K.; Bligaard, T.; Logadottir, A.; Kitchin, J. R.; Chen, J. G.; Pandelov, S.; Stimming, U. Trends in the Exchange Current for Hydrogen Evolution. *J. Electrochem. Soc.* 2005, 152 (3), J23. <https://doi.org/10.1149/1.1856988>.
- (38) Kim, K.-Y.; Zikmund, E.; Logan, B. E. Impact of Catholyte Recirculation on Different 3-Dimensional Stainless Steel Cathodes in Microbial Electrolysis Cells. *Int. J. Hydrogen Energy* 2017, 42 (50), 29708–29715. <https://doi.org/10.1016/j.ijhydene.2017.10.099>.
- (39) Lu, L.; Hou, D.; Fang, Y.; Huang, Y.; Ren, Z. J. Nickel Based Catalysts for Highly Efficient H₂ Evolution from Wastewater in Microbial Electrolysis Cells. *Electrochim. Acta* 2016, 206, 381–387. <https://doi.org/10.1016/j.electacta.2016.04.167>.
- (40) Yuan, H.; He, Z. Platinum Group Metal-Free Catalysts for Hydrogen Evolution Reaction in Microbial Electrolysis Cells. *Chem. Rec.* 2017, 17 (7), 641–652. <https://doi.org/10.1002/tcr.201700007>.
- (41) Hrapovic, S.; Manuel, M.-F.; Luong, J. H. T.; Guiot, S. R.; Tartakovsky, B. Electrodeposition of Nickel Particles on a Gas Diffusion Cathode for Hydrogen Production in a Microbial Electrolysis Cell. *Int. J. Hydrogen Energy* 2010, 35 (14), 7313–7320. <https://doi.org/10.1016/j.ijhydene.2010.04.146>.
- (42) Jayabalan, T.; Matheswaran, M.; Radhakrishnan, T. K.; Naina Mohamed, S. Influence of Nickel Molybdate Nanocatalyst for Enhancing Biohydrogen Production in Microbial Electrolysis Cell Utilizing Sugar Industrial Effluent. *Bioresour. Technol.* 2021, 320, 124284. <https://doi.org/10.1016/j.biortech.2020.124284>.
- (43) Ribot-Llobet, E.; Nam, J.-Y.; Tokash, J. C.; Guisasola, A.; Logan, B. E. Assessment of Four Different Cathode Materials at Different Initial PHs Using Unbuffered Catholytes in Microbial Electrolysis Cells. *Int. J. Hydrogen Energy* 2013, 38 (7), 2951–2956. <https://doi.org/10.1016/j.ijhydene.2012.12.037>.
- (44) Selembo, P. A.; Merrill, M. D.; Logan, B. E. Hydrogen Production with Nickel Powder Cathode Catalysts in Microbial Electrolysis Cells. *Int. J. Hydrogen Energy* 2010, 35 (2), 428–437. <https://doi.org/10.1016/j.ijhydene.2009.11.014>.
- (45) Jeremiassie, A. W.; Hamelers, H. V. M.; Saakes, M.; Buisman, C. J. N. Ni Foam Cathode Enables High Volumetric H₂ Production in a Microbial Electrolysis Cell. *Int. J. Hydrogen Energy* 2010, 35 (23), 12716–12723. <https://doi.org/10.1016/j.ijhydene.2010.08.131>.
- (46) Kim, K.-Y.; Logan, B. E. Nickel Powder Blended Activated Carbon Cathodes for Hydrogen Production in Microbial Electrolysis Cells. *Int. J. Hydrogen Energy* 2019, 44 (26), 13169–13174. <https://doi.org/10.1016/j.ijhydene.2019.04.041>.
- (47) Rozendal, R. A.; Hamelers, H. V. M.; Rabaey, K.; Keller, J.; Buisman, C. J. N. Towards Practical Implementation of Bioelectrochemical Wastewater Treatment. *Trends Biotechnol.* 2008, 26 (8), 450–459. <https://doi.org/10.1016/j.tibtech.2008.04.008>.
- (48) Mitov, M.; Chorbadzhiyska, E.; Nalbandian, L.; Hubenova, Y. Nickel-Based

- Electrodeposits as Potential Cathode Catalysts for Hydrogen Production by Microbial Electrolysis. *J. Power Sources* 2017, 356, 467–472. <https://doi.org/10.1016/j.jpowsour.2017.02.066>.
- (49) Zhang, B.; Wen, Z.; Ci, S.; Chen, J.; He, Z. Nitrogen-Doped Activated Carbon as a Metal Free Catalyst for Hydrogen Production in Microbial Electrolysis Cells. *RSC Adv.* 2014, 4 (90), 49161–49164. <https://doi.org/10.1039/C4RA08555H>.
- (50) Mastragostino, M.; Arbizzani, C.; Meneghelli, L.; Paraventi, R. Electronically Conducting Polymers and Activated Carbon: Electrode Materials in Supercapacitor Technology. *Adv. Mater.* 1996, 8 (4), 331–334. <https://doi.org/10.1002/adma.19960080409>.
- (51) DITZIG, J.; LIU, H.; LOGAN, B. Production of Hydrogen from Domestic Wastewater Using a Bioelectrochemically Assisted Microbial Reactor (BEAMR). *Int. J. Hydrogen Energy* 2007, 32 (13), 2296–2304. <https://doi.org/10.1016/j.ijhydene.2007.02.035>.
- (52) Carmona-Martínez, A. A.; Trably, E.; Milferstedt, K.; Lacroix, R.; Etcheverry, L.; Bernet, N. Long-Term Continuous Production of H₂ in a Microbial Electrolysis Cell (MEC) Treating Saline Wastewater. *Water Res.* 2015, 81, 149–156. <https://doi.org/10.1016/j.watres.2015.05.041>.
- (53) Zikmund, E.; Kim, K. Y.; Logan, B. E. Hydrogen Production Rates with Closely-Spaced Felt Anodes and Cathodes Compared to Brush Anodes in Two-Chamber Microbial Electrolysis Cells. *Int. J. Hydrogen Energy* 2018, 43 (20), 9599–9606. <https://doi.org/10.1016/j.ijhydene.2018.04.059>.
- (54) Cario, B. P.; Rossi, R.; Kim, K.-Y.; Logan, B. E. Applying the Electrode Potential Slope Method as a Tool to Quantitatively Evaluate the Performance of Individual Microbial Electrolysis Cell Components. *Bioresour. Technol.* 2019, 287 (May), 121418. <https://doi.org/10.1016/j.biortech.2019.121418>.
- (55) Liu, H.; Grot, S.; Logan, B. E. Electrochemically Assisted Microbial Production of Hydrogen from Acetate. *Environ. Sci. Technol.* 2005, 39 (11), 4317–4320. <https://doi.org/10.1021/es050244p>.
- (56) Jin, T.; Han, Q.; Jiao, L.; Jin, T.; Han, Q.; Jiao, L. Binder-Free Electrodes for Advanced Sodium-Ion Batteries. *Adv. Mater.* 2020, 32 (3), 1806304. <https://doi.org/10.1002/ADMA.201806304>.
- (57) Chu, N.; Wang, D.; Wang, H.; Liang, Q.; Chang, J.; Gao, Y.; Jiang, Y.; Zeng, R. J. Flow-Electrode Microbial Electrosynthesis for Increasing Production Rates and Lowering Energy Consumption. *Engineering* 2021. <https://doi.org/10.1016/j.eng.2021.09.015>.
- (58) Zhang, C.; Ma, J.; Wu, L.; Sun, J.; Wang, L.; Li, T.; Waite, T. D. Flow Electrode Capacitive Deionization (FCDI): Recent Developments, Environmental Applications, and Future Perspectives. *Environ. Sci. Technol.* 2021, 55 (8), 4243–4267. <https://doi.org/10.1021/acs.est.0c06552>.
- (59) Mourshed, M.; Niya, S. M. R.; Ojha, R.; Rosengarten, G.; Andrews, J.; Shabani, B. Carbon-Based Slurry Electrodes for Energy Storage and Power Supply Systems. *Energy Storage Mater.* 2021, 40, 461–489. <https://doi.org/10.1016/j.ensm.2021.05.032>.
- (60) Jeon, S.; Park, H.; Yeo, J.; Yang, S.; Cho, C. H.; Han, M. H.; Kim, D. K. Desalination via a New Membrane Capacitive Deionization Process Utilizing Flow-Electrodes. *Energy Environ. Sci.* 2013, 6 (5), 1471. <https://doi.org/10.1039/c3ee24443a>.
- (61) Hatzell, K. B.; Hatzell, M. C.; Cook, K. M.; Boota, M.; Housel, G. M.; McBride, A.; Kumbur, E. C.; Gogotsi, Y. Effect of Oxidation of Carbon Material on Suspension Electrodes for Flow Electrode Capacitive Deionization. *Environ. Sci. Technol.* 2015, 49 (5), 3040–3047. <https://doi.org/10.1021/es5055989>.
- (62) Yang, S.; Jeon, S.; Kim, H.; Choi, J.; Yeo, J.; Park, H.; Kim, D. K. Stack Design and Operation for Scaling Up the Capacity of Flow-Electrode Capacitive Deionization Technology. *ACS Sustain. Chem. Eng.* 2016, 4 (8), 4174–4180. <https://doi.org/10.1021/acssuschemeng.6b00689>.
- (63) Cho, Y.; Lee, K. S.; Yang, S.; Choi, J.; Park, H.; Kim, D. K. A Novel Three-Dimensional Desalination System Utilizing Honeycomb-Shaped Lattice Structures for Flow-Electrode Capacitive Deionization. *Energy Environ. Sci.* 2017, 10 (8), 1746–1750.

- (64) He, C.; Lian, B.; Ma, J.; Zhang, C.; Wang, Y.; Mo, H.; Waite, T. D. Scale-up and Modelling of Flow-Electrode CDI Using Tubular Electrodes. *Water Res.* 2021, 203, 117498. <https://doi.org/10.1016/j.watres.2021.117498>.
- (65) Hatzell, K. B.; Iwama, E.; Ferris, A.; Daffos, B.; Urita, K.; Tzedakis, T.; Chauvet, F.; Taberna, P.-L.; Gogotsi, Y.; Simon, P. Capacitive Deionization Concept Based on Suspension Electrodes without Ion Exchange Membranes. *Electrochim. commun.* 2014, 43, 18–21. <https://doi.org/10.1016/j.elecom.2014.03.003>.
- (66) Carmona-Orbezo, A.; Dryfe, R. A. W. Understanding the Performance of Flow-Electrodes for Capacitive Deionization through Hydrodynamic Voltammetry. *Chem. Eng. J.* 2021, 406, 126826. <https://doi.org/10.1016/j.cej.2020.126826>.
- (67) Boota, M.; Hatzell, K. B.; Alhabeb, M.; Kumbur, E. C.; Gogotsi, Y. Graphene-Containing Flowable Electrodes for Capacitive Energy Storage. *Carbon N. Y.* 2015, 92, 142–149. <https://doi.org/10.1016/j.carbon.2015.04.020>.
- (68) Porada, S.; Lee, J.; Weingarth, D.; Presser, V. Continuous Operation of an Electrochemical Flow Capacitor. *Electrochim. commun.* 2014, 48, 178–181. <https://doi.org/10.1016/j.elecom.2014.08.023>.
- (69) Song, J.; Ma, J.; Zhang, C.; He, C.; Waite, T. D. Implication of Non-Electrostatic Contribution to Deionization in Flow-Electrode CDI: Case Study of Nitrate Removal From Contaminated Source Waters. *Front. Chem.* 2019, 7. <https://doi.org/10.3389/fchem.2019.00146>.
- (70) Zhang, C.; Wang, M.; Xiao, W.; Ma, J.; Sun, J.; Mo, H.; Waite, T. D. Phosphate Selective Recovery by Magnetic Iron Oxide Impregnated Carbon Flow-Electrode Capacitive Deionization (FCDI). *Water Res.* 2021, 189, 116653. <https://doi.org/10.1016/j.watres.2020.116653>.
- (71) Xie, J.; Ma, J.; Zhang, C.; Waite, T. D. Direct Electron Transfer (DET) Processes in a Flow Anode System–Energy-Efficient Electrochemical Oxidation of Phenol. *Water Res.* 2021, 203, 117547. <https://doi.org/10.1016/J.WATRES.2021.117547>.
- (72) Youssry, M.; Madec, L.; Soudan, P.; Cerbelaud, M.; Guyomard, D.; Lestriez, B. Formulation of Flowable Anolyte for Redox Flow Batteries: Rheo-Electrical Study. *J. Power Sources* 2015, 274, 424–431. <https://doi.org/10.1016/j.jpowsour.2014.10.076>.
- (73) Li, X.; Zhao, L.; Yu, J.; Liu, X.; Zhang, X.; Liu, H.; Zhou, W. Water Splitting: From Electrode to Green Energy System. *Nano-Micro Lett.* 2020, 12 (1), 131. <https://doi.org/10.1007/s40820-020-00469-3>.
- (74) Yang, N.; Zhou, Q.; Zhan, G.; Liu, Y.; Luo, H.; Li, D. Comparative Evaluation of Simultaneous Nitritation/Denitritation and Energy Recovery in Air-Cathode Microbial Fuel Cells (ACMFCs) Treating Low C/N Ratio Wastewater. *Sci. Total Environ.* 2021, 788, 147652. <https://doi.org/10.1016/j.scitotenv.2021.147652>.
- (75) Xiao, L.; Ge, Z.; Kelly, P.; Zhang, F.; He, Z. Evaluation of Normalized Energy Recovery (NER) in Microbial Fuel Cells Affected by Reactor Dimensions and Substrates. *Bioresour. Technol.* 2014, 157, 77–83. <https://doi.org/10.1016/j.biortech.2014.01.086>.
- (76) Thakur, S.; Das, B. Performance Evaluation of Microbial Fuel Cell with Sewage Wastewater and RO Concentrate Using Composite Anode Made of Luffa Aegyptiaca. *Environ. Prog. Sustain. Energy* 2021, 40 (1), e13504. <https://doi.org/10.1002/ep.13504>.
- (77) Cusick, R. D.; Bryan, B.; Parker, D. S.; Merrill, M. D.; Mehanna, M.; Kiely, P. D.; Liu, G.; Logan, B. E. Performance of a Pilot-Scale Continuous Flow Microbial Electrolysis Cell Fed Winery Wastewater. *Appl. Microbiol. Biotechnol.* 2011, 89 (6), 2053–2063. <https://doi.org/10.1007/s00253-011-3130-9>.
- (78) Cotterill, S. E.; Dolfing, J.; Jones, C.; Curtis, T. P.; Heidrich, E. S. Low Temperature Domestic Wastewater Treatment in a Microbial Electrolysis Cell with 1 m² Anodes: Towards System Scale-Up. *Fuel Cells* 2017, 17 (5), 584–592. <https://doi.org/10.1002/fuce.201700034>.
- (79) Singh, L.; Miller, A. G.; Wang, L.; Liu, H. Scaling-up up-Flow Microbial Electrolysis Cells with a Compact Electrode Configuration for Continuous Hydrogen Production. *Bioresour.*

- Technol. 2021, 331 (January), 125030. <https://doi.org/10.1016/j.biortech.2021.125030>.
- (80) Baeza, J. A.; Martínez-Miró, Á.; Guerrero, J.; Ruiz, Y.; Guisasola, A. Bioelectrochemical Hydrogen Production from Urban Wastewater on a Pilot Scale. *J. Power Sources* 2017, 356, 500–509. <https://doi.org/10.1016/j.jpowsour.2017.02.087>.
- (81) Rossi, R.; Baek, G.; Saikaly, P. E.; Logan, B. E. Continuous Flow Microbial Flow Cell with an Anion Exchange Membrane for Treating Low Conductivity and Poorly Buffered Wastewater. *ACS Sustain. Chem. Eng.* 2021, 9 (7), 2946–2954. <https://doi.org/10.1021/acssuschemeng.0c09144>.
- (82) Mostazo-López, M. J.; Ruiz-Rosas, R.; Morallón, E.; Cazorla-Amorós, D. Generation of Nitrogen Functionalities on Activated Carbons by Amidation Reactions and Hofmann Rearrangement: Chemical and Electrochemical Characterization. *Carbon N. Y.* 2015, 91, 252–265. <https://doi.org/10.1016/j.carbon.2015.04.089>.
- (83) Moreno-Castilla, C.; Ferro-Garcia, M. A.; Joly, J. P.; Bautista-Toledo, I.; Carrasco-Marín, F.; Rivera-Utrilla, J. Activated Carbon Surface Modifications by Nitric Acid, Hydrogen Peroxide, and Ammonium Peroxydisulfate Treatments. *Langmuir* 1995, 11 (11), 4386–4392. <https://doi.org/10.1021/la00011a035>.
- (84) Chingombe, P.; Saha, B.; Wakeman, R. J. Surface Modification and Characterisation of a Coal-Based Activated Carbon. *Carbon N. Y.* 2005, 43 (15), 3132–3143. <https://doi.org/10.1016/j.carbon.2005.06.021>.
- (85) Kim, K.-Y.; Moreno-Jimenez, D. A.; Efstathiadis, H. Electrochemical Ammonia Recovery from Anaerobic Centrate Using a Nickel-Functionalized Activated Carbon Membrane Electrode. *Environ. Sci. Technol.* 2021, 55 (11), 7674–7680. <https://doi.org/10.1021/acs.est.1c01703>.
- (86) Slack, J. J.; Brodt, M.; Cullen, D. A.; Reeves, K. S.; More, K. L.; Pintauro, P. N. Impact of Polyvinylidene Fluoride on Nanofiber Cathode Structure and Durability in Proton Exchange Membrane Fuel Cells. *J. Electrochem. Soc.* 2020, 167 (5), 054517. <https://doi.org/10.1149/1945-7111/ab77fb>.
- (87) Li, Q.; Chen, Y.; Lee, D. J.; Li, F.; Kim, H. Preparation of Y-Zeolite/CoCl₂ Doped PVDF Composite Nanofiber and Its Application in Hydrogen Production. *Energy* 2012, 38 (1), 144–150. <https://doi.org/10.1016/j.energy.2011.12.021>.
- (88) Logan, B.; Cheng, S.; Watson, V.; Estadt, G. Graphite Fiber Brush Anodes for Increased Power Production in Air-Cathode Microbial Fuel Cells. *Environ. Sci. Technol.* 2007, 41 (9), 3341–3346. <https://doi.org/10.1021/es062644y>.
- (89) Jeremiasse, A. W.; Hamelers, H. V. M.; Kleijn, J. M.; Buisman, C. J. N. Use of Biocompatible Buffers to Reduce the Concentration Overpotential for Hydrogen Evolution. *Environ. Sci. Technol.* 2009, 43 (17), 6882–6887. <https://doi.org/10.1021/es9008823>.
- (90) Ivanov, I.; Ren, L.; Siegert, M.; Logan, B. E. A Quantitative Method to Evaluate Microbial Electrolysis Cell Effectiveness for Energy Recovery and Wastewater Treatment. *Int. J. Hydrogen Energy* 2013, 38 (30), 13135–13142. <https://doi.org/10.1016/j.ijhydene.2013.07.123>.
- (91) Murthy, A. P.; Theerthagiri, J.; Madhavan, J. Insights on Tafel Constant in the Analysis of Hydrogen Evolution Reaction. *J. Phys. Chem. C* 2018, 122 (42), 23943–23949. <https://doi.org/10.1021/acs.jpcc.8b07763>.
- (92) Foo, K. Y.; Hameed, B. H. Insights into the Modeling of Adsorption Isotherm Systems. *Chem. Eng. J.* 2010, 156 (1), 2–10. <https://doi.org/10.1016/j.cej.2009.09.013>.
- (93) Dujeanic-Stephane, K.; Gupta, M.; Kumar, A.; Sharma, V.; Pandit, S.; Bocchetta, P.; Kumar, Y. The Effect of Modifications of Activated Carbon Materials on the Capacitive Performance: Surface, Microstructure, and Wettability. *J. Compos. Sci.* 2021, Vol. 5, Page 66 2021, 5 (3), 66. <https://doi.org/10.3390/JCS5030066>.
- (94) Bleda-Martínez, M. J.; Lozano-Castelló, D.; Morallón, E.; Cazorla-Amorós, D.; Linares-Solano, A. Chemical and Electrochemical Characterization of Porous Carbon Materials. *Carbon N. Y.* 2006, 44 (13), 2642–2651. <https://doi.org/10.1016/j.carbon.2006.04.017>.
- (95) Hang, B. T.; Okada, S.; Yamaki, J. Effect of Binder Content on the Cycle Performance of Nano-Sized Fe₂O₃-Loaded Carbon for Use as a Lithium Battery Negative Electrode. *J.*

- (96) Power Sources 2008, 178 (1), 402–408. <https://doi.org/10.1016/j.jpowsour.2007.12.001>.
- (96) Son, S.; Koo, B.; Chai, H.; Tran, H. V. H.; Pandit, S.; Jung, S. P. Comparison of Hydrogen Production and System Performance in a Microbial Electrolysis Cell Containing Cathodes Made of Non-Platinum Catalysts and Binders. *J. Water Process Eng.* 2021, 40, 101844. <https://doi.org/10.1016/j.jwpe.2020.101844>.
- (97) Tang, J.; Bian, Y.; Jin, S.; Sun, D.; Ren, Z. J. Cathode Material Development in the Past Decade for H₂ Production from Microbial Electrolysis Cells. *ACS Environ. Au* 2022, 2 (1), 20–29. <https://doi.org/10.1021/acsenvironau.1c00021>.
- (98) Grandi, M.; Rohde, S.; Liu, D. J.; Gollas, B.; Hacker, V. Recent Advancements in High Performance Polymer Electrolyte Fuel Cell Electrode Fabrication – Novel Materials and Manufacturing Processes. *Journal of Power Sources*. Elsevier April 1, 2023, p 232734. <https://doi.org/10.1016/j.jpowsour.2023.232734>.
- (99) Majlan, E. H.; Rohendi, D.; Daud, W. R. W.; Husaini, T.; Haque, M. A. Electrode for Proton Exchange Membrane Fuel Cells: A Review. *Renew. Sustain. Energy Rev.* 2018, 89, 117–134. <https://doi.org/10.1016/j.rser.2018.03.007>.
- (100) Yang, W.; Chen, S. Recent Progress in Electrode Fabrication for Electrocatalytic Hydrogen Evolution Reaction: A Mini Review. *Chem. Eng. J.* 2020, 393, 124726. <https://doi.org/10.1016/j.cej.2020.124726>.
- (101) Lin, R.; Li, B.; Hou, Y. P.; Ma, J. M. Investigation of Dynamic Driving Cycle Effect on Performance Degradation and Micro-Structure Change of PEM Fuel Cell. *Int. J. Hydrogen Energy* 2009, 34 (5), 2369–2376. <https://doi.org/10.1016/J.IJHYDENE.2008.10.054>.
- (102) Baria, D. N.; Hulbert, H. M. Reduction of Crotonic Acid with Hydrogen on a Slurry Electrode. *J. Electrochem. Soc.* 1973, 120 (10), 1333. <https://doi.org/10.1149/1.2403257/XML>.
- (103) Bian, Y.; Chen, X.; Lu, L.; Liang, P.; Ren, Z. J. Concurrent Nitrogen and Phosphorus Recovery Using Flow-Electrode Capacitive Deionization. *ACS Sustain. Chem. Eng.* 2019, 7 (8), 7844–7850. <https://doi.org/10.1021/acssuschemeng.9b00065>.
- (104) Lim, J.; Shin, Y. U.; Son, A.; Hong, S. W.; Hong, S. TiO₂ Nanotube Electrode for Organic Degradation Coupled with Flow-Electrode Capacitive Deionization for Brackish Water Desalination. *npj Clean Water* 2022 51 2022, 5 (1), 1–9. <https://doi.org/10.1038/s41545-022-00150-9>.
- (105) Wei, Q.; Tang, L.; Ramalingam, K.; Liang, M.; Ma, J.; Shi, Y.; Hui, K. N.; Hui, K. S.; Chen, F. Redox-Catalysis Flow Electrode Desalination in an Organic Solvent. *J. Mater. Chem. A* 2021, 9 (39), 22254–22261. <https://doi.org/10.1039/D1TA05350G>.
- (106) Nam, J. Y.; Logan, B. E. Enhanced Hydrogen Generation Using a Saline Catholyte in a Two Chamber Microbial Electrolysis Cell. *Int. J. Hydrogen Energy* 2011, 36 (23), 15105–15110. <https://doi.org/10.1016/J.IJHYDENE.2011.08.106>.
- (107) Park, B. H.; Choi, J. H. Improvement in the Capacitance of a Carbon Electrode Prepared Using Water-Soluble Polymer Binder for a Capacitive Deionization Application. *Electrochim. Acta* 2010, 55 (8), 2888–2893. <https://doi.org/10.1016/J.ELECTACTA.2009.12.084>.
- (108) Technology, N. I. of S. and. Spectroscopy, NIST X-ray Photoelectron database. NIST Standard Reference Database Number 20. doi:10.18434/T4T88K (accessed 2023-02-26). <https://doi.org/10.18434/T4T88K>.
- (109) Rossi, R.; Nicolas, J.; Logan, B. E. Using Nickel-Molybdenum Cathode Catalysts for Efficient Hydrogen Gas Production in Microbial Electrolysis Cells. *J. Power Sources* 2023, 560, 232594. <https://doi.org/10.1016/J.JPOWSOUR.2022.232594>.
- (110) Dubey, P.; Kaurav, N.; Devan, R. S.; Okram, G. S.; Kuo, Y. K. The Effect of Stoichiometry on the Structural, Thermal and Electronic Properties of Thermally Decomposed Nickel Oxide. *RSC Adv.* 2018, 8 (11), 5882–5890. <https://doi.org/10.1039/C8RA00157J>.
- (111) Huang, Q.; Wang, X.; Li, J.; Dai, C.; Gamboa, S.; Sebastian, P. J. Nickel Hydroxide/Activated Carbon Composite Electrodes for Electrochemical Capacitors. *J. Power Sources* 2007, 164 (1), 425–429. <https://doi.org/10.1016/j.jpowsour.2006.09.066>.
- (112) Kuan-Xin, H.; Quan-Fu, W.; Xiao-gang, Z.; Xin-Lei, W. Electrodeposition of Nickel and

- Cobalt Mixed Oxide/Carbon Nanotube Thin Films and Their Charge Storage Properties. *J. Electrochem. Soc.* 2006, 153 (8), A1568. <https://doi.org/10.1149/1.2208735/XML>.
- (113) Yuan, G. H.; Jiang, Z. H.; Aramata, A.; Gao, Y. Z. Electrochemical Behavior of Activated-Carbon Capacitor Material Loaded with Nickel Oxide. *Carbon N. Y.* 2005, 43 (14), 2913–2917. <https://doi.org/10.1016/J.CARBON.2005.06.027>.
- (114) Liang, P.; Sun, X.; Bian, Y.; Zhang, H.; Yang, X.; Jiang, Y.; Liu, P.; Huang, X. Optimized Desalination Performance of High Voltage Flow-Electrode Capacitive Deionization by Adding Carbon Black in Flow-Electrode. *Desalination* 2017, 420, 63–69. <https://doi.org/10.1016/J.DESAL.2017.05.023>.
- (115) Choo, K. Y.; Yoo, C. Y.; Han, M. H.; Kim, D. K. Electrochemical Analysis of Slurry Electrodes for Flow-Electrode Capacitive Deionization. *J. Electroanal. Chem.* 2017, 806, 50–60. <https://doi.org/10.1016/j.jelechem.2017.10.040>.
- (116) Rommerskirchen, A.; Kalde, A.; Linnartz, C. J.; Bongers, L.; Linz, G.; Wessling, M. Unraveling Charge Transport in Carbon Flow-Electrodes: Performance Prediction for Desalination Applications. *Carbon N. Y.* 2019, 145, 507–520. <https://doi.org/10.1016/J.CARBON.2019.01.053>.
- (117) Ďurovič, M.; Hnát, J.; Bouzek, K. Electrocatalysts for the Hydrogen Evolution Reaction in Alkaline and Neutral Media. A Comparative Review. *J. Power Sources* 2021, 493, 229708. <https://doi.org/10.1016/j.jpowsour.2021.229708>.
- (118) Kalantarifard, S.; Bikas, R.; Nandy, S.; Lis, T.; Chae, K. H.; Najafpour, M. M. Water Oxidation in the Presence of a Nickel Coordination Compound: Decomposition Products, Fe Impurity in the Electrolyte, and a Candidate as a Catalyst. *J. Phys. Chem. C* 2022, 126 (23), 9753–9761. <https://doi.org/10.1021/acs.jpcc.2c02611>.
- (119) Mahmood, N.; Yao, Y.; Zhang, J. W.; Pan, L.; Zhang, X.; Zou, J. J. Electrocatalysts for Hydrogen Evolution in Alkaline Electrolytes: Mechanisms, Challenges, and Prospective Solutions. *Adv. Sci.* 2018, 5 (2). <https://doi.org/10.1002/advs.201700464>.
- (120) Xia, J.; Dhaka, K.; Volokh, M.; Peng, G.; Wu, Z.; Fu, Y.; Caspary Toroker, M.; Wang, X.; Shalom, M. Nickel Phosphide Decorated with Trace Amount of Platinum as an Efficient Electrocatalyst for the Alkaline Hydrogen Evolution Reaction. *Sustain. Energy Fuels* 2019, 3 (8), 2006–2014. <https://doi.org/10.1039/C9SE00221A>.
- (121) Sheng, W.; Zhuang, Z.; Gao, M.; Zheng, J.; Chen, J. G.; Yan, Y. Correlating Hydrogen Oxidation and Evolution Activity on Platinum at Different PH with Measured Hydrogen Binding Energy. *Nat. Commun.* 2015, 6 (1), 1–6. <https://doi.org/10.1038/ncomms6848>.
- (122) Dennison, C. R.; Beidaghi, M.; Hatzell, K. B.; Campos, J. W.; Gogotsi, Y.; Kumbur, E. C. Effects of Flow Cell Design on Charge Percolation and Storage in the Carbon Slurry Electrodes of Electrochemical Flow Capacitors. *J. Power Sources* 2014, 247, 489–496. <https://doi.org/10.1016/j.jpowsour.2013.08.101>.
- (123) Heidian, A.; Cheung, S. C. P.; Ojha, R.; Rosengarten, G. Effects of Current Collector Shape and Configuration on Charge Percolation and Electric Conductivity of Slurry Electrodes for Electrochemical Systems. *Energy* 2022, 239, 122313. <https://doi.org/10.1016/j.energy.2021.122313>.
- (124) Peng, L.; Ren, Y.; Yin, Z.; Wang, Z.; Wu, X.; Zhang, L. Current Collectors' Effects on the Electrochemical Performance of $\text{LiNi}_0\cdot6\text{Co}_0\cdot2\text{Mn}_0\cdot2\text{O}_2$ Suspension Electrodes for Lithium Slurry Battery. *Green Energy Environ.* 2023. <https://doi.org/10.1016/j.gee.2023.03.002>.
- (125) Mourshed, M.; Nguyen, H. Q.; Shabani, B. Using Electrical Conductivity to Determine Particle Sedimentation Status of Carbon-Based Slurry Electrodes in Electrochemical Energy Storage Systems. *Mater. Sci. Energy Technol.* 2023, 6, 290–300. <https://doi.org/10.1016/j.mset.2023.02.003>.
- (126) Kastening, B.; Boinowitz, T.; Heins, M. Design of a Slurry Electrode Reactor System. *J. Appl. Electrochem.* 1997, 27 (2), 147–152. <https://doi.org/10.1023/A:1018443705541/METRICS>.
- (127) Tam, V.; Wainright, J. Electrochemical Behavior of Low Loading Slurry Electrodes for

- Redox Flow Batteries. *J. Electrochem. Soc.* 2023, 170 (1), 010538. <https://doi.org/10.1149/1945-7111/acb10a>.
- (128) Forschner, L.; Artmann, E.; Jacob, T.; Engstfeld, A. K. Electric Potential Distribution Inside the Electrolyte during High Voltage Electrolysis. *J. Phys. Chem. C* 2023, 127, 4387–4394. <https://doi.org/10.1021/acs.jpcc.2c07873>.
- (129) Mourshed, M.; Rezaei Niya, S. M.; Shabani, B. Electronical Conductivity Improvement of Carbon-Based Slurry Electrodes Using Carbon Foams for Enhanced Performance in Advanced Electrochemical Energy Storage Systems. *ACS Omega* 2023, 8 (11), 10525–10544. <https://doi.org/10.1021/acsomega.3c00278>.
- (130) Heidarian, A.; Wehner, M.; Padligur, M.; Keller, R.; Cheung, S. C. P.; Blanch, E. W.; Wessling, M.; Rosengarten, G. A Microfluidic Proton Flow Reactor System: In-Situ Visualisation of Hydrogen Evolution and Storage in Carbon-Based Slurry Electrodes. *J. Power Sources* 2023, 569, 233026. <https://doi.org/10.1016/j.jpowsour.2023.233026>.
- (131) Kastening, B.; Busscher, N.; Asskamp, U. Electrochemical Polarization of Activated Carbon and Graphite Powder Suspensions. Part III. Charge Transfer during a Single Collisions and Contact Resistance. *J. Electroanal. Chem. Interfacial Electrochem.* 1989, 265 (1–2), 77–101. [https://doi.org/10.1016/0022-0728\(89\)80181-0](https://doi.org/10.1016/0022-0728(89)80181-0).
- (132) Lohaus, J.; Rall, D.; Kruse, M.; Steinberger, V.; Wessling, M. On Charge Percolation in Slurry Electrodes Used in Vanadium Redox Flow Batteries. *Electrochim. commun.* 2019, 101, 104–108. <https://doi.org/10.1016/J.ELECOM.2019.02.013>.
- (133) Rossi, R.; Cario, B. P.; Santoro, C.; Yang, W.; Saikaly, P. E.; Logan, B. E. Evaluation of Electrode and Solution Area-Based Resistances Enables Quantitative Comparisons of Factors Impacting Microbial Fuel Cell Performance. *Environ. Sci. Technol.* 2019, 53 (7), 3977–3986. <https://doi.org/10.1021/acs.est.8b06004>.